NASA Contractor Report 3339

Solid State SPS Microwave Generation and Transmission Study

Volume II - Phase II Final Report, Appendices

Owen E. Maynard

CONTRACT NAS8-33157
NOVEMBER 1980

NASA

NASA Contractor Report 3339

Solid State SPS Microwave Generation and Transmission Study

Volume II - Phase II Final Report, Appendices

Owen E. Maynard
Raytheon Company
Wayland, Massachusetts

Prepared for
Marshall Space Flight Center
under Contract NAS8-33157

National Aeronautics
and Space Administration

**Scientific and Technical
Information Branch**

1980

Technical Note

SPS Pilot Beam Ionospheric Effects - Discussion of Critical Issues

1. INTRODUCTION

The ionosphere will introduce phase errors in the pilot beam system through a combination of "bias" and stochastic fluctuations effects. Specific actions must be taken to remove these errors in order to make the pilot beam system capable of performing its assigned function.

The approach available for the solution of the problem involves the use of averaging processes. However, in order to perform them in an effective manner, we must first measure and remove from the arriving phase of the pilot beam the steady state ionospheric "bias". The dual frequency scheme assumed for the SPS Pilot Beam Baseline System (October 1978 version) employing two tones one at either side of the carrier of the downcoming power beam, each separated from this carried by Δf = 100 MHz, cannot accomplish this task. An alternative scheme based on the use of three frequencies can, on the contrary, do it. We review here-under its basic principle, which could be applied to a broad family of mechanizations. Once the "bias" is removed, we have to cope with the stochastic fluctuations. Starting point of any action in this sense must be a reliable estimate of the expected stochastic phase errors. This note also addresses this critical issue.

2. The 3-frequency versus the 2-frequency method for the removal of the ionospheric "bias"

The SPS Pilot Beam Baseline System (October 1978 version) suggested to implement the pilot beam approach with a dual frequency arrangement. Two carriers were allocated at either side of the 2.45 GHz carrier of the downcoming power beam, each with a typical separation from it of Δf = 100 MHz. From phase measurements performed at these two carriers, it was claimed that it would be possible, through suitable processes, to remove the ionospheric effects.

Unfortunately this is not the case. In fact, it can be shown that the two-frequency method cannot work unless the spacing between the two frequencies is at least one order of magnitude smaller than the spacing chosen in the Baseline System design. The reason is that there is a severe ambiguity in the value of the measured phase, that does not make it possible to remove the ionospheric bias. A numerical example will clarify the difficulty.

The value of the phase path length over a transionospheric path with geometric length L and total electron content $\int Ndl$, is given at the frequency f by the expression:

$$\phi_{rad} = 2\pi \frac{1}{v_1} \left(fL - \frac{40}{f} \int Ndl \right) \qquad (1)$$

where v_1 is the velocity of light in free space.

By specializing Equation (1) to the frequencies f_1 and f_2, by then multiplying ϕ_1 (at frequency f_1) by the ratio f_2/f_1, and by finally subtracting from this product the quantity ϕ_2 (phase at the frequency f_2) we obtain:

$$\Delta\phi_{rad} = \phi_1 \frac{f_2}{f_1} - \phi_2 = 2\pi \cdot \frac{40}{v_1} \left(\frac{1}{f_2} - \frac{f_2}{f_1^2} \right) \int Ndl \qquad (2)$$

In Equation (2) we have:

$v_1 = 3 \times 10^8$ m/sec
$f_1 = 2.35\ 10^9$ Hz
$f_2 = 2.55\ 10^9$ Hz
} Values chosen by the Baseline System Design

$\int Ndl = 10^{18}$ el/m^2 (We assume here a large value for this quantity, a value, however, that is not uncommon at all)

Under these assumptions, we have

$$\Delta\phi = 9.2 \times 2\pi$$

This is an unacceptable value for $\Delta\phi$. The reason is that phase measuring instrumentation of every conceivable type will read for the $\Delta\phi$ above the erroneous value $0.2 \times 2\pi$, from which an incorrect value for $\int Ndl$ would be derived. In other words, no instrumentation or approach exists that could eliminate the 2π ambiguity (in this case a 9 fold ambiguity) from the measurements.

Equation (2) shows that in order to keep $\Delta\phi < 2\pi$, for $\int Ndl = 10^{18}$ el/m^2 and for $f_2 = 2.55\ 10^9$ Hz, we must keep $\Delta f < 10$ MHz, a spacing an order of magnitude smaller than contemplated by the Baseline System Design (by adopting $\Delta f = 10$ MHz, we would have $\Delta\phi = 0.89 \times 2\pi$). However, in the SPS case, it is not

advisable to allocate the carriers of the pilot beam system so close to the power beam carrier.

This fundamental limitation of the 2-frequency method was recognized twenty years ago by Prof. Von R. Eshleman of Stanford University. He solved the problem of achieving wide carrier-to-carrier separation in an ionospheric correction link and still avoided the 2π ambiguity problem, with his scheme known as the "3-frequency method" (Eshleman et al, 1960; Burns and Fremouw, 1970).

The basic principle of the method can be illustrated as follows. Let us consider three frequencies

$$f_1 = f_0 - \Delta f$$

$$f_0,$$

$$f_2 = f_0 + \Delta f,$$

and let's call ϕ_1, ϕ_0 and ϕ_2 the phase path lengths in a transionospheric link, respectively at f_1, f_0 and f_2.

The following expressions apply for the two phase differences $(\phi_1 - \phi_0)$ and $(\phi_0 - \phi_2)$:

$$\Delta\phi_A = \phi_1 - \phi_0 = 2\pi \cdot \frac{1}{v_1} \left\{ (f_1 - f_0)\, L - 40 \left(\frac{1}{f_1} - \frac{1}{f_0} \right) \int \mathrm{Ndl} \right\}$$

$$\Delta\phi_B = \phi_0 - \phi_2 = 2\pi \frac{1}{v_1} \left\{ (f_0 - f_2)\, L - 40 \left(\frac{1}{f_0} - \frac{1}{f_2} \right) \int \mathrm{Ndl} \right\}$$

At this point, the method goes further than is usually the case with the dual frequency approach, and requires the computation of the difference of the two differences above:

$$\Delta\phi_A - \Delta\phi_B = 2\pi \frac{40}{v_1} \left(\frac{2\Delta f^2}{f_0^3} \right) \int \mathrm{Ndl} \qquad (3)$$

This is the fundamental observable, from which $\int \mathrm{Ndl}$ is computed.

A numerical evaluation of Equation (3) shows that for $\int Ndl = 10^{18}$ el/m^2 and for $f_0 = 2.55\ 10^9$ Hz,

$$\Delta\phi_A - \Delta\phi_B \approx 2\pi\ (1.6 \times 10^{-17})\ \Delta f^2$$

With the use of the three frequencies, the avoidance of the 2π ambiguity brings forth the following requirement for the maximum allowable value of the frequency separation among the various tones:

$$\Delta f_2 \leq \frac{1}{1.6 \times 10^{-12}}$$

$$\Delta f \leq 249 \text{ MHz}$$

We conclude therefore that we can easily meet the requirements of keeping any carrier of the multifrequency pilot beam system at least 100 MHz away from the frequency of the downcoming power beam and still retain the ability of correcting for the ionospheric "bias" without 2π ambiguities.

Figure 1 shows a possible way in which the various frequencies could be allocated. Several other suitable allocations are also possible. See Appendix A for a possible mechanization of the 3-frequency scheme.

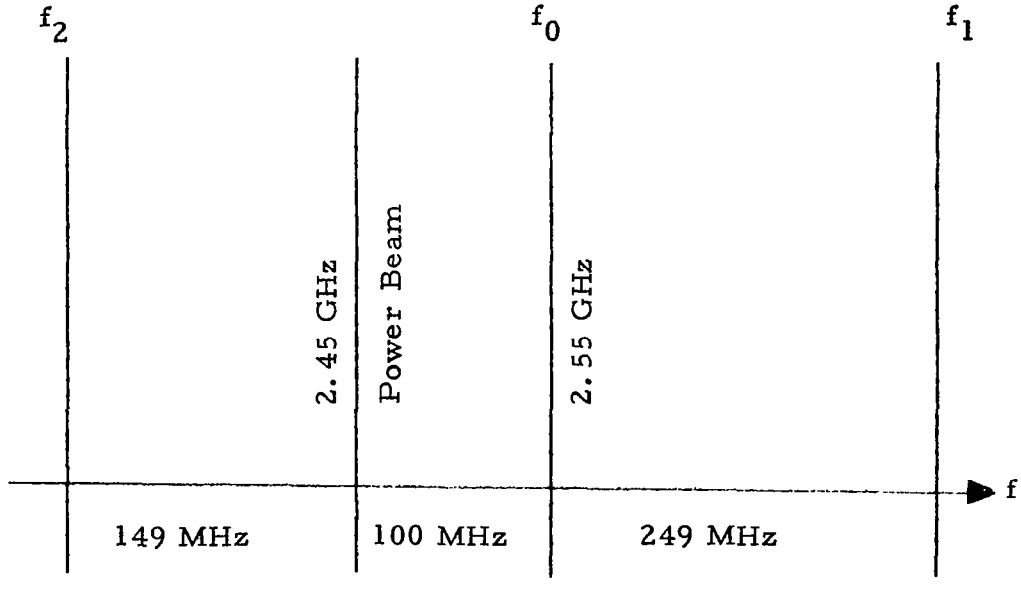

Figure 1. Possible Frequency Allocation

Once that, with the use of the three frequency method, it has been possible to remove from the measured phase the effect of the ionospheric "bias" at the wanted pilot beam frequency, we can properly apply to the residuals suitable averaging processes in order to reduce the effect of the stochastic fluctuations due to ionospheric inhomogeneities.

3. Stochastic Phase Fluctuations due to Ionospheric Inhomogeneities

In this past decade surprising results have been obtained by researchers active in the area of ionospheric scintillation, while experimenting with trans-ionospheric paths at microwave. Unexpectedly, large scintillation indeces have been observed at microwave in space-to-ground links that cross the nighttime F region of the ionosphere at equatorial, tropical and auroral latitudes. Observed phase fluctuations were found to be much larger than could be expected from such analytical approaches as the "thin scattering layer" theory. In fact, by applying thin scattering theory to the spectral density distribution $\frac{\delta n/n}{\sqrt{Km^{-1}}}$ versus K(wave number, Km^{-1}) of the electron density inhomogeneities actually measured in the ionosphere with rockets and other means, the phase fluctuations that would be computed for a microwave link that crosses the region containing these inhomogeneities are much smaller than experimentally ascertained. A "workman-like approach" to solve at least temporarily the difficulty (while a suitable new theory is being worked out) is the one suggested by Basu and Basu (1976). It involves altering "phenomenologically" the spectral density distribution of Figure 2 by moving the curve A-A to the B-B location and using the new curve as the basis for the computation of phase fluctuations with the thin scattering theory formula. In this way, results are obtained that match the observations. The applicable formula is (Costa and Kelly, 1976):

$$\Phi_0^2 = \frac{\sqrt{2}}{2} \pi (r_e \lambda)^2 \frac{\alpha}{\beta} (L \sec \theta) \frac{(\delta n)^2}{K_o} \qquad (4)$$

where:

Φ_0 = rms phase fluctuation, rad.

r_e = classical radius of electrons = $2.818\ 10^{-15}$ m

θ = angle between the ray path and the vertical

L = thickness of the irregular layer, m (at ionospheric F_2 layer heights)

λ = wavelength of the propagating wave, free space value, m (λ = 0.12245 m at 2.45 GHz)

$\beta^2 = \cos^2 \psi + \alpha^2 \sin^2 \psi$, where ψ is the angle between the direction of the Earth magnetic field and the ray path and where α is the axial ratio

$\frac{\alpha}{\beta} \cong 1$ for equatorial paths ($\psi = 90°$, $\beta^2 = \alpha^2$)

K = wave number = $\frac{2\pi}{\lambda_s}$ (where λ_s is the spatial wavelength of the irregularities)

K_o = outer scale wave number

For equatorial transionospheric paths, we have in (4) $L = 2 \times 10^5$ m, $K_o = 0.31$ Km^{-1} $\frac{\alpha}{\beta} \cong 1$, sec $\theta \cong 1$.

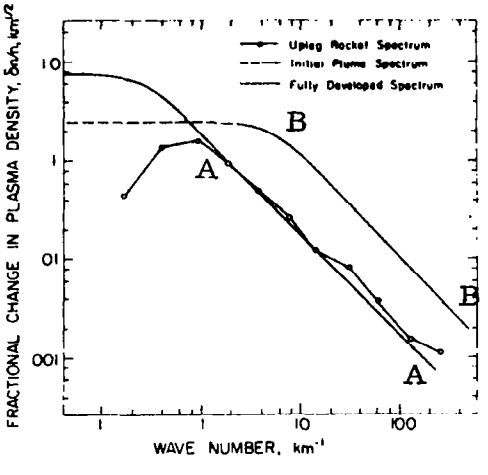

Figure 2. The dashed line is a model spectrum used by Costa and Kelley (1976) to characterize the breakup of density gradients in upwelling structures. The solid line is a spectrum used by Basu and Basu (1976) to typify extended topside irregularities.
(From Basu and Kelley, 1977)

To proceed in the computation, we must define the wave number interval in the x-axis of Figure 2, across which to integrate the spectral density curve. This interval must include all spatial wavelengths equal to or smaller than the "size" of the pilot beam ray at ionospheric heights. This could not be derived from purely geometrical considerations (where a 10 meter spatial size F layer height would be obtained). The value obtained this way would not have physical meaning. On the contrary, physically meaningful results are obtained by constructing the Fresnel ellipsoid(Fagot et al, 1959) for the ground-to-space pilot beam link (Figure 3). The radius of the first Fresnel zone at ionospheric height is the rational representation of the "size" of the ray. From Figure 3, we have that this radius is:

$$\text{radius of the first Fresnel zone} = FB = \sqrt{\frac{\lambda \times d_1 \times d_2}{d_1 + d_2}}$$

In the case of the peak of the F layer, $d_1 \cong 400$ Km, $d_2 = 37500$ Km and therefore

$$FB = 2.2 \times 10^2 = 220 \text{ meters.}$$

The interval of integration in Figure 2 must therefore be extended from at least a spatial wavelength equal to this value down to all smaller wavelengths (wave numbers from ~ 28 Km^{-1} to ~ 300 Km^{-1}). Figure 2 yields:

$$\frac{\delta n}{n} \cong \frac{0.025}{2} \sqrt{272} \cong 0.2$$

and with an electron density in the F2 layer of $2.5\ 10^{-11}$ m^{-3}, Equation (4) gives

$$\Phi_0 = 1.3 \times 10^{-11}(\delta n) = 1.3\ 10^{-11} \times 0.2 \times 2.5\ 10^{-11}_{\text{rad}} \cong 38^\circ$$

This value of Φ_0 is a realistic estimate for the phase fluctuations to be expected at 2.45 GHz in transionospheric paths crossing perturbed regions such as the equatorial or the auroral ionosphere. In fact, this estimate is substantiated by the experimental evidence collected by the DNA wideband satellite (Fremouw et al, 1978). Figures 4 and 5 show fluctuations upwards of 35° which is comparable with the above calculation. We are reminded that the DNA satellite could not see,

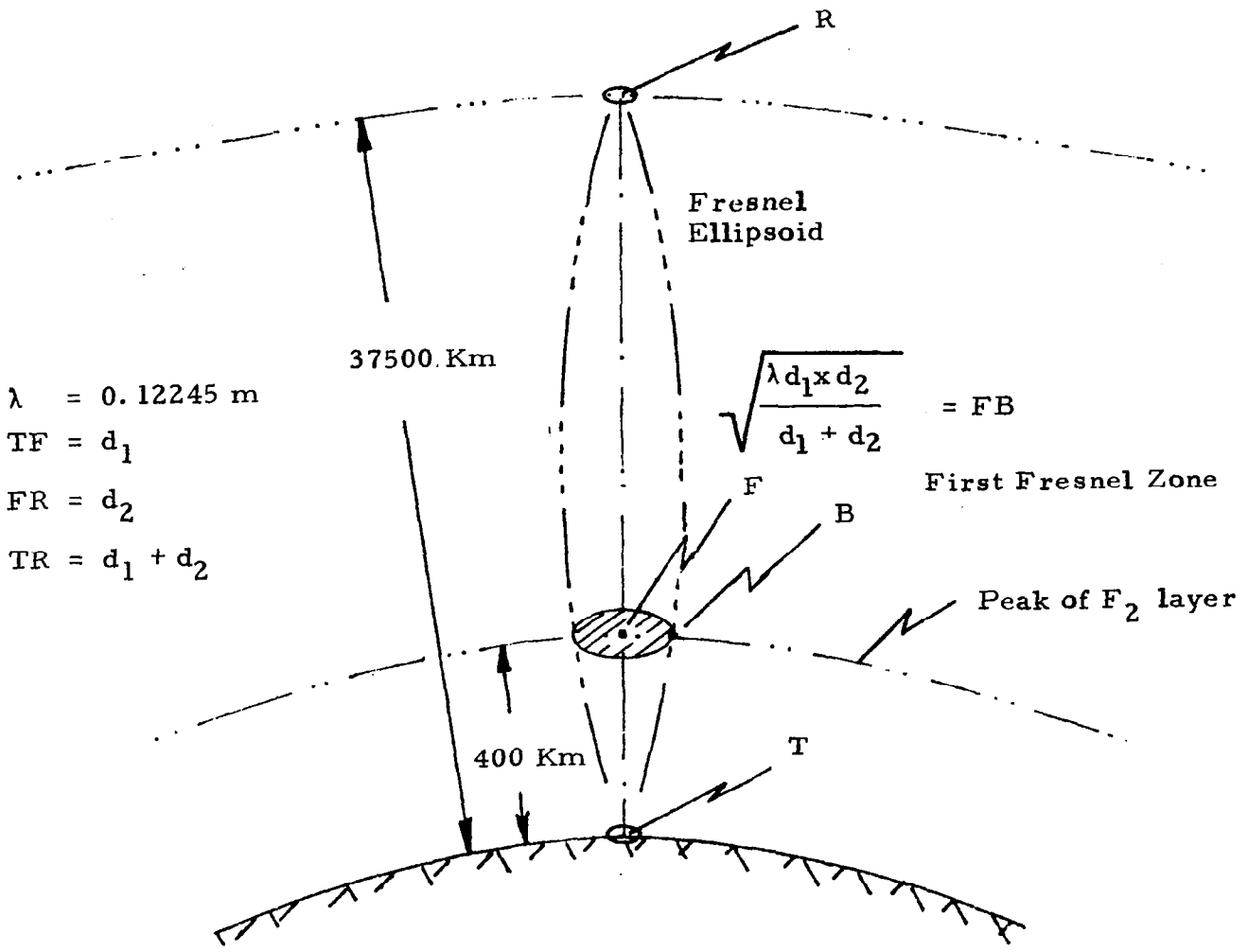

Figure 3. Fresnel Ellipsoid of the Pilot Beam Ray

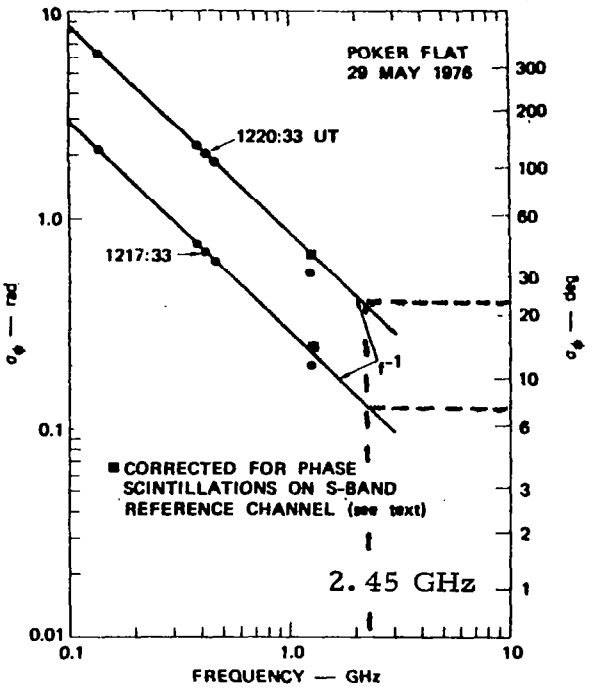

Figure 4. Frequency dependence of phase-scintillation index, during two 20 sec periods of the pass above Poker Flat, 29 May 1976 compared with an f^{-1} dependence. (from Fremouw et al, 1978)

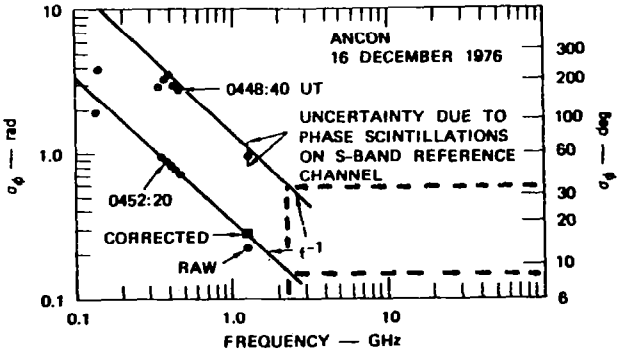

Figure 5. Frequency dependence of phase scintillation index during two 20 sec periods of pass recorded at Ancon on 16 Dec. 1976, compared with an f^{-1} dependence arbitarily passed through the 413 MHz data point. (from Fremouw et al, 1978)

(because of the integration time used in the measurements), spatial wavelengths shorter than approximately 25 m. However, because of the size of the Fresnel zone, (approximately 200 m), these results apply to our case. The question now is: what value for Φ_0 should be adopted in the design of, and associated experiments for, the SPS pilot beam system that is expected to cross the ionosphere at middle latitudes? There are two opposite factors that play a role in this decision:

1. Natural ionospheric inhomogeneities at mid latitude are smaller than at the equator and in the auroral zones. Vessot and Levine (1977) measured in a mid latitude transionospheric path phase fluctuations with rms value of about 4° at S-band on a very quiet day, with the 3-frequency gravitational red-shift rocket probe experiment that they performed for NASA-MSFC. No data base exists, however, that would make it possible to compute the percentage of time during which, (in spread F events or other occurrences of mid latitude ionospheric perturbations), the value Φ_0, (that typically applies to equatorial paths), could be reached or even exceeded. However small that percentage might be, it could be significant in the overall performance of the pilot beam system;

2. The medium where the pilot beam will propagate in the SPS case is expected to be heated and perturbed by the downcoming power beam. The interactions phenomena could resemble the natural phenomena of field aligned striations and similar structures formation occurring at the magnetic equator and in the auroral zones. These are the natural causes of the phase perturbations illustrated in Figures 2, 4 and 5. Therefore, while waiting for the results of the ionospheric/magnetospheric heating experimental program (which is part of the SPS environmental assessment effort), it is advisable to adopt the equatorial or the auroral situations as representative of what is to be expected for the pilot beam when the SPS high-power radiation is "on". In other words, it is advisable to make the assumption that the phase fluctuations in a mid latitude transionospheric link perturbed by the SPS power beam heating will be of similar intensity to the ones observed as naturally occurring at the equator or in aurora-crossing transionospheric links.

It appears from the above that it is advisable, in Raytheon's opinion, to adopt the value $\Phi_0 \cong 40^\circ$ for the expected phase fluctuations in the SPS pilot beam system and to design a system that can cope with this expectation as well as to design experiments that will address these parameters during the GBED program.

4. Conclusions

The ionospheric effects on the pilot beam phase stability and phase measurement accuracy will not be inconsequential and require the project's attention. However, several approaches are potentially suited to the solution of the various problems and could be adopted to make the pilot beam capable of operating within rational performance specifications in the expected conditions of ionospheric bias and stochastic fluctuations.

Developing further this approach should not add to the system complexity to the point that it could possibly lead to a potential program stoppage. On the contrary, the inclusion in the system of features that would make it work under the conditions above could only reinforce the SPS case.

5. References

Basu, S. and Kelley, M. C., "Review of Equatorial Scintillation Phenomena in Light of Recent Developments in the Theory and Measurement of Equatorial Irregularities," J. Atmos. and Terres. Physics, Vol. 39, No. 9/12, pp 1229-1242, 1977.

Costa, E. and Kelley, M. C., "Calculations of Equatorial Scintillation at UHF and GHz Frequencies Based on a New Model of the Disturbed Equatorial Ionosphere," Geophys. Res. Lett. 3, 677-680, 1976.

Basu, Sunanda and Basu, Santimay, "Correlated Measurements of Scintillations and In-Situ F-Region Irregularities From OGO-6,"Geophys, Res. Lett., 3, 681-684, 1976.

Fremouw, E. J. et al, "Early Results From The DNA Wideband Satellite Experiment-Complex-Signal Scintillation," Radio Science, 13, pp 167-187, 1978.

Vessot, R. F. C., and Levine, M. W. (1977), "A Preliminary Report on the Gravitational Red-Shift Rocket-Probe Experiment," Proc. International Symposium on Experimental Gravitation, Pavia, Italy, 17-20 September 1976.

Eshleman, V. R., Gallagher, D. B., and Barthle, R. C. (1960), "Radar Methods of Measuring the Cislunar Electron Density," J. G. R., Volume 65, pp 3079-3086, October.

Burns, A. A., and Fremouw, E. J., (1970), "A Real-Time Correction Technique For Transionospheric Ranging Error," IEEE Transactions on Antenna and Propagation, Vol. AP-18, No. 6, pp 785-790, November.

Fagot, T., and Mague, P. (1959), La Modulation de frequence - Theorie Applicatic aux Faisceaux Hertziens Publisher; Soc. Fran Doc Electronique, Paris, Frai

APPENDIX A

A POSSIBLE MECHANIZATION OF THE 3-FREQUENCY SCHEME

A POSSIBLE MECHANIZATION OF THE 3-FREQUENCY SCHEME

Figure A-1 illustrates the simplified block diagram of one of the possible mechanizations of the 3-frequency approach. The diagram follows closely the Stanford University design guidelines contained in the paper by Burns and Fremouw (1970).

We are reminded that it is quite all right to perform arithmetic manipulations on the phases of the arriving signals. This fully preserves phase coherence, and it is currently done in ionospheric correction schemes. Figure A-2 gives an example of the 3-frequency scheme adopted by Vessot and Levine (1977) to cancel the ionospheric bias error in their gravitational red-shift experiment, conducted for NASA-MSFC. Their 3-frequency scheme characterized by extensive arithmetic manipulations of the phases worked perfectly and the ionospheric bias was eliminated from the phase observations (NASA awarded to Dr. Vessot the Gold Medal for Exceptional Achievement, in connection with this experiment). Raytheon has no doubt that the technology exists today to implement the ionospheric correction scheme recommended for SPS in Section 2.

Literature References for Appendix A

Burns, A. A., and Fremouw, E. J., (1970), "A Real-Time Correction Technique For Transionospheric Ranging Error," IEEE Transactions on Antenna and Propagation, Vol. AP-18, No. 6, pp 785-790, November.

Vessot, R. F. C., and Levine, M. W. (1977), "A Preliminary Report on the Gravitational Red-Shift Rocket-Probe Experiment," Proc. International Symposium on Experimental Gravitation, Pavia, Italy, 17-20 September 1976.

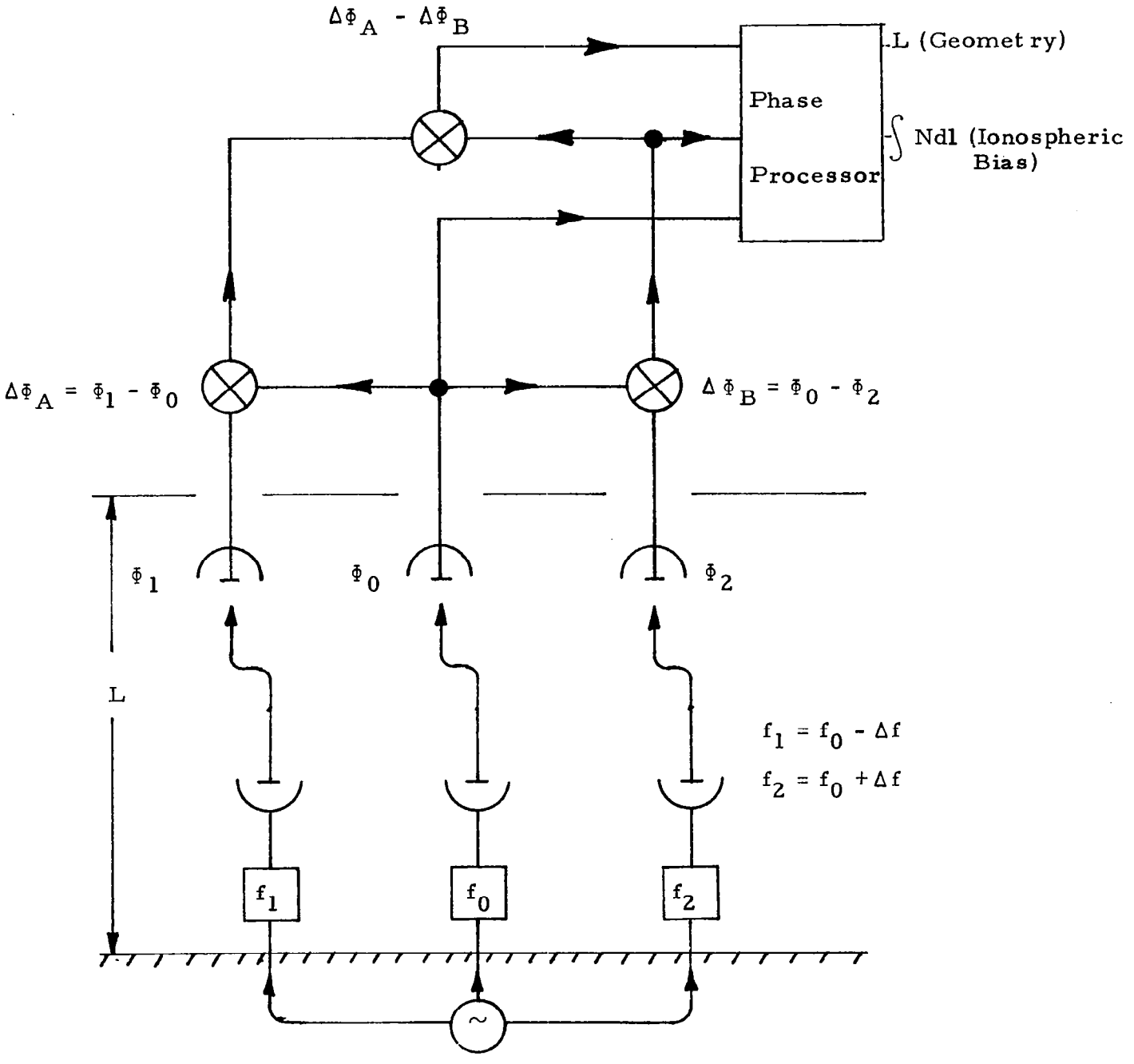

Figure A-1. Three Frequency Approach - Simplified Block Diagram of Proposed Mechanization

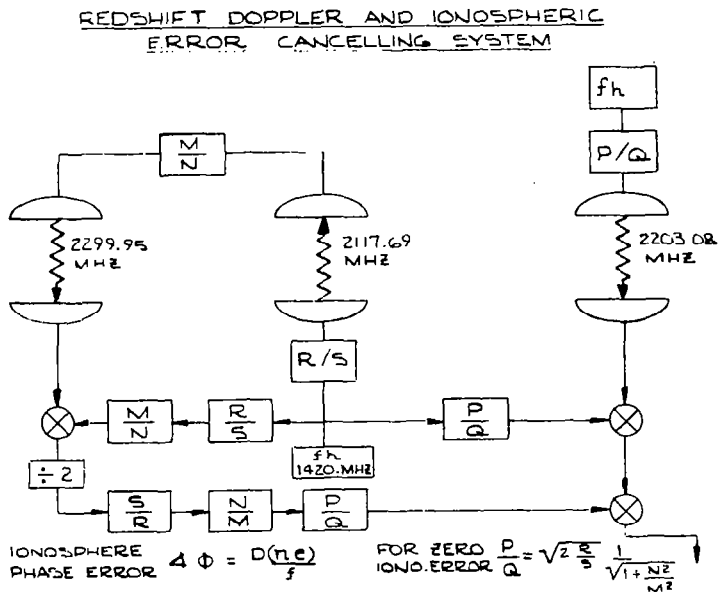

Figure A-2. Schematic Concept of the Doppler-Cancelling System. (Vessot and Levine, 1977)

IONOSPHERIC COLUMNAR ELECTRON DENSITY

- This function is a random process in the time domain. It has a non-zero mean.

- This mean value is called the ionospheric "bias."

- The "bias" is slowly changing with time (1 sample every 15 minutes is an appropriate sampling rate).

- Superimposed to the "bias" there are random fluctuations (ionospheric scintillation phenomenon). Typical scintillation rates are between 0.1/minute to 10/minute, requiring sampling rates of approximately one every 3 minutes to one every 2 seconds respectively.

APPENDIX B

MICROWAVE POWER TRANSMISSION ANTENNA ANALYSES

I. Introduction

Antenna tradeoffs are described for the application of solid state technology to microwave power transmission from space. The concept is illustrated in Figure B-1. Solar power impinges on mirrors which concentrates the sun's rays on a panel of solar cells. The solar power is converted to DC to power solid state RF amplifiers for subsequent beaming to earth[1].

The excitation for the amplifier modules is derived from a pilot signal from earth which is combined, frequency shifted, phase conjugated, and divided among the amplifiers. The power output per GaAs FET amplifier is expected to range between 5 and 30 watts at 80% efficiency.

The pilot signal is transmitted from the ground at several frequencies simultaneously as listed in Table B-1, thereby averaging the pilot electromagnetic transmission characteristics through the ionosphere. The received pilot wavefront at the spacetenna is retrodirected by dedicated phase conjugation and reference circuitry forming a pencil beam pointed back to earth. Here a large rectenna is used to collect the microwave power for conversion to DC and subsequent AC distribution to the utility power grid.[2], [3], [4]

The beam of electromagnetic power transmitted to the ground is at 2.45 GHz (.121 m wavelength) under the tentative constraint of 23 mW/cm^2 power density at the beam peak in the ionosphere. The objective is to deliver the maximum power to the utility grid at lowest cost without exceeding this power density.

II. Parametric Studies

The objective is to deliver to the utility grid the maximum power at the lowest cost under the 23 mW/cm^2 ionospheric power density constraint. The power delivered to the grid is given by

$$P_g = P_T \eta_B \eta_o \qquad \text{(B-1)}$$

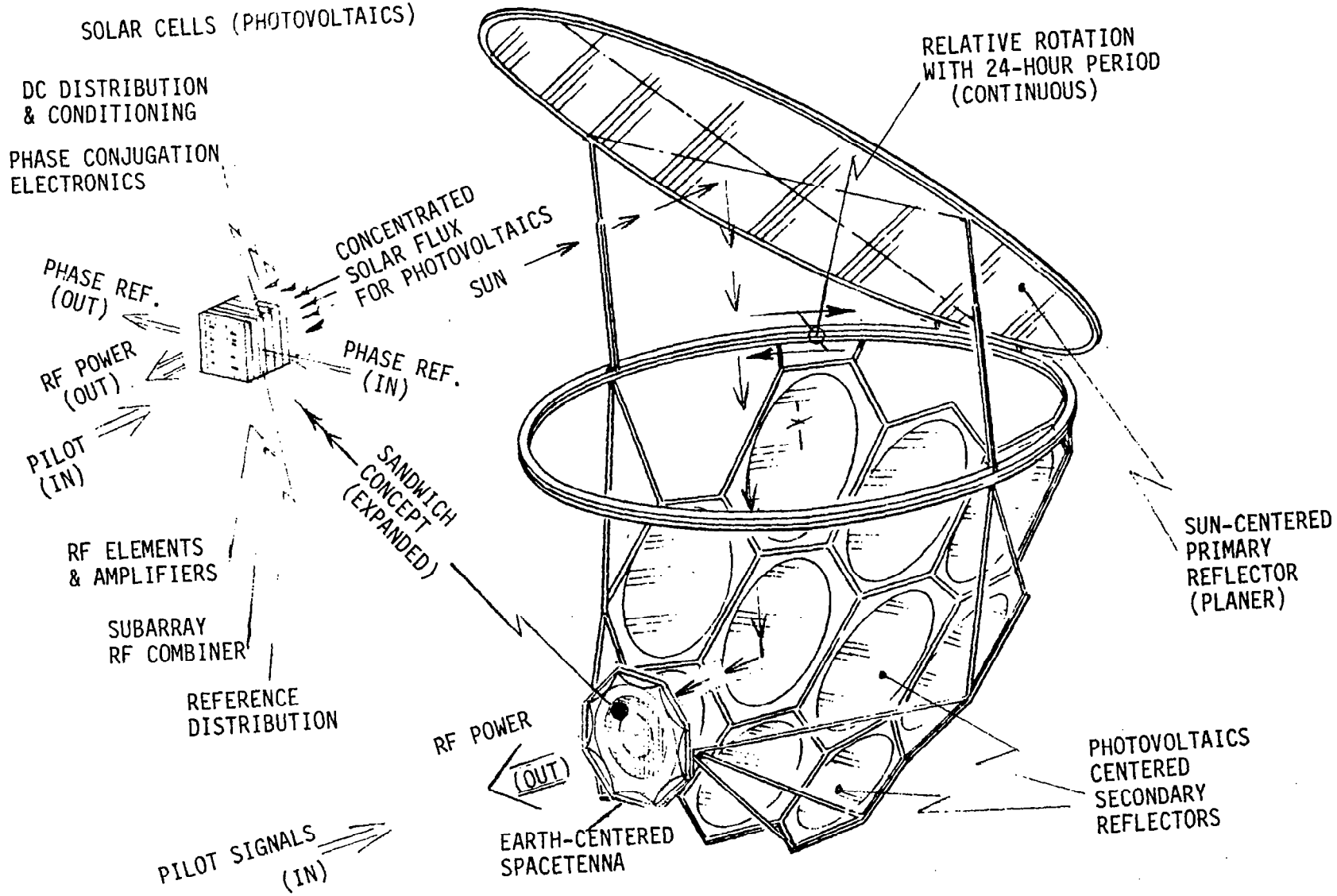

Figure B-1. Solid-State Sandwich - Typical SPS Concept

Table B-1 Solid State MPTS Parameters and Constraints

FREQUENCY (TRANSMIT)	= 2.450 GHz
FREQUENCIES (PILOT)	= 2.301 GHz 2.550 2.799
SYNCHRONOUS ORBIT RANGE	= 37×10^3 kM
POWER DENSITY LIMITS	
AT IONOSPHERE	23 mW/sq cm
AT EDGE OF RECTENNA	1 mW/sq cm
PEOPLE SAFETY	0.1 mW/sq cm
ELECTROMAGNETIC INTERFERENCE	- 154 dBW/m^2/4 kHz
SOLAR FLUX	
NOMINAL	1350 W/m^2
USEFUL	820 W/m^2

where P_T is the total available power at the output of the active transmit elements. η_B is the beam efficiency and η_o includes the atmospheric efficiency (η_{AT}) the array efficiency (η_A), the rectenna conversion efficiency (η_{RF-DC}), and the power grid interface efficiency (η_i).

The cost to develop this power is critically dependent on the size and weight of the spacetenna and secondarily on the size of the rectenna and on the real estate at the ground site. It is therefore desirable to have the smallest diameter spacetenna with amplifier modules and radiating elements arranged to transmit at the maximum power density.

It is also noted that the maximum power density capability of the active elements is dependent on thermal considerations which include primarily: junction temperature, amplifier junction waste heat, waste heat from the rest of the active element, waste heat from the DC distribution system, solar load on the microwave side and solar cell waste heat. These are discussed more completely in Sections 6 and 8.

A uniformly illuminated aperture with each active element operating at the same power level would satisfy this objective except for η_B, the beam efficiency. The beam efficiency is the ratio of the power subtended by a given solid angle of the beam to the total power radiated.[11] A uniformly illuminated aperture has high sidelobes which are not collected by the rectenna, therefore wasting power and resulting in a lower beam efficiency. Other illumination functions such as hyperspheroidal and Gaussian are known to result in higher beam efficiencies.[5] These as well as uniform have been included in the parametric study; the necessary formulas are described below.

The power density at the ionosphere is given by

$$P_{d_i} = \frac{P_T G_T}{4\pi R_o^2} \eta_{AR} \eta_{AT} \qquad \text{(B-2)}$$

where P_T is the total power transmitted, G_T the gain of the spacetenna, η_{AR} the array losses, η_{AT} the atmospheric losses and R_o the synchronous orbit range.

The spacetenna gain is given by

$$G_T = \frac{4\pi A_T}{\lambda_o^2} \eta_i \qquad \text{(B-3)}$$

where A_T is the area of the transmitting antenna ($A_T = \frac{\pi}{4} D_T^2$ for circular aperture), λ_o is the transmitting wavelength and η_i is the illumination taper efficiency.

The available transmitted power is

$$P_T = P_o A_T F \tag{B-4}$$

where P_o is the transmit power density at the active element and F is the power taper factor.

It has been determined that hyperspheroidal is the illumination with the highest beam efficiency. Gaussian illumination taper closely approximates this function and has therefore been used in the parametric study.

The Gaussian illumination power density is given by

$$P = P_o e^{-2Kr^2} \tag{B-5}$$

This results in an available transmitted power level of

$$P_T = \int_0^{R_T} \int_0^{2\pi} P_o e^{-2Kr^2} \, r dr d\phi \tag{B-6}$$

$$P_T = \frac{P_o \pi}{2k} \left(1 - e^{-2KR_T^2}\right) \tag{B-7}$$

K is related to the edge taper B in dB and the spacetenna radius

$$K = \frac{.115\ B}{R_t^2} \tag{B-8}$$

$$F = \frac{(1 - 10^{-B/10})}{0.23B} \tag{B-9a}$$

and substituting for F in Equation (B-4),

$$P_T = \frac{P_o A_t (1 - 10^{-B/10})}{.23\ B} \tag{B-9b}$$

The power density at the ionosphere is a function of the power available as well as the illumination taper efficiency η_i.

$$P_{d_i} = \frac{P_T A_T}{(R_o \lambda_o)^2} \eta_{AV} \eta_{AT} \eta_i \tag{B-10}$$

The illumination taper efficiency is given by the ratio of the power at the peak of the beam to the total available power in the aperture,

$$\eta_i = \frac{\left[\int_0^{R_T} \int_0^{2\pi} \sqrt{P_o} e^{-K\gamma^2} \, r dr d\phi \right]^2}{\frac{P_o A_t (1 - 10^{-B/10})}{.2313}} \tag{B-11}$$

$$\eta_i = \frac{2 (1 - 10^{-B/20})^2}{.115B(1 - 10^{-B/10})} \tag{B-12}$$

From (B-7), (B-10) and (B-12) the diameter of the spacetenna can be determined as follows:

$$D_T = 2 \left(\frac{P_{d_i}}{P_o \eta_{AR} \eta_{AT}} \right)^{.25} \sqrt{\lambda_o R_o} \sqrt{\frac{.115B}{\pi (1 - 10^{-B/20})}} \tag{B-13}$$

The diameter of the spacetenna as a function of the edge taper for various element power densities is plotted in Figure B-2.

The parameters for uniform illumination are obtained from (B-10) for $\eta_i = 1$ and from (B-4) for F = 1 where

$$P_{d_i} = \frac{P_o A_T^2}{(R_o \lambda_o)^2} \eta_{AV} \eta_{AT} \tag{B-14}$$

and

$$D_T = 2 \left(\frac{P_{d_i}}{P_o \eta_{AR} \eta_{AT}} \right)^{.25} \sqrt{\frac{\lambda_o R_o}{\pi}} \tag{B-15}$$

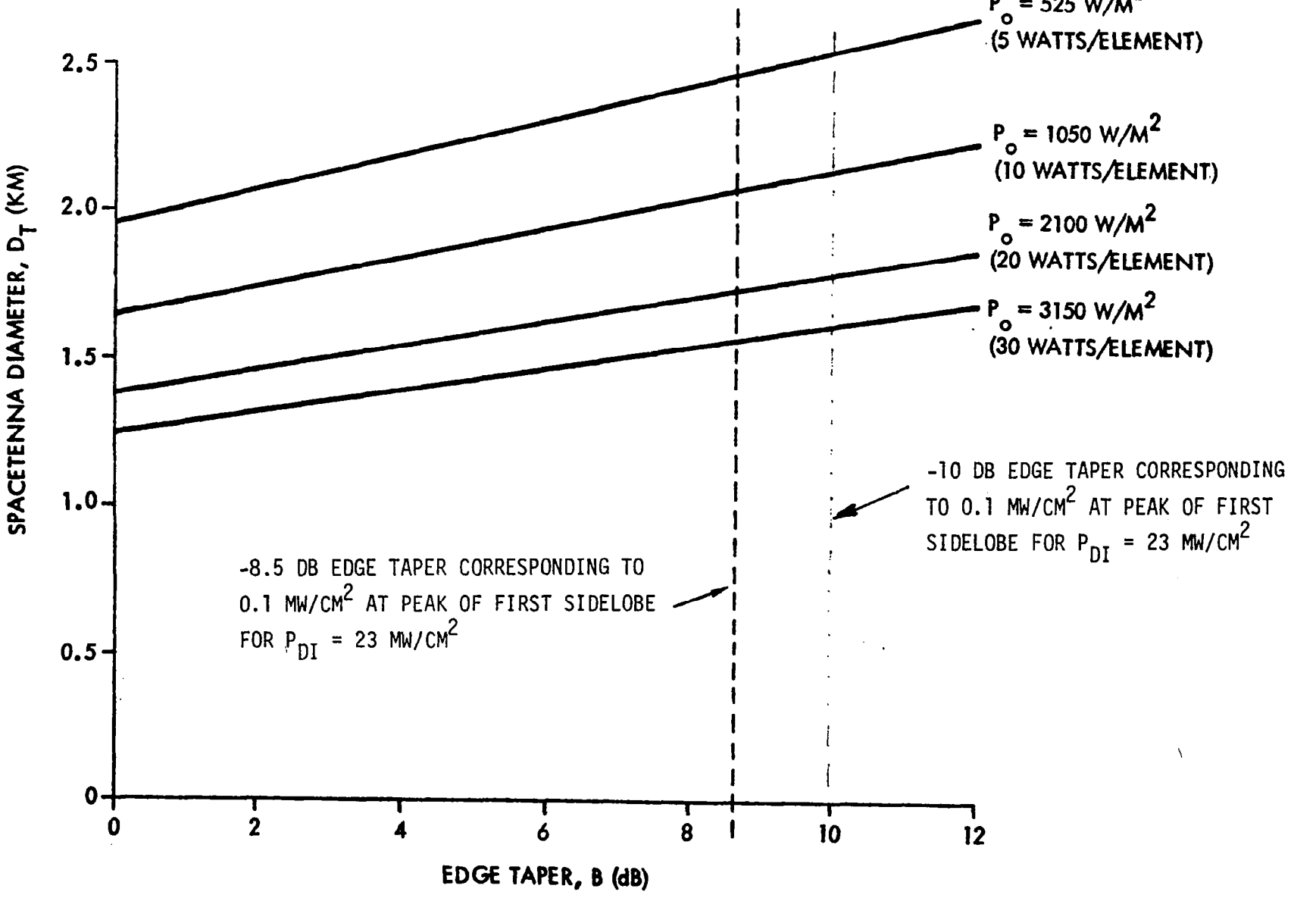

Figure B-2 Spacetenna Diameter and Power Density Vs Edge Taper

which is the same result obtained by substituting $10^{-B/20} \simeq 1 - .115B + (.115B)^2$ into Equation (B-13) and letting B 0 dB edge taper.

Determining the power delivered to the grid requires exploration of the second constraint which is to restrict the power density outside of the rectenna diameter to be less than 1 mW/cm^2. There is also a third constraint which is for the power density outside of a fenced area to be less than 0.1 mW/cm^2. This third constraint has a cost impact associated with land acquisition. These two constraints can be examined using similar formulations which depend on the antenna pattern of the spacetenna.

A circular Gaussian illumination taper has been assumed on the spacetenna which for 0 dB edge taper encompasses uniform illumination. For this Gaussian illumination the first sidelobe level versus edge taper is shown in Figure B-3[8]. In Figure B-4 is plotted the angular location from the aim-axis corresponding to the -13.6 dB (1 mW/cm^2 and the -23.6 dB (0.1 mW/cm^2) levels in terms of

$$U = \frac{D_T}{\lambda} \sin \theta \qquad \text{(B-16)}$$

Assuming that the spacetenna line of sight is perpendicular to a plane at the earth's surface, then the pattern of equi-amplitude contours will intersect this plane in concentric circles whose diameter is

$$D = 2R_o \tan \theta \qquad \text{(B-17)}$$

From (B-16), (B-17) and (B-13),

$$D = \left(\frac{P_o \eta_{AR} \eta_{AT}}{P_{d_i}} \right)^{1/4} \sqrt{\frac{\lambda_o R_o \pi (1 - 10^{-B/20})}{.115B}}\, u$$

where P_{d_i} is the power density at the peak of the main lobe at the ground.

From this equation, the rectenna diameter has been computed and plotted in Figure B-5 versus edge taper and corresponds to the spacetenna diameters and peak power densities listed in Figure B-2.

Examples of the far field antenna patterns and rectenna and fence locations for uniform illumination and 10 dB Gaussian edge taper are shown in Figures B-6 and B-7. A 10 dB Gaussian taper can use a smaller rectenna and fenced area but requires a larger spacetenna than the corresponding uniform illumination case.

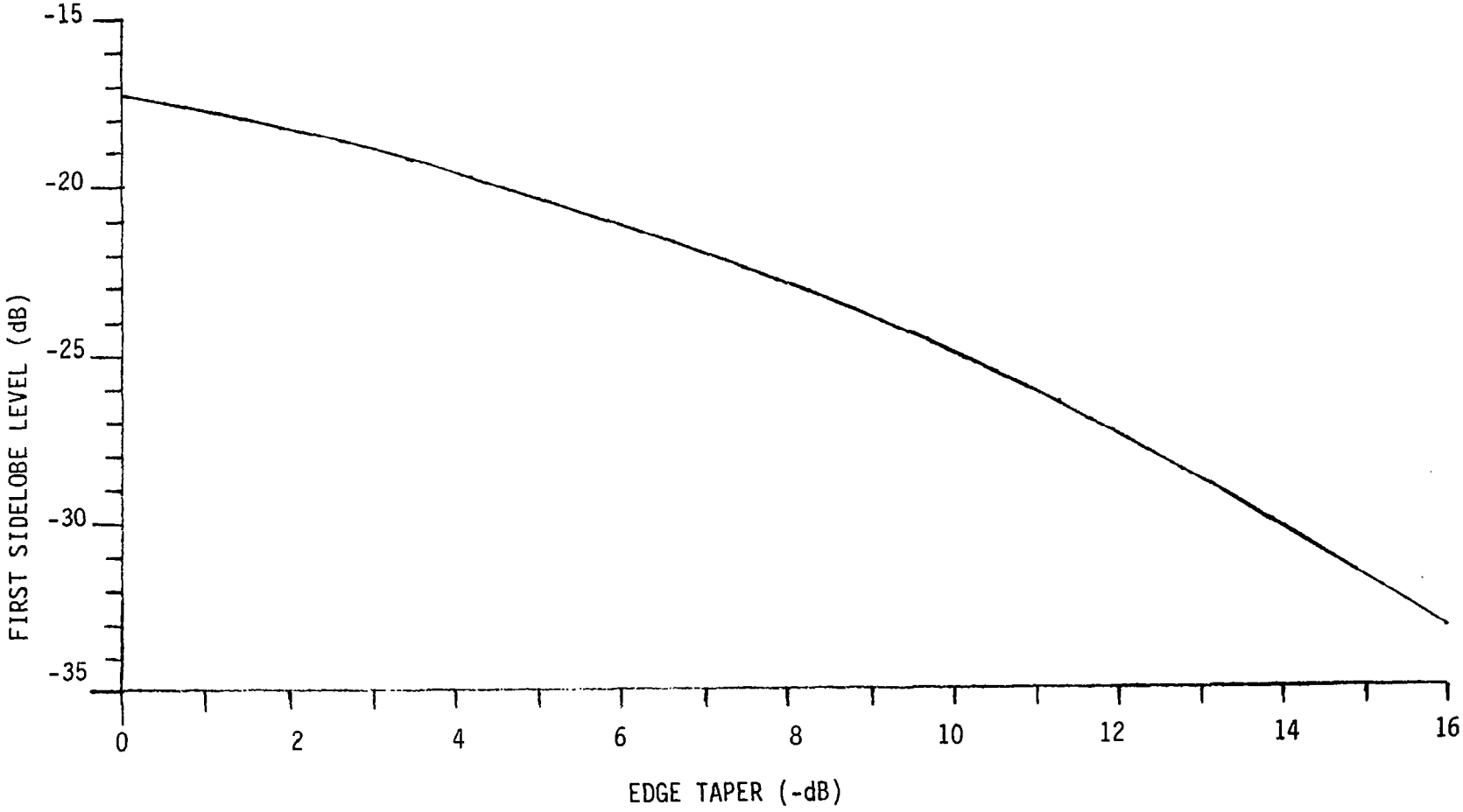

Figure B-3 First Sidelobe Level for Truncated Gaussian Taper

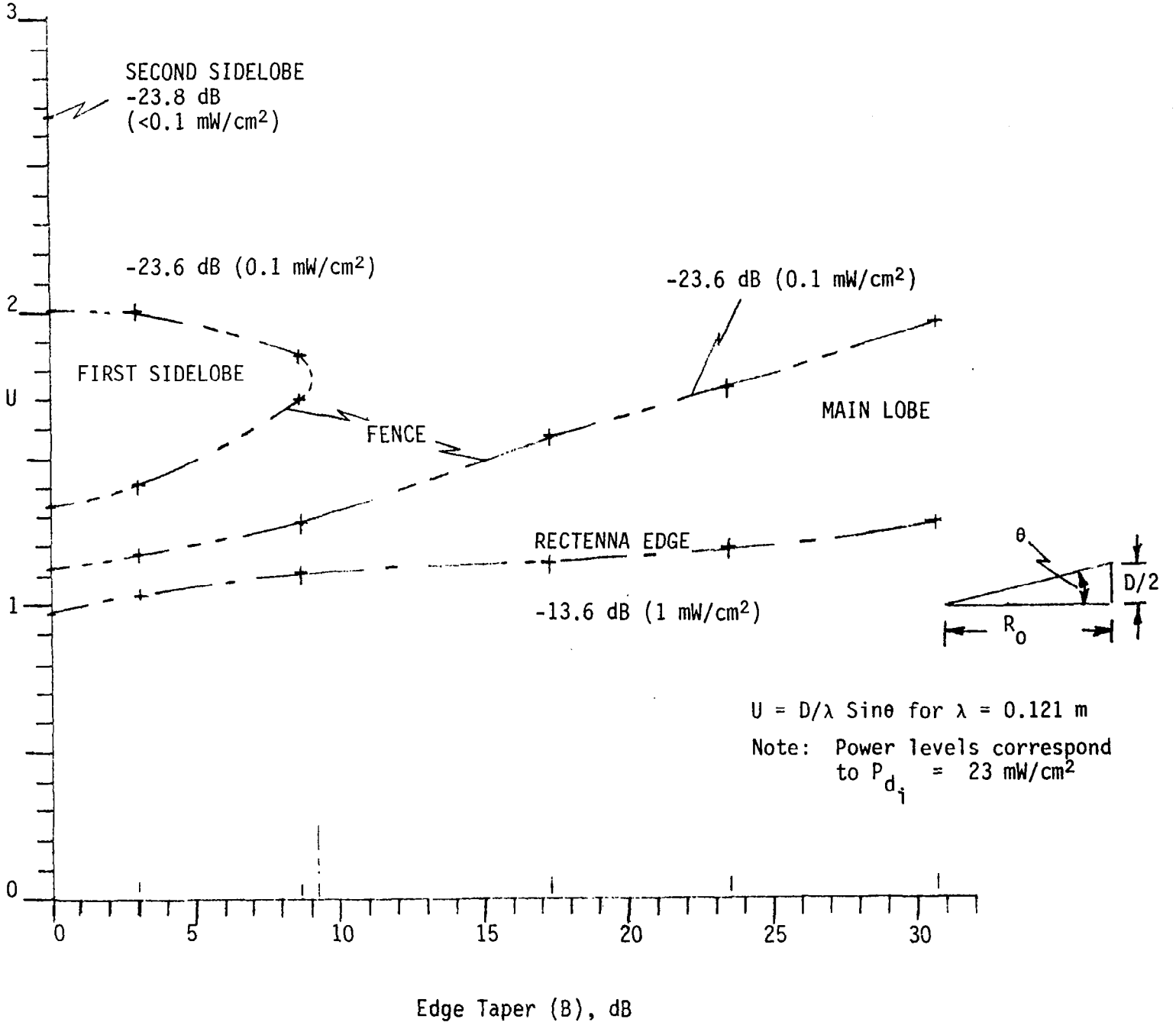

Figure B-4 Location of Power Density Limits on Ground for Gaussian Illumination Tapers at the Spacetenna

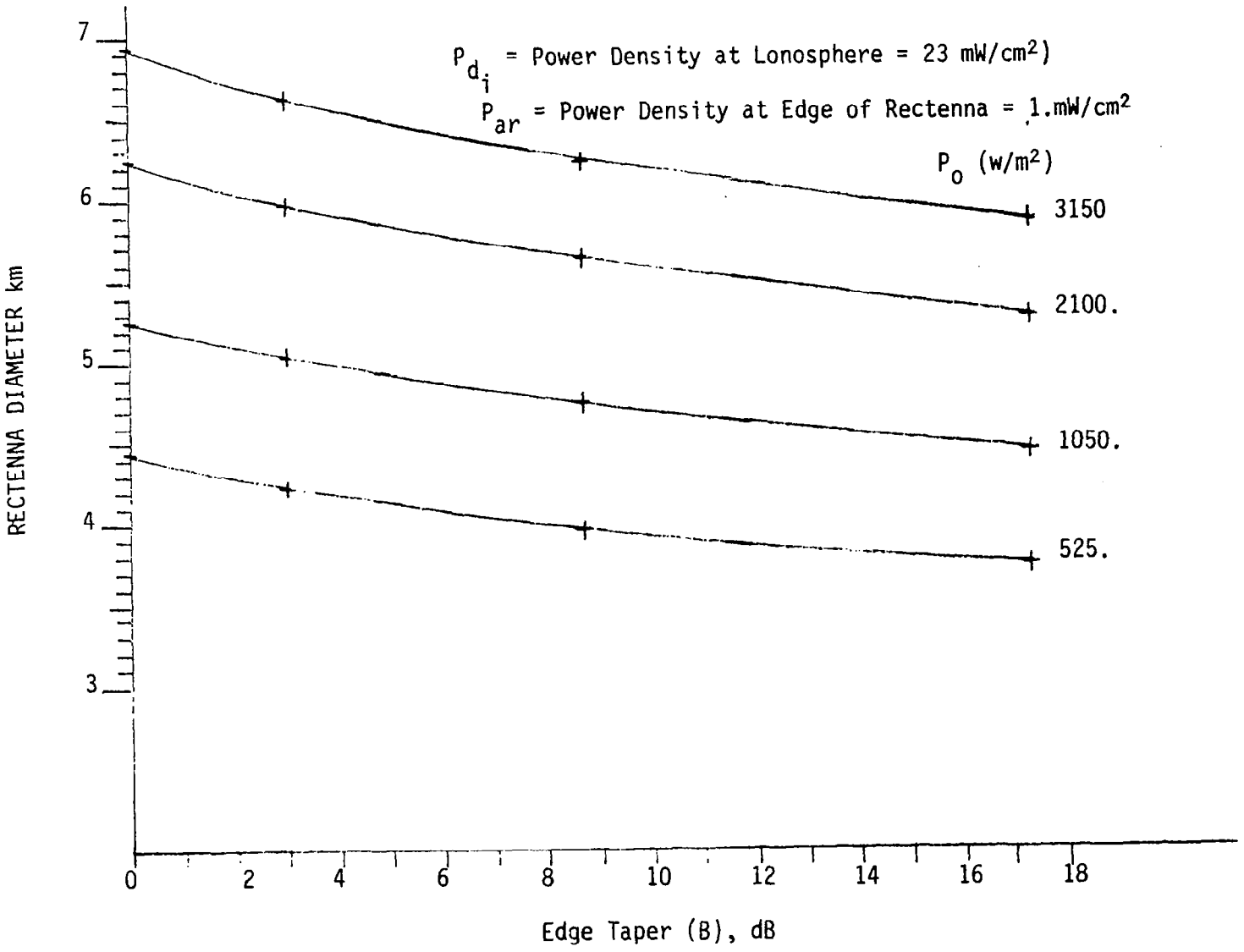

Figure B-5 Rectenna Diameter vs Gaussian Edge Taper

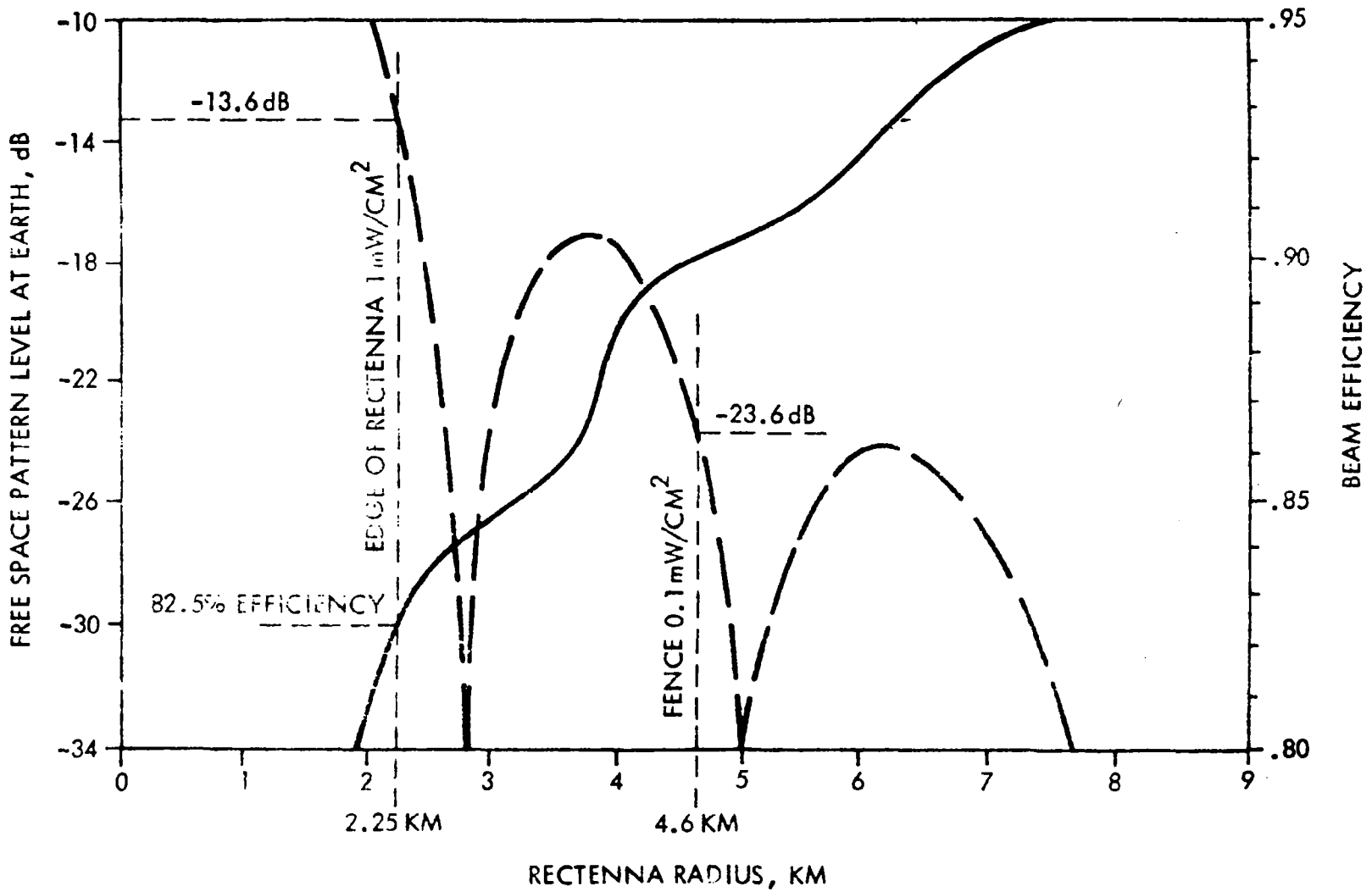

Figure B-6 Rectenna Size Vs Beam Efficiency - Uniform Illumination

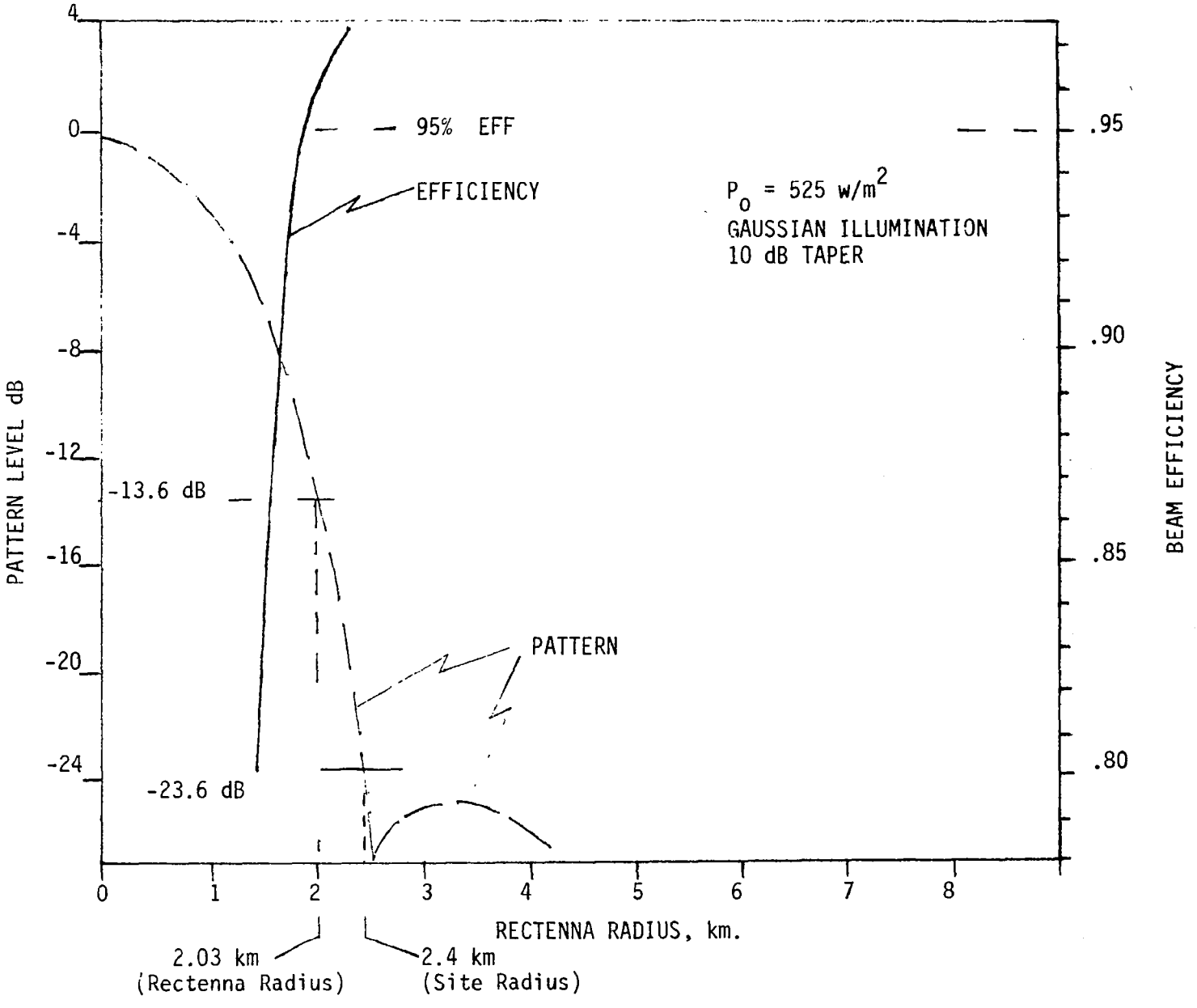

Figure B-7 Rectenna Size vs Beam Efficiency - Tapered Illumination

One other antenna pattern related quantity in the power grid formula of Equation (B-1) is the beam efficiency. For the uniform case the rectenna would collect 82.5% of the available radiated power while the 10 dB Gaussian taper case would collect 95% of the available radiated power.

The parameters for uniform illumination and for -10 dB taper are summarized in Table B-2. The tapered case requires a 30% larger spacetenna to deliver 23% less power than uniform; the rectenna diameter is 11% smaller and approximately 27% of the land area is required. The costs for the land facilities are less but the spacetenna and the transportation costs will be much greater. The cost comparison is covered in a parametric format in Section 3.10.

Based on the above parametrics the uniformly illuminated spacetenna was selected as a baseline.

As indicated earlier in this appendix, thermal considerations must be included in the evaluation of an optimum design. These are covered in Sections 6 and 8.

Also certain land use aspects play an important role in the antenna system selection.

Concerning this latter item, it became of interest to reduce the first and second sidelobes in the uniformly illuminated patterns; the first to bring in the fence thereby requiring less land use and the second to demonstrate that power densities of lower than 0.1 mW/cm^2 were achievable outside the fenced area. In order to accomplish these goals in a practical implementation, a single step taper was investigated.

Results of the single step taper investigation are reported in Appendix C.

Table B-2

Comparison Between Uniform and -10 dB Gaussian Taper for Spacetenna

Antenna Illumination	D_T (km)	P_T (GW)	η_B	η_o	P_g (GW)	D_R (km)	D_S (km)
Uniform	1.95	1.568	.825	.829	1.072	4.5	9.2
Gaussian - 10 dB	2.545	1.045	.95	.829	0.823	4.0	4.8

References

[1] Finnell, W., "MSFC Solid State SPS Concepts and Design Description," Material from presentation at NASA Headquarters, February 22, 1979.

[2] Brown, W.C., "The Technology and Application of Free Space Power Transmission by Microwave Beam," Proc. IEEE, Vol. 62, No. 1, January 1974.

[3] Brown, W.C. and O.E. Maynard, "The Adaptation of Free Space Power Transmission Technology to the SSPS Concept," AIAA/AAS Solar Energy for Earth Conference, #75-642, April 1975.

[4] Nalos, E.J., "New Developments in Electromagnetic Energy Beaming," Proc. IEEE, Vol. 66, No. 3, March 1978.

[5] Borgiotti, G.V., "Design of Circular Apertures for High Beam Efficiency and Low Sidelobes," Alta Frequenza, Vol. XL, 1971.

[6] Borgiotti, G.V., "Maximum Power Transfer Between Two Planar Apertures in the Fresnel Zone," Vol. AP-14, No. 2, March 1966.

[7] Sherman, J.W., "Properties of Focused Apertures in the Fresnel Region," Vol. AP- , July 1962.

[8] Barton, D.K. and H.R. Ward, "Handbook of Radar Measurement," Prentice-Hall, 1969.

[9] Kay, A.F., "Near Field of Aperture Antennas, Vol. AP- , November 1960.

[10] Goubau, G., "Microwave Power Transmission," Journal of Microwave Power, Vol. 5, No. 4, 1970.

[11] Young, L., "Advances in Microwaves," Academic Press, Vol. 3, 1969.

[12] Maynard, O., "Microwave Power Transmission System Studies," NASA CR-134886, December 1975.

APPENDIX C
SINGLE STEP TAPER

The objective of investigating the single step taper was to reduce spacetenna pattern sidelobes. Reduction of the first sidelobe would result in requiring less real estate at the fenced-in rectenna site and reduction of the second and other sidelobes would demonstrate that power densities lower than 0.1 mW/cm^2 were achievable outside the fenced-in area.

The single step taper illuminaton is illustrated in Figure C-1. This is considered to be a practical illumination which can be implemented using active elements operating at two different power levels.

The step taper illumination has been designed so that the power density at the center of the spacetenna aperture and power density at the peak of the beam are equal to those obtained with uniform illumination. This requires an increase in aperture diameter ($2k_2a$) to offset the step in aperture voltage (C); the inner diameter of the step being $2k_1a$.

By equating the power at the beam peak for the uniform and step taper cases, the illumination parameters are related as follows:

$$k_2 = \left[\frac{1 - k_1^2(1 - C)}{C} \right]^{1/2} \qquad (C\text{-}1)$$

$$k_1 = \left[\frac{1 - k_2^2 C}{1 - C} \right]^{1/2}$$

For example, if C = 0.4 and k_1 = 0.8, then k_2 = 1.24 which results in a 24% increase in aperture diameter. This is derived as follows:

Uniform:

$$E_u(o) = \pi a^2 \qquad (C\text{-}2)$$

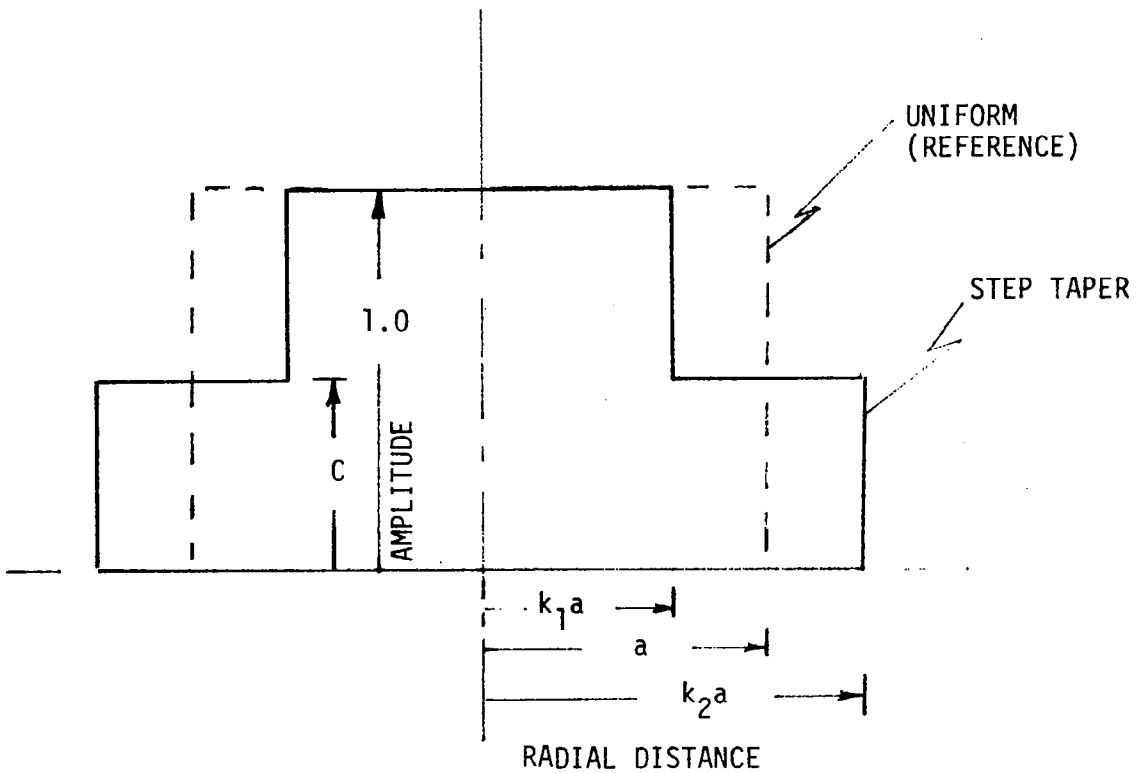

Figure C-1 Spacetenna Step-Taper Aperture Illumination

Step:

$$E(o) \int_0^{k_2 a} \int_0^{2\pi} C \, r dr d\psi = \int_0^{k_1 a} \int_0^{2\pi} (1 - C) \, r dr d\psi \tag{C-3}$$

$$E_s(o) = \pi(k_2 a)^2 C + \pi(k_1 a)^2 (1 - C) \tag{C-4}$$

when $E_u(o) = E_s(o)$,

$$1 = k_2^2 C + k_1^2 (1 - C) \tag{C-5}$$

and Equation (C-1) is obtained.

The far field pattern for a uniformly illuminated circular aperture

$$E(u) = \frac{2 J_1(u)}{u} \tag{C-6}$$

and the corresponding patterns for the single step taper are obtained by superimposing uniform illumination patterns of the step of amplitude C and the step of amplitude 1 - C with the following results:

$$E(u) = 2 \left[k_2^2 C \frac{J_1(u_2)}{(u_2)} + 1 - C \, k_1^2 \frac{J_1(u_1)}{u_1} \right] \tag{C-7}$$

where

$$u = \frac{2 \pi a}{\lambda} \sin \theta \tag{C-8}$$

$$u_1 = k_1 u \tag{C-9}$$

$$u_2 = k_2 u \tag{C-10}$$

When $C = 1$, $k_2 = 1$ then Equation (C-7) is the pattern of a uniformly illuminated circular aperture, as shown in Figure C-2.

Examples of the patterns obtained by stepping the illumination under the above constraints are shown in Figure C-3. Here power steps of 1/3 and 1/4

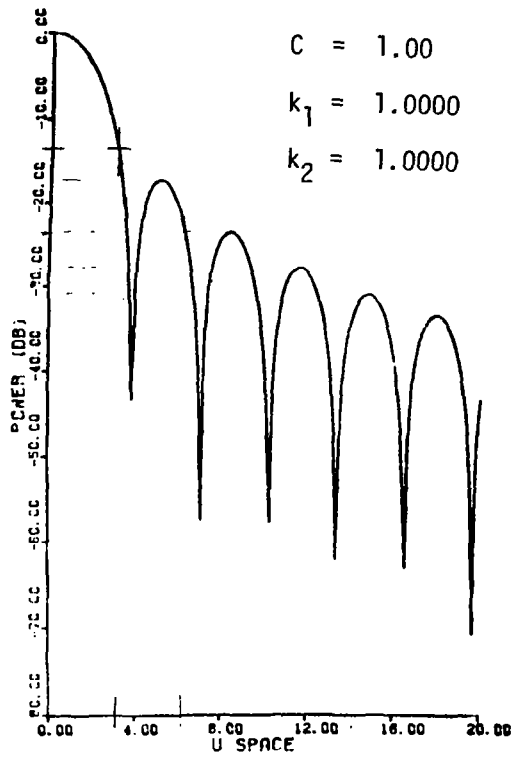

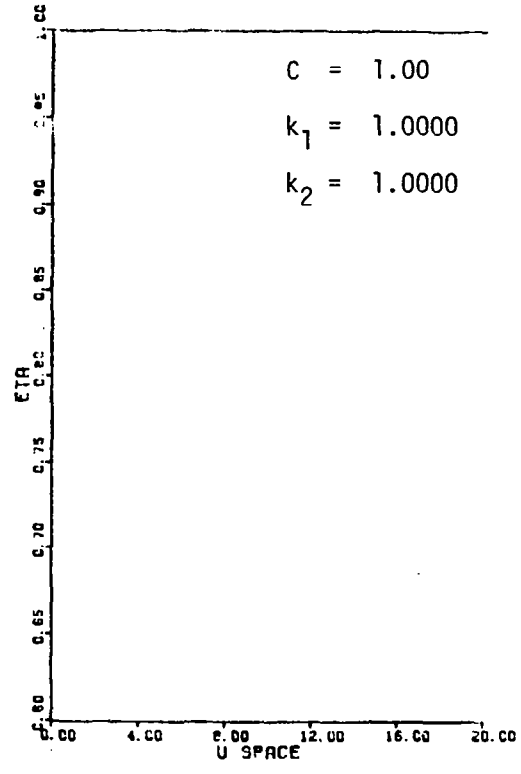

Figure C-2 Antenna Pattern - Uniform Illumination

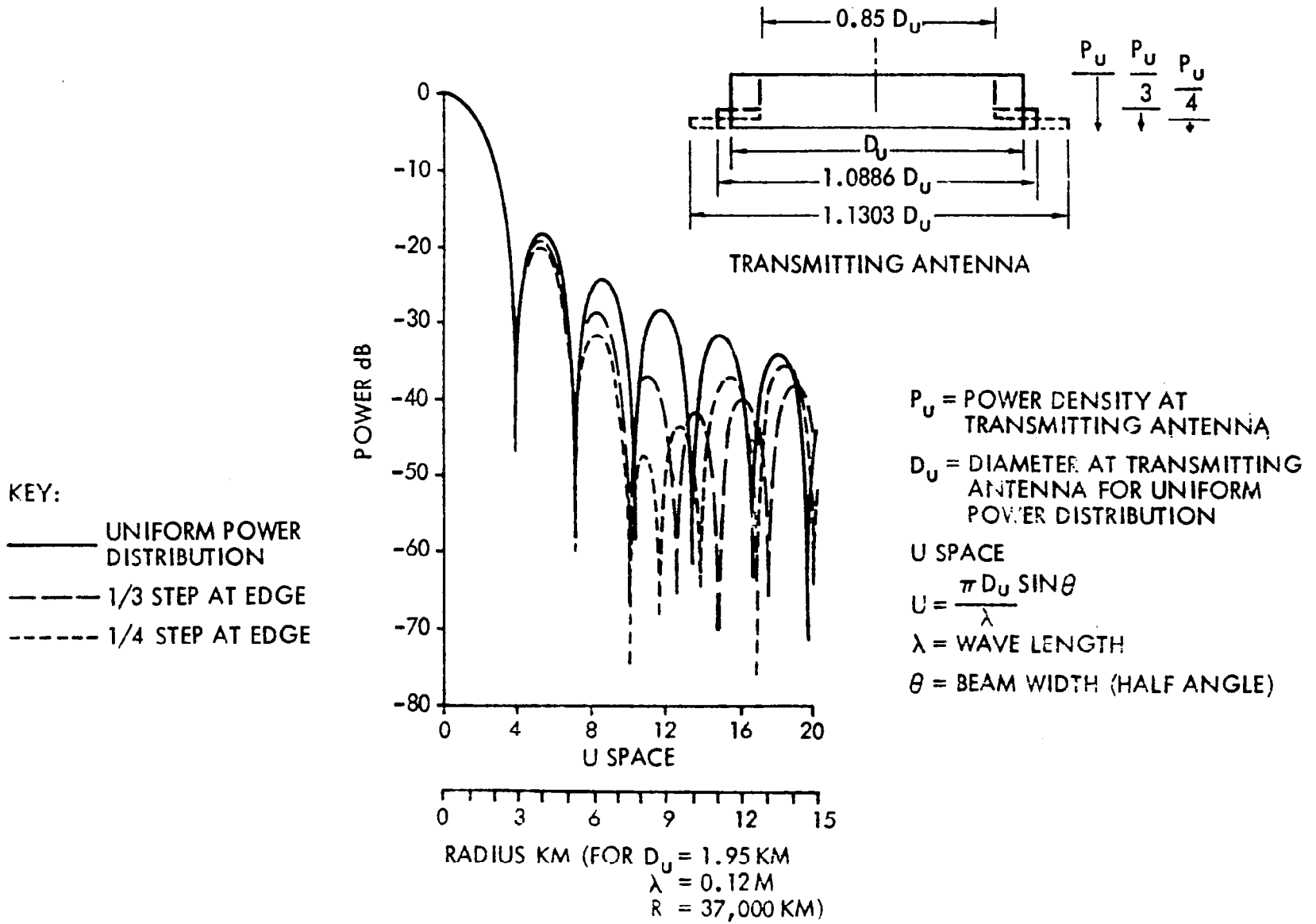

Figure C-3 Sidelobe Comparison of Uniform Power Distribution With Two Examples of Single Step Edge Taper

(.58 and .5 voltage) result in significant second sidelobe reduction (between 5 and 10 dB) with a resulting increase in aperture size of between 8.9% and 13%.

The lower power region of the spacetenna diameter has excess potential solar cell area which can be used to provide power for inboard active elements. The thermal and power distribution considerations that permit this redistribution of power are discussed in Sections 6 and 8.

Another characteristic of the single step taper is that it results in a reduction in available power as compared to the uniform case as follows:

$$\frac{P_{TT}}{P_{TU}} = k_1^2(1 - C^2) + C^2k_2^2 \qquad \text{(C-11)}$$

where

P_{TT} = Total transmitted power in the tapered case;

P_{TU} = Total transmitted power in the untapered case.

The results of applying this formula are shown in Figure C-4 where the available power ratio is plotted versus the spacetenna diameter ratio for various amplitude steps. For the cases shown in Figure C-3 the available power is 91% for the 1/3 power step and 85% for the 1/4 power step as compared to that available for uniform illumination.

Formula (C-12) for the available power has been derived by integrating the power in the circular aperture:

$$P = \int_0^{k_1 a} \int_0^{2\pi} (1)^2 \, r dr d\psi + \int_0^{k_2 a} \int_0^{2\pi} C^2 \, r dr d\psi \qquad \text{(C-12)}$$

The remaining pattern characteristic to be evaluated is beam efficiency. This has been computed relative to the uniform case. The power collected for uniform illumination versus pattern angle is determined from the beam efficiency

$$\eta_u = \frac{\int_0^{w'} \left(2 \, \frac{J_1(w)}{w} \right)^2 w dw}{P_{AV}} \qquad \text{(C-13)}$$

where $w = (2\pi a/\lambda) \sin\theta$ and $P_{vu} = \pi a^2$ is the power available for 1 volt amplitude.

The uniform illumination far field pattern is

$$E(w) = 2\pi a^2 \frac{J_1(w)}{w} \tag{C-14}$$

The power collected for the step taper case relative to uniform is determined from the step taper beam efficiency,

$$\eta_s = \frac{4 \int_0^{w'} \left[\frac{k_2^2 \, C \, J_1(w_2)}{w_2} + \frac{(1 - C) \, K_1^2 \, J_1(w_1)}{w_1} \right]^2 wdw}{P_{vu}} \tag{C-15}$$

where $w_1 = k_1 w$ and $w_2 = k_2 w$.

The relative efficiency of the step taper case is

$$\eta_{sr} = \frac{\eta_s}{\eta_u} = \frac{\int_0^{w'} \left[\frac{k_2^2 \, C \, J_1(w_2)}{w_2} + \frac{(1 - C) k_1^2 \, J_1(w_1)}{w_1} \right]^2 wdw}{\int_0^{w'} \left(\frac{J_1(w)}{w} \right)^2 wdw} \tag{C-16}$$

and w' ranges from 0 to $\pm$ 20.

The numerator approaches the power available ratio in the limit as plotted in Figure C-4.

The antenna patterns and relative efficiency ratio have been plotted for voltage step ratios between .2 and .8 over a range of spacetenna diameter ratios from 1 to 1.6 as shown in Figure C-5.

Sidelobe envelopes and efficiency η_{TA} are presented in Figures C-6 , C-7 and C-8 for power tapers of .04, .09 and .16 respectively.

Figure C-9 shows the efficiency η_{TA} due to the step-tapered aperture power distribution. For uniform power distribution the first sidelobe is at -17.4 dB. The dotted curve shows the combinations of C^2 and k_2 to reduce the first sidelobe to -23.6 dB, thus eliminating the need for fences out of the main lobe. There

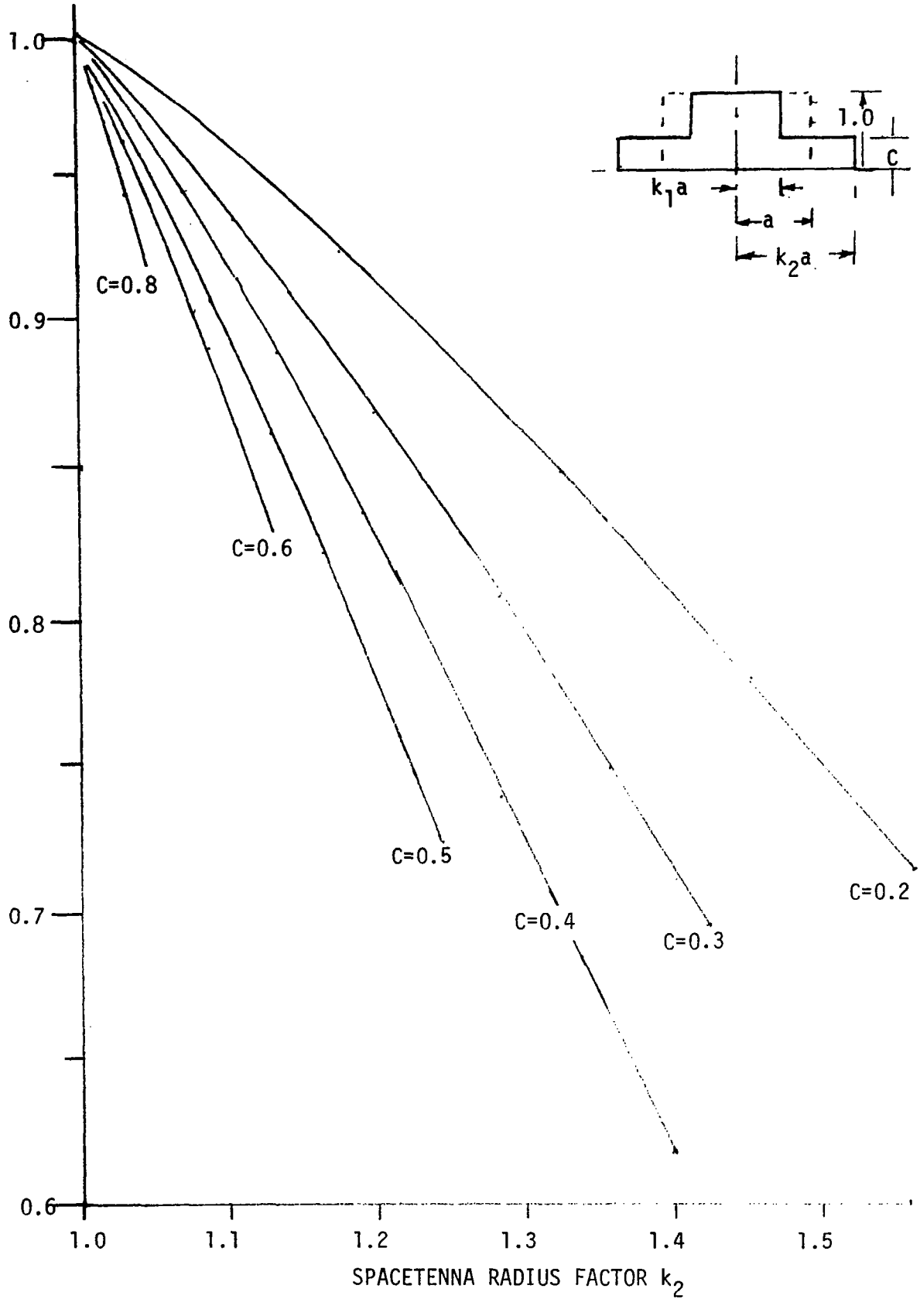

Figure C-4 Step Taper Power Ratio Vs Radius Factor

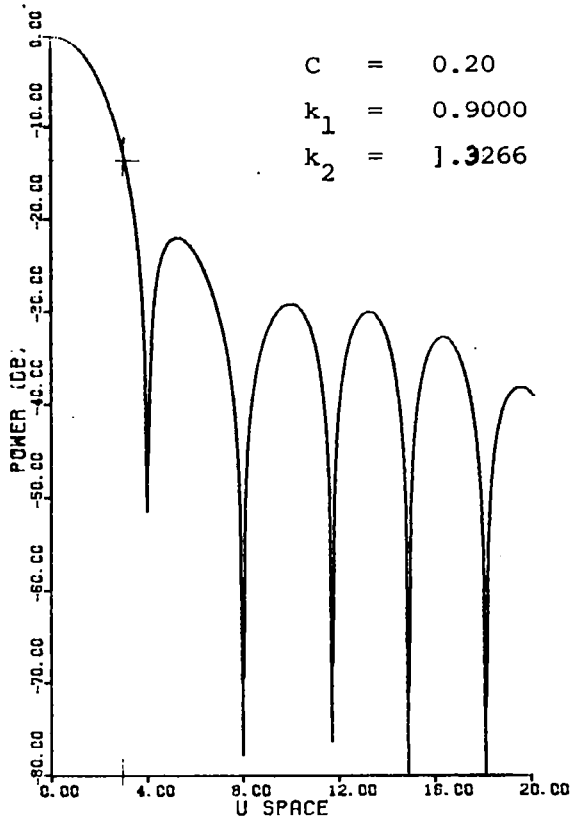

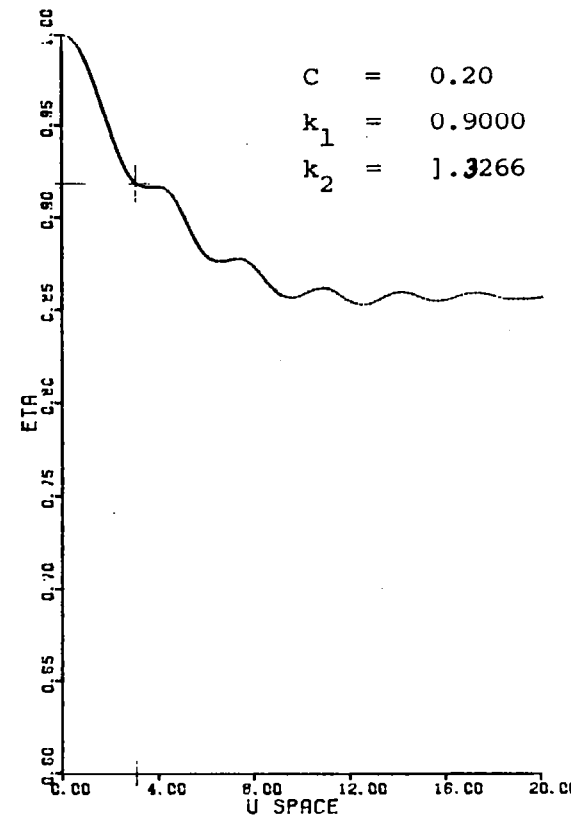

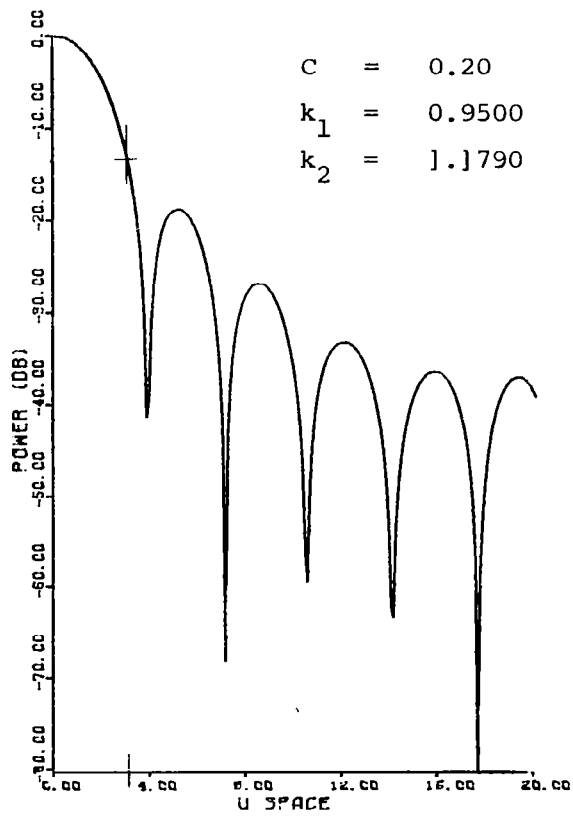

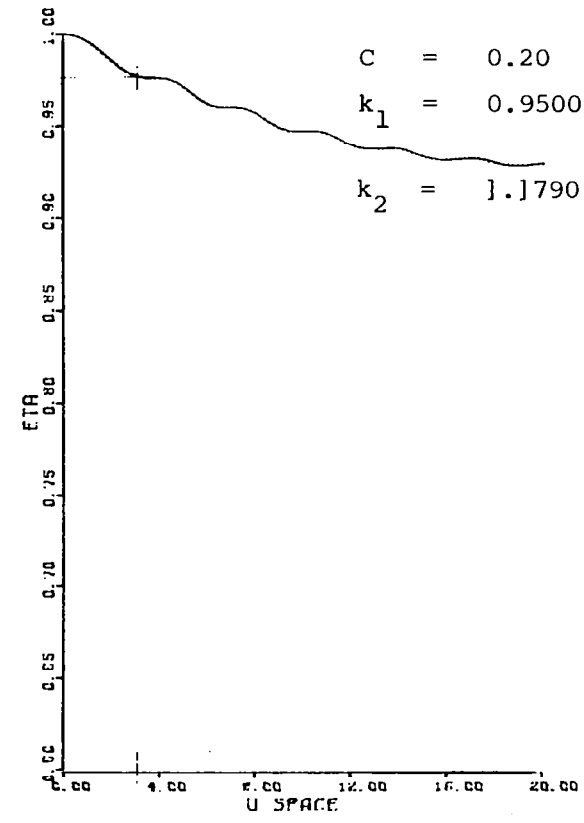

Figure C-5 Near-In Sidelobe and Relative Efficiency Data

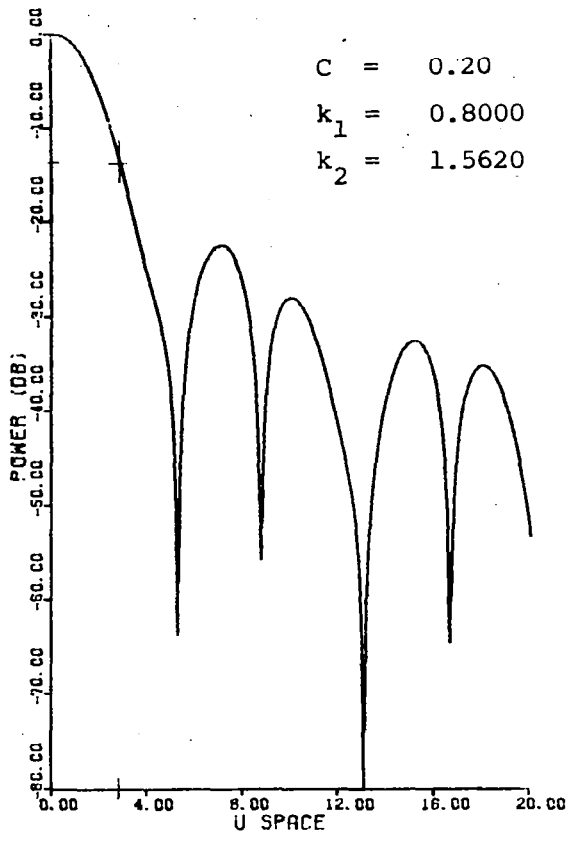

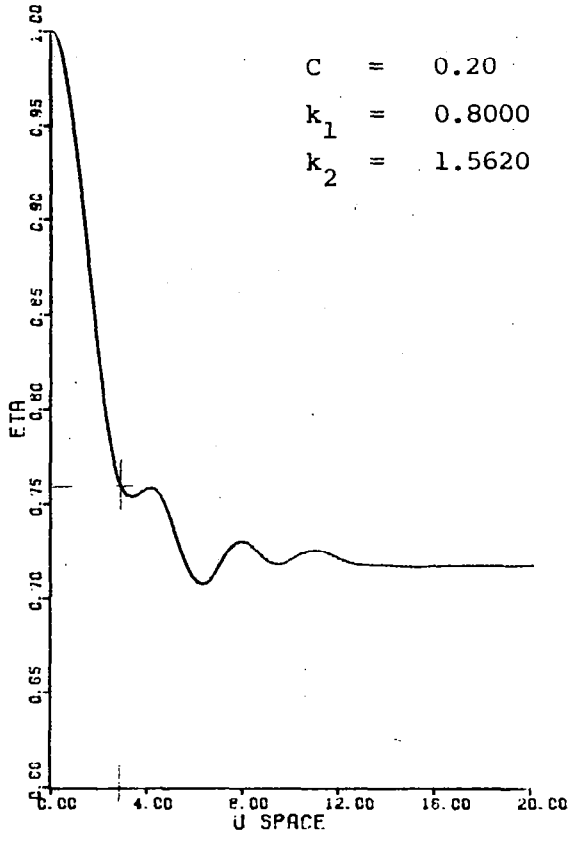

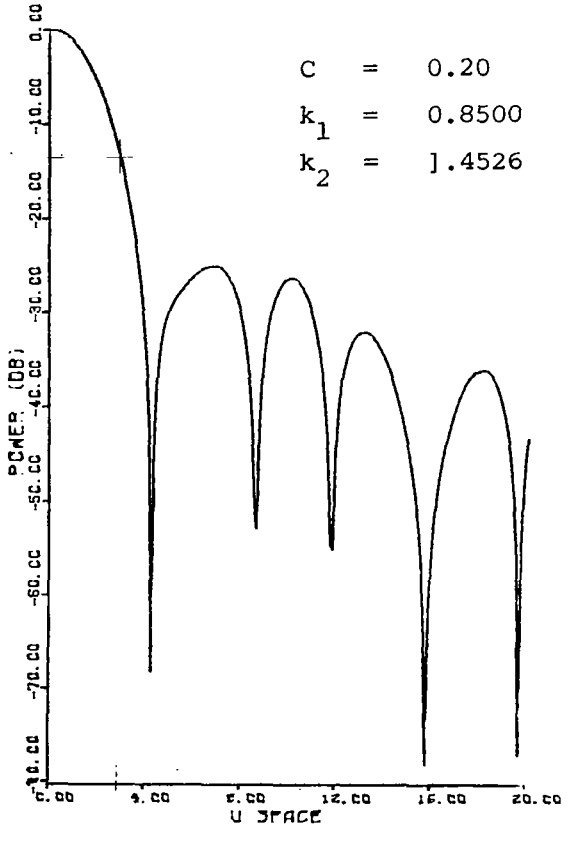

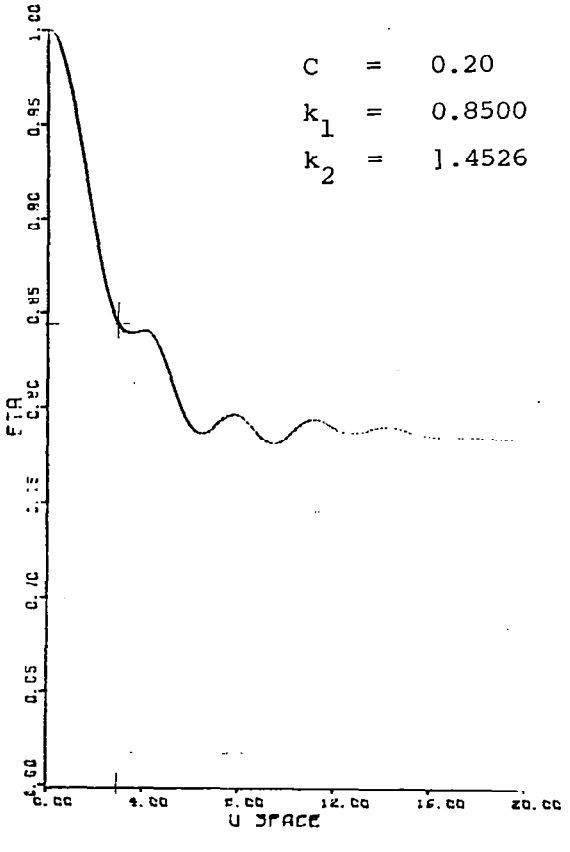

Figure C-5 -- Continued

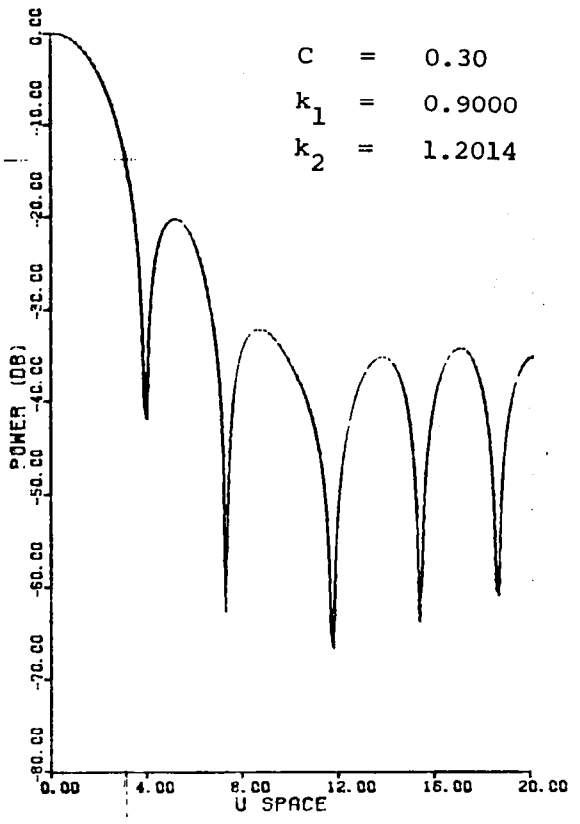

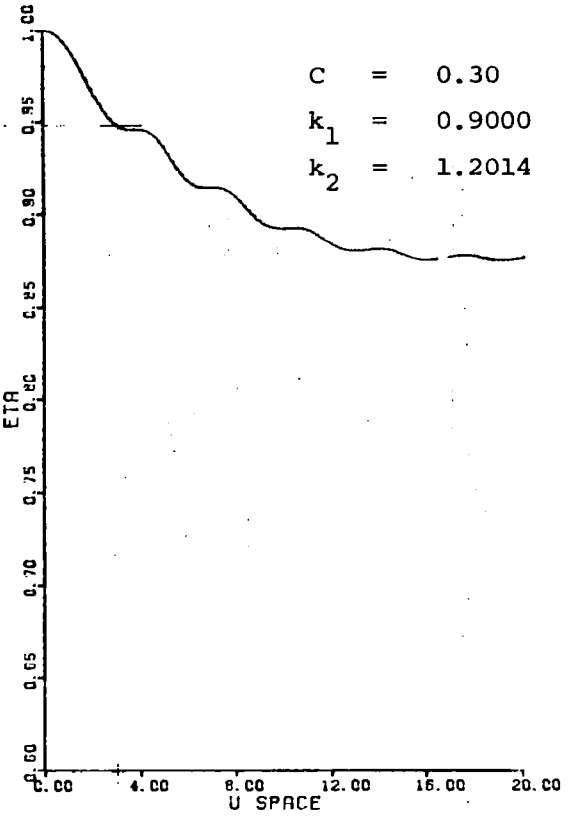

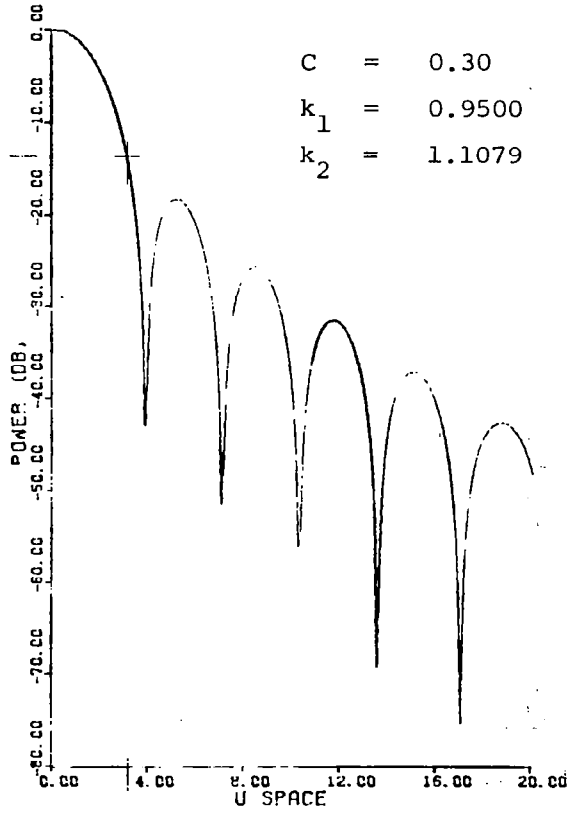

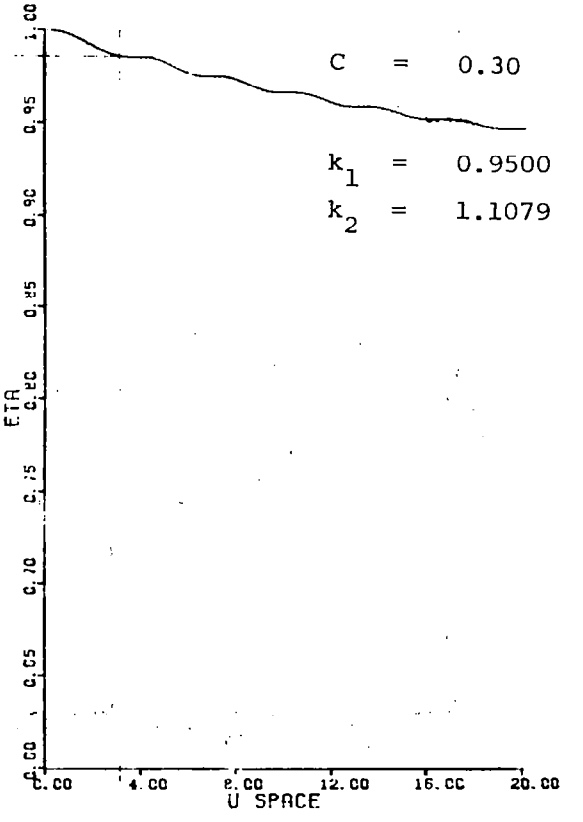

Figure C-5 -- Continued

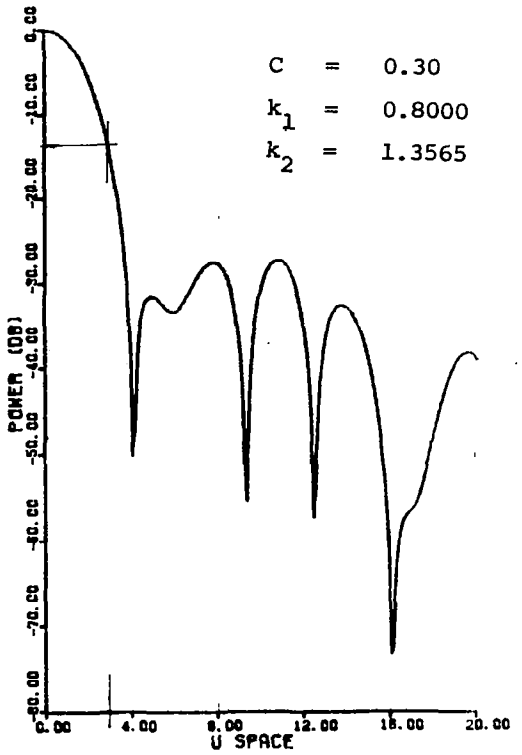

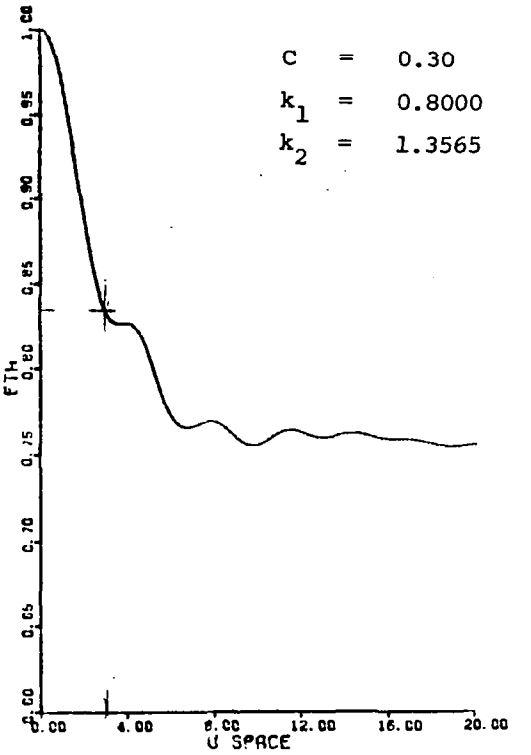

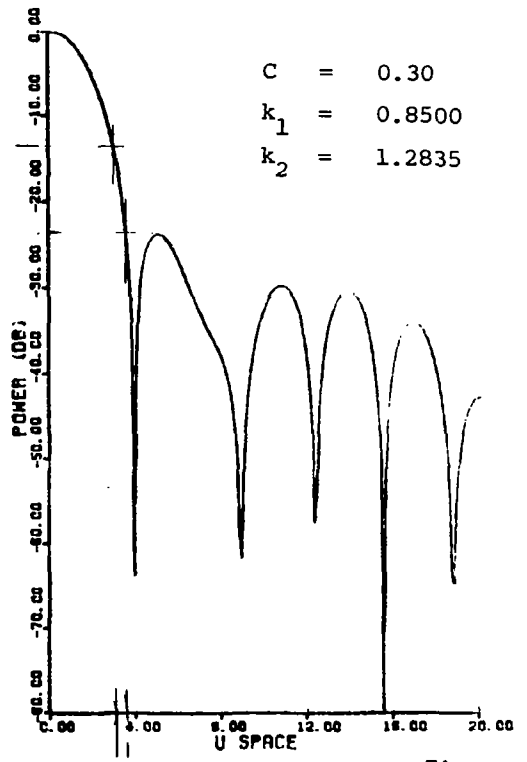

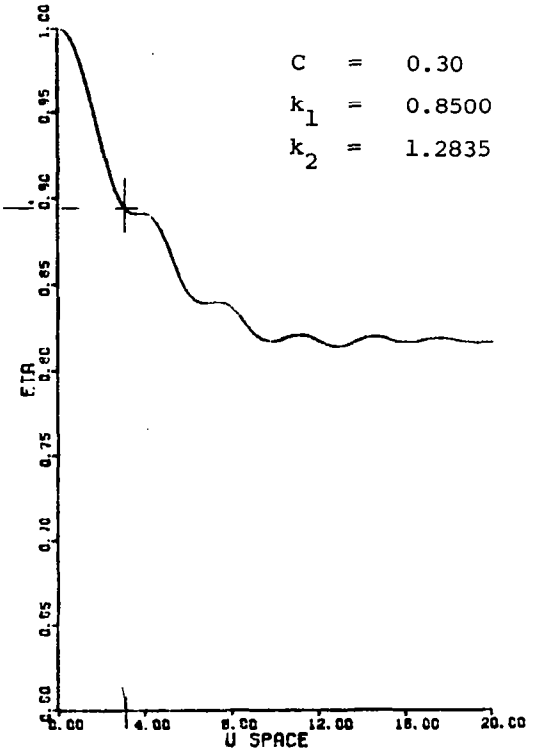

Figure C-5 -- Continued

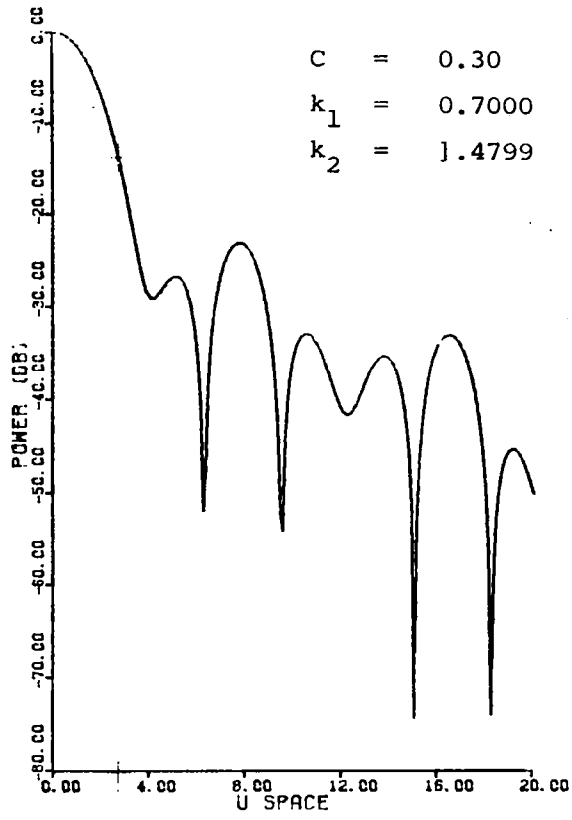

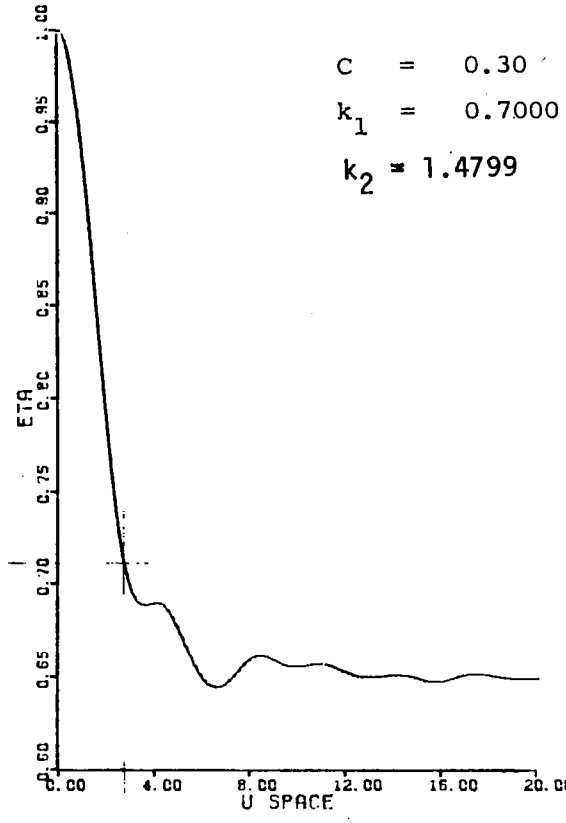

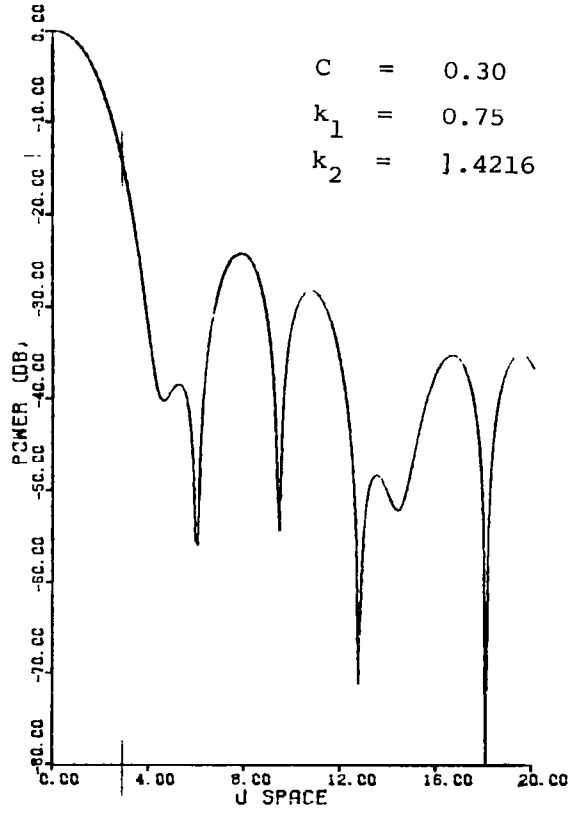

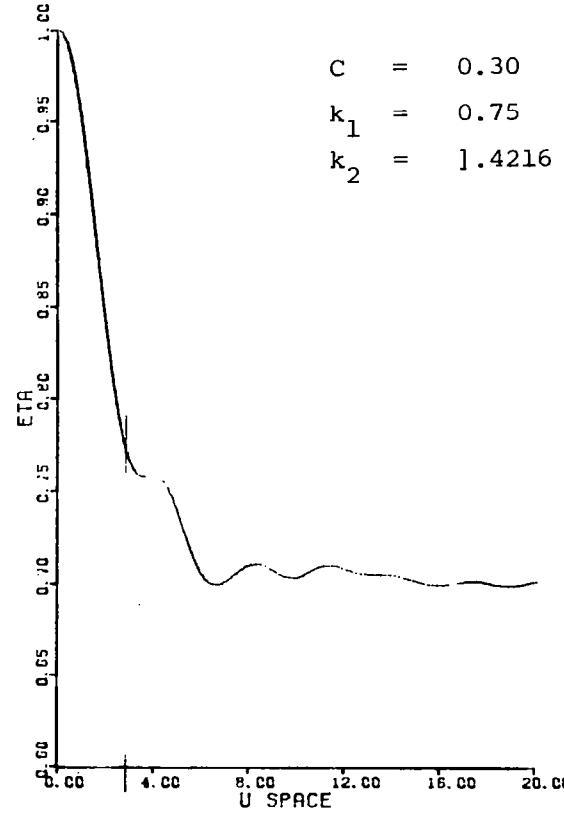

Figure C-5 -- Continued

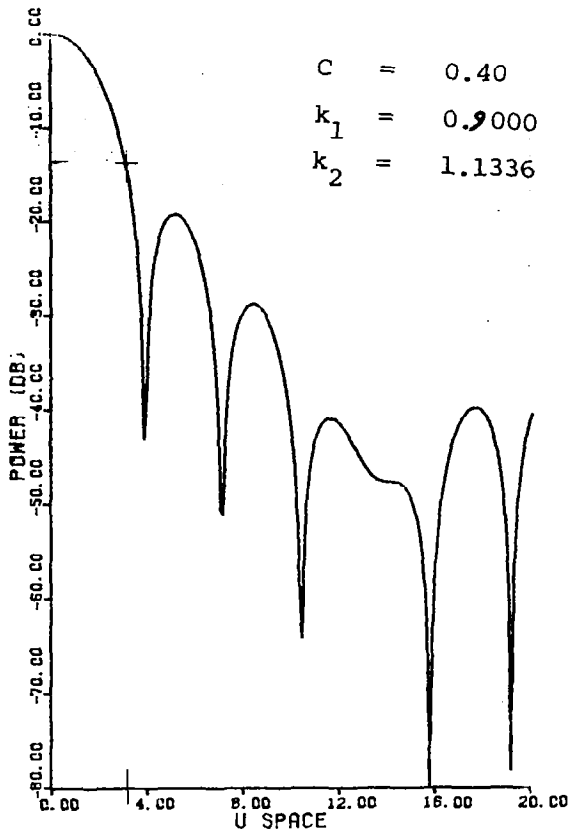

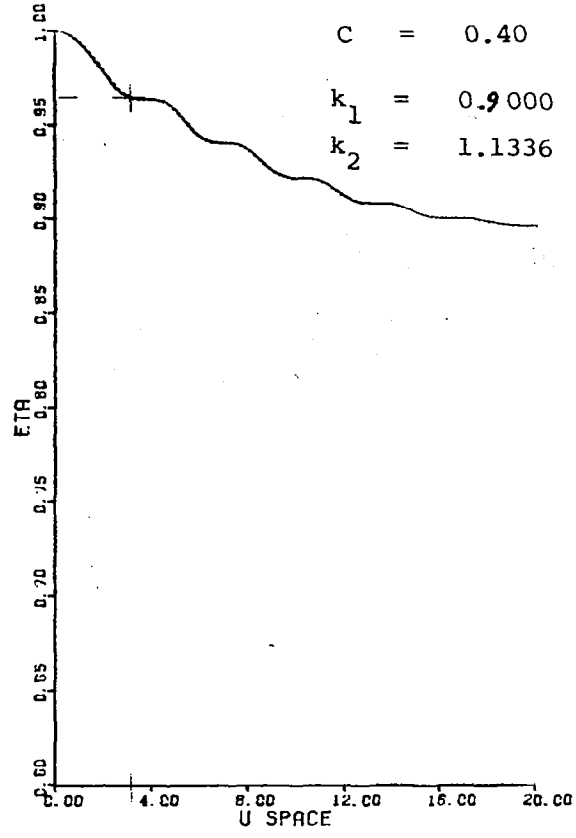

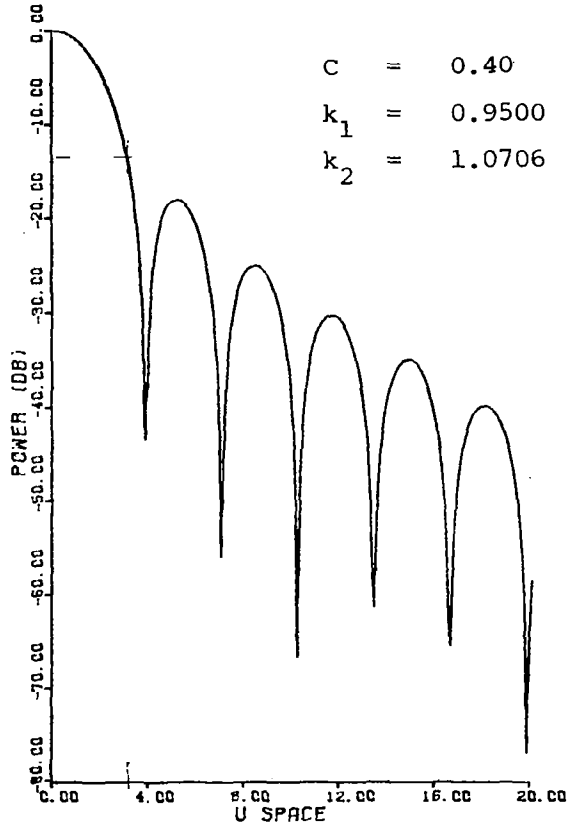

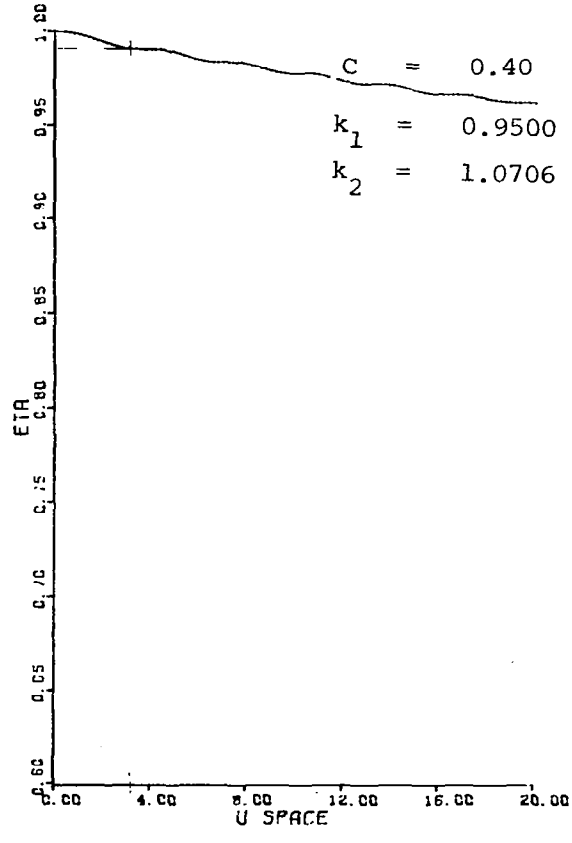

Figure C-5 -- Continued

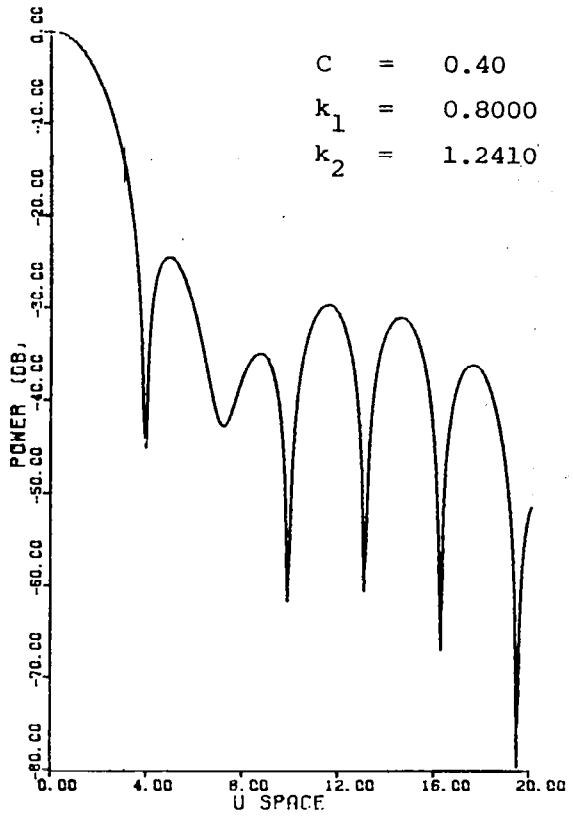

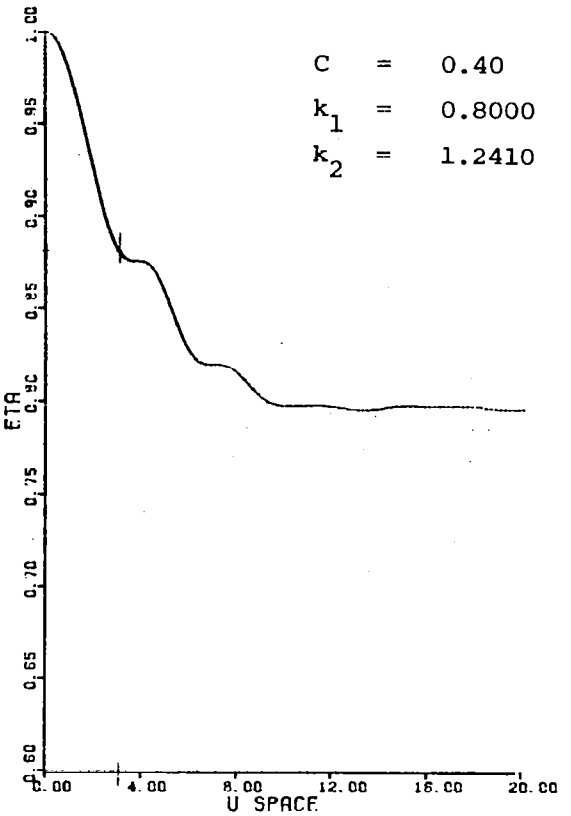

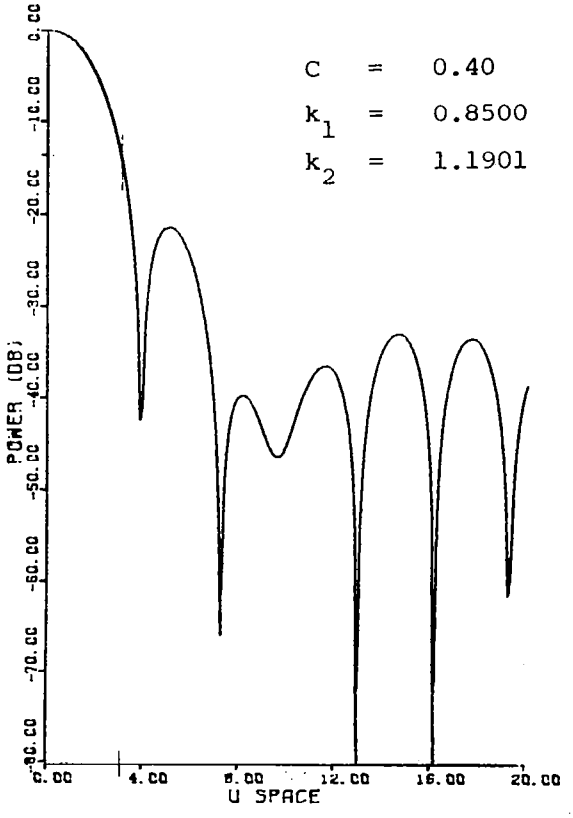

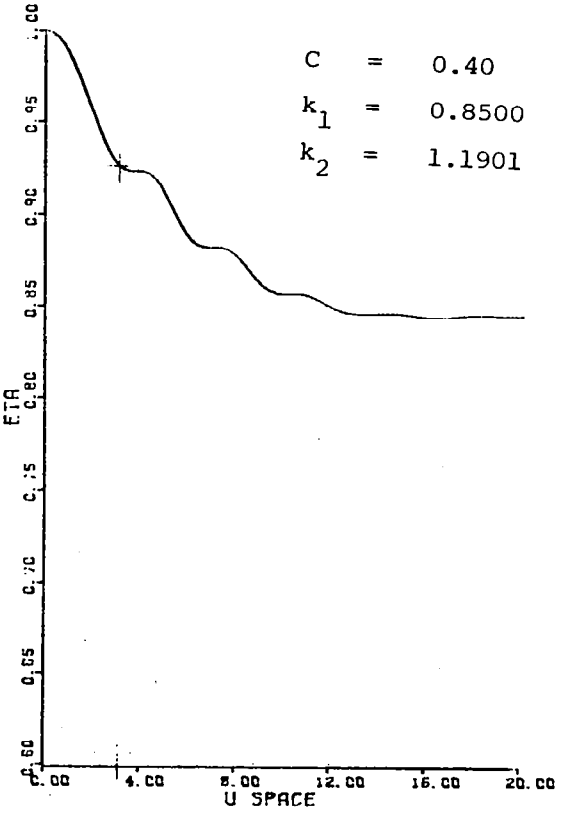

Figure C-5 -- Continued

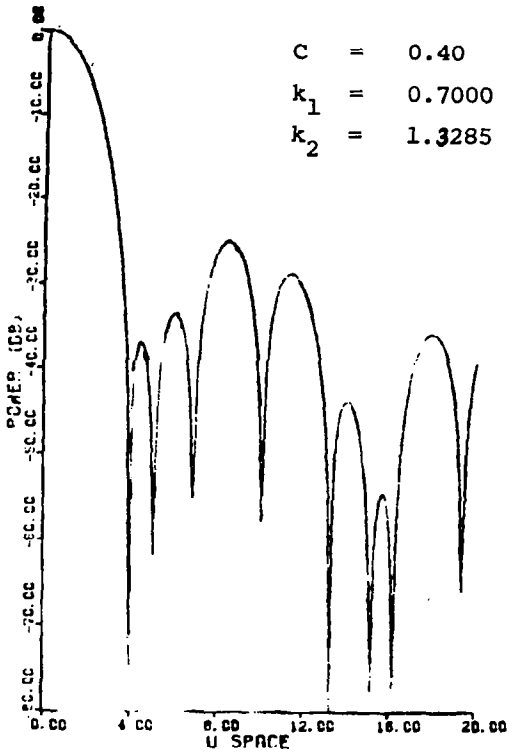

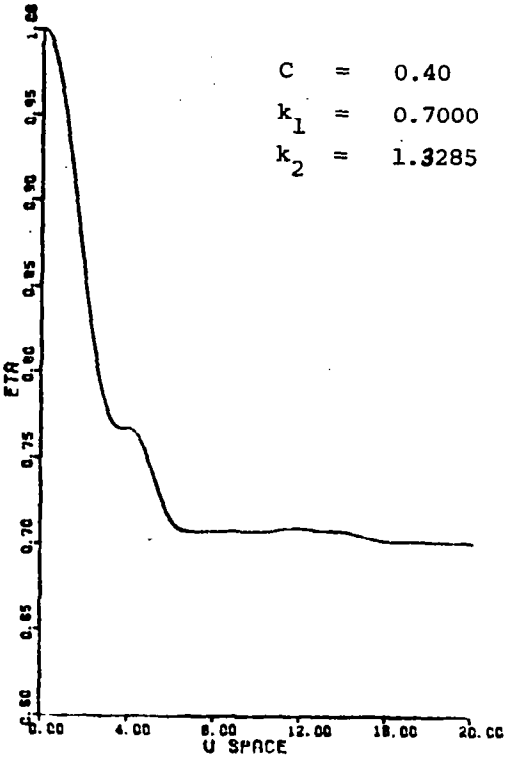

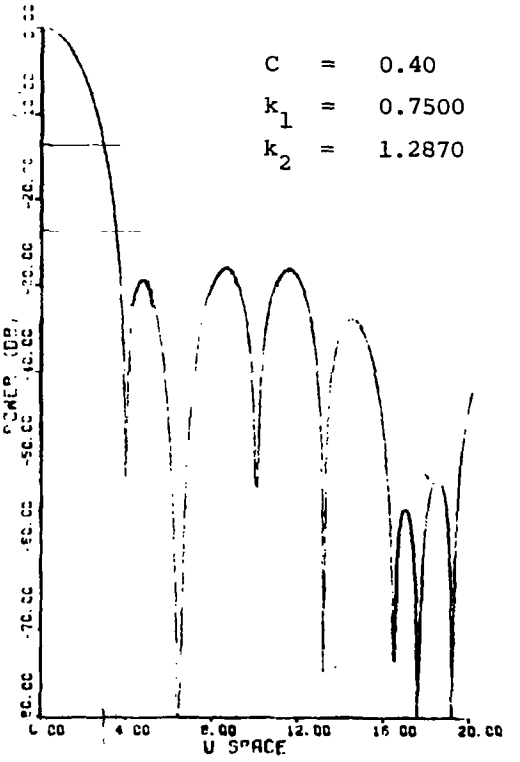

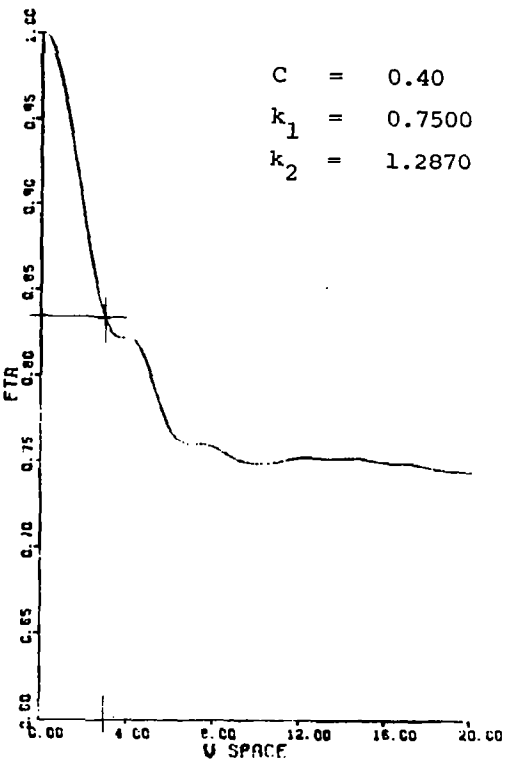

Figure C-5 -- Continued

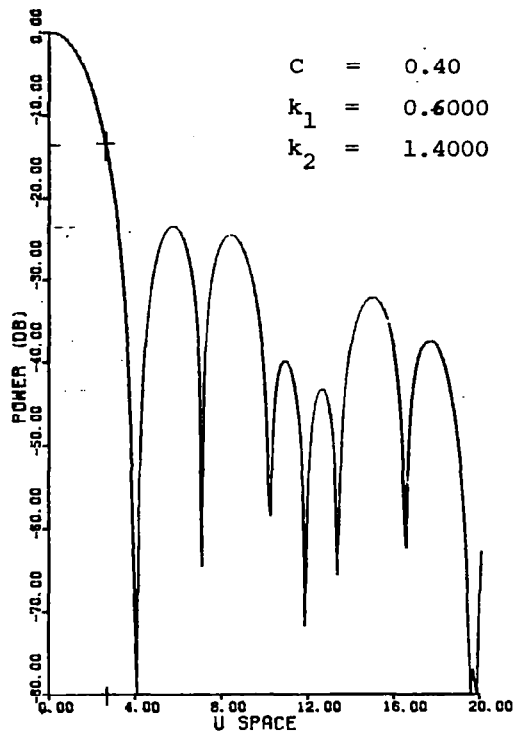

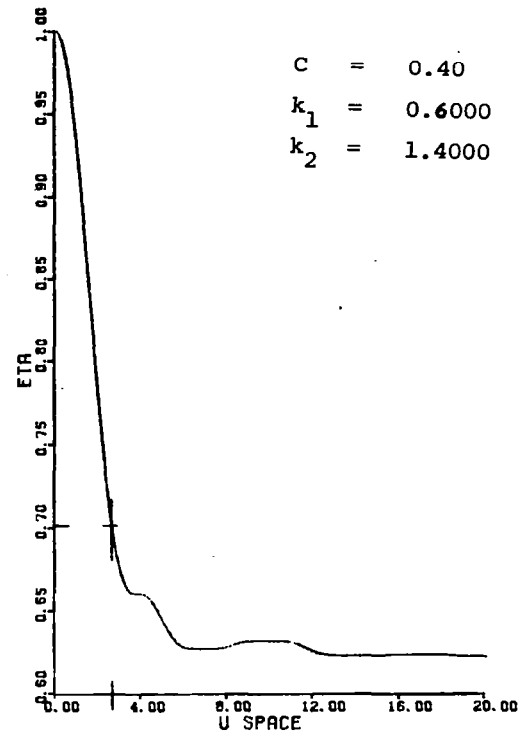

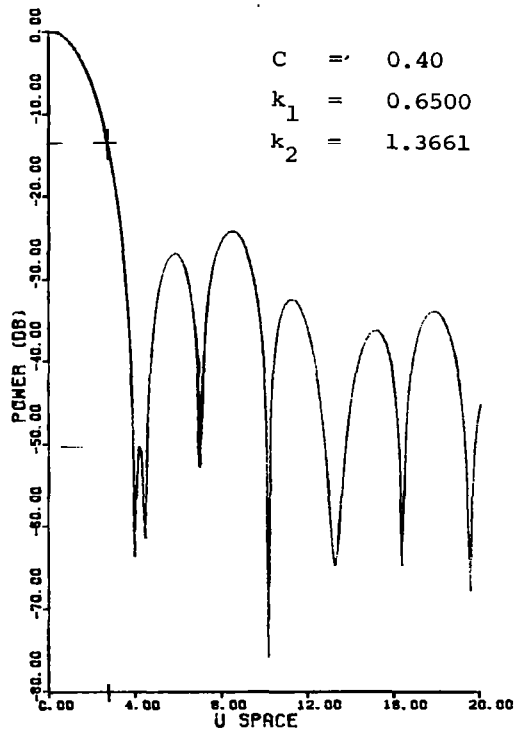

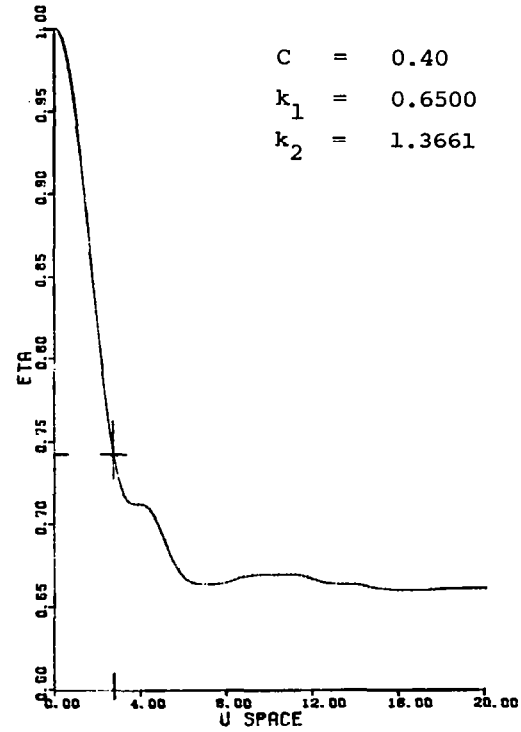

Figure C-5 -- Continued

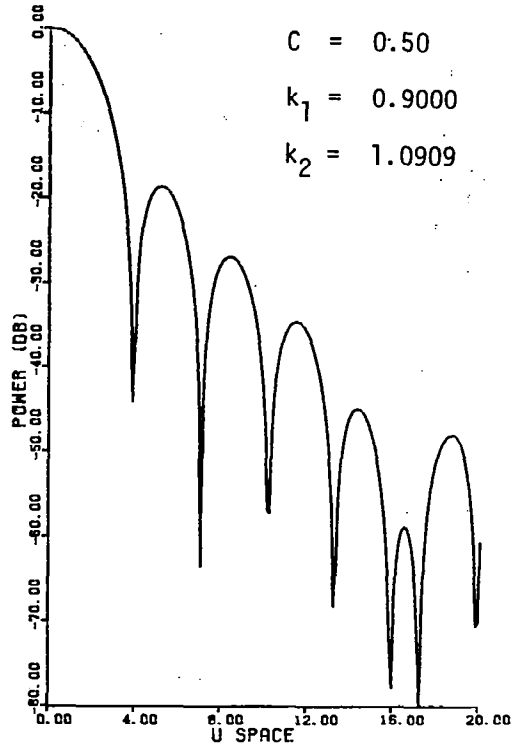

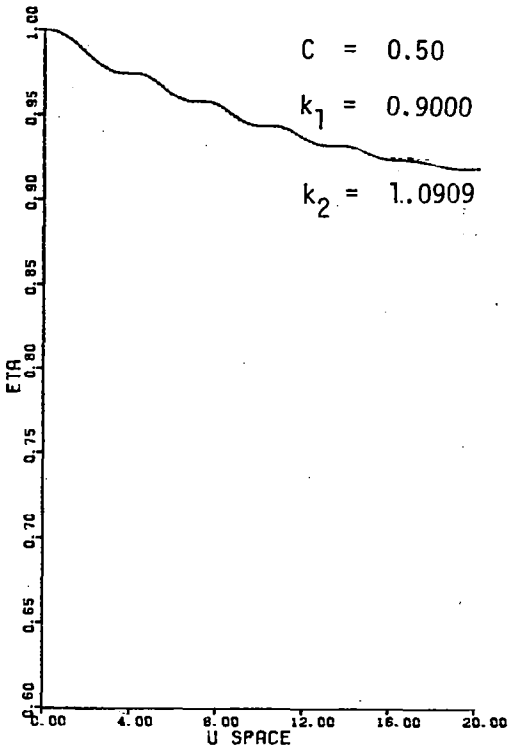

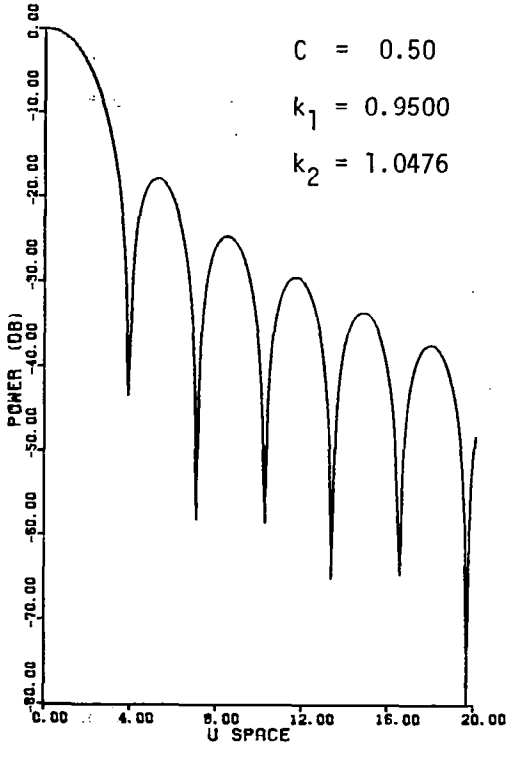

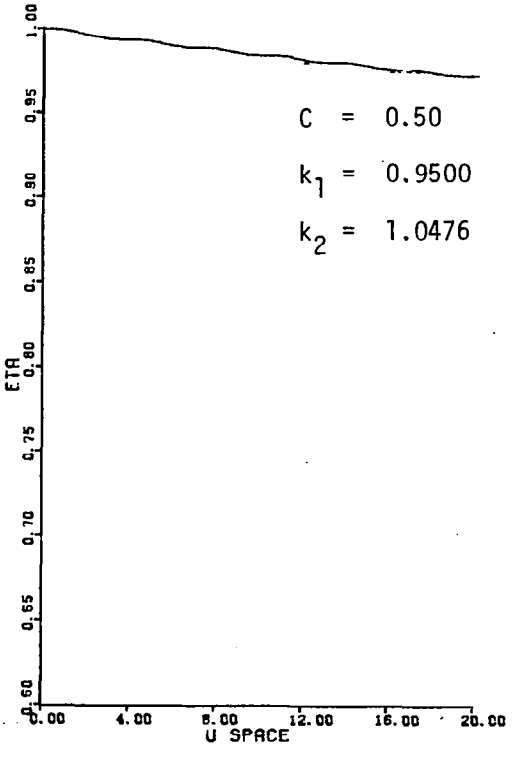

Figure C-5 -- Continued

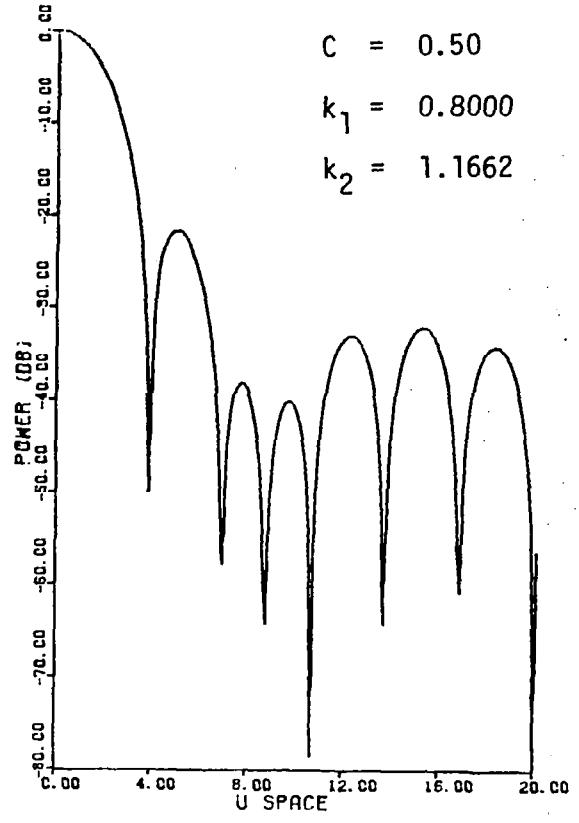

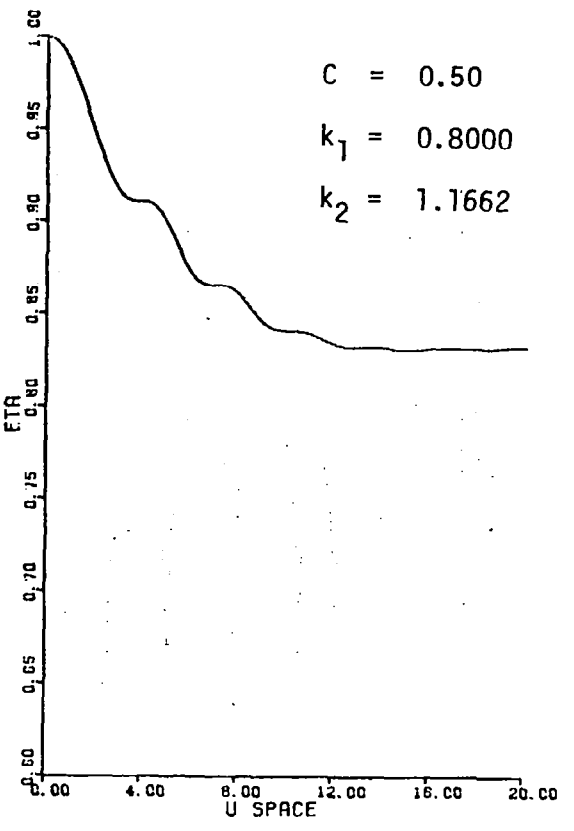

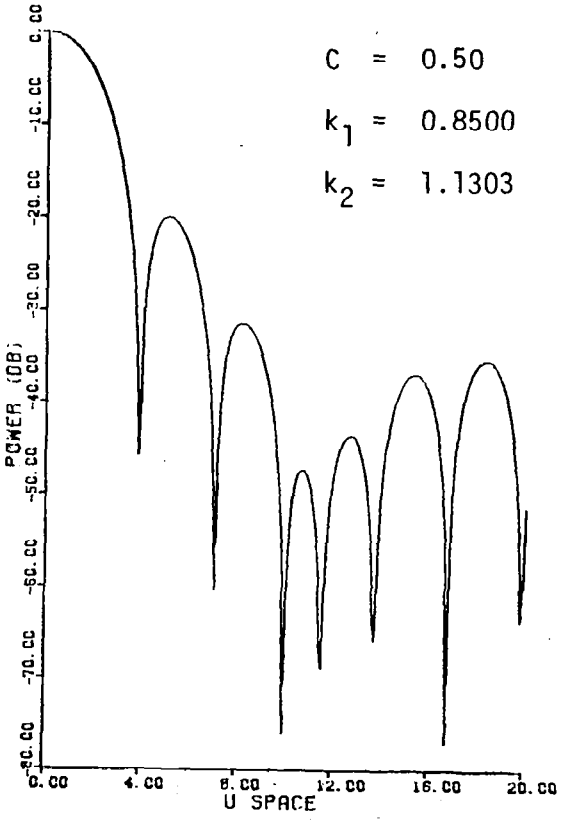

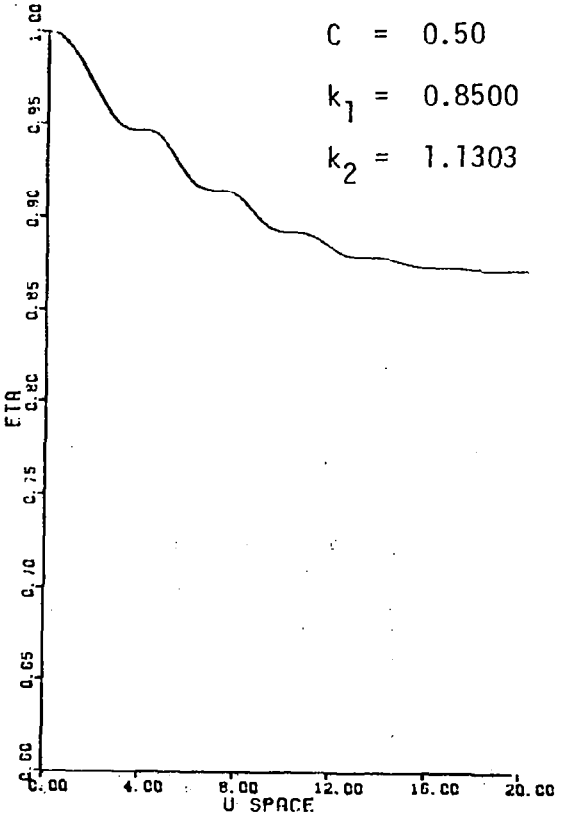

Figure C-5 -- Continued

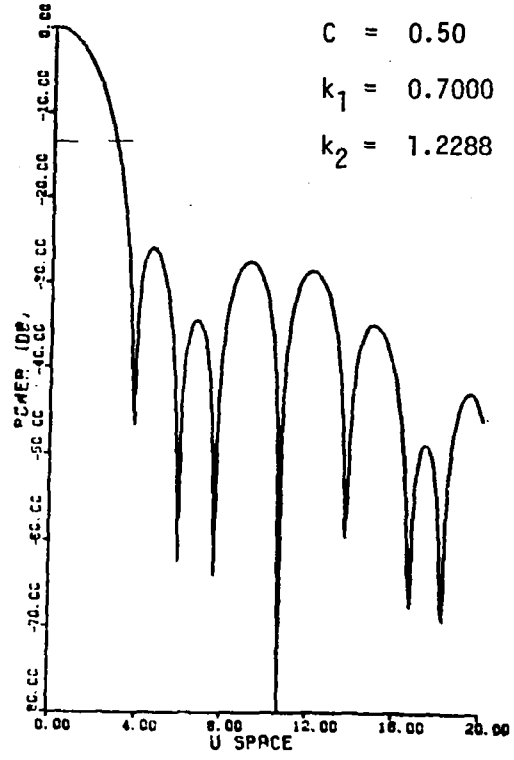

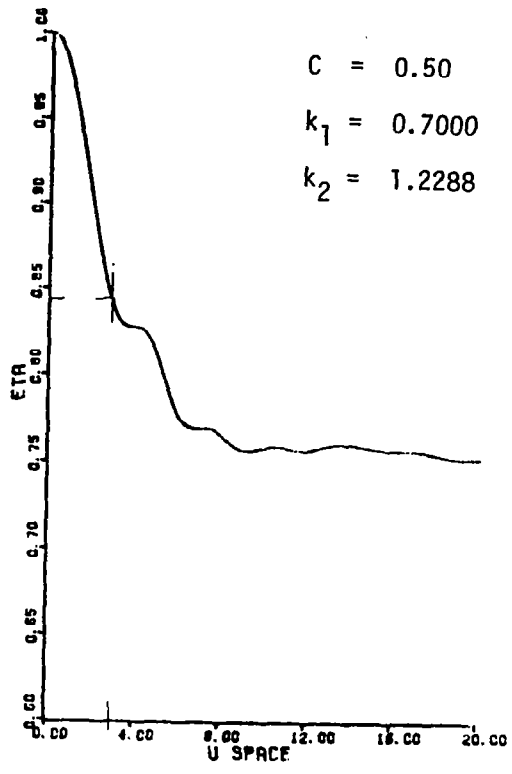

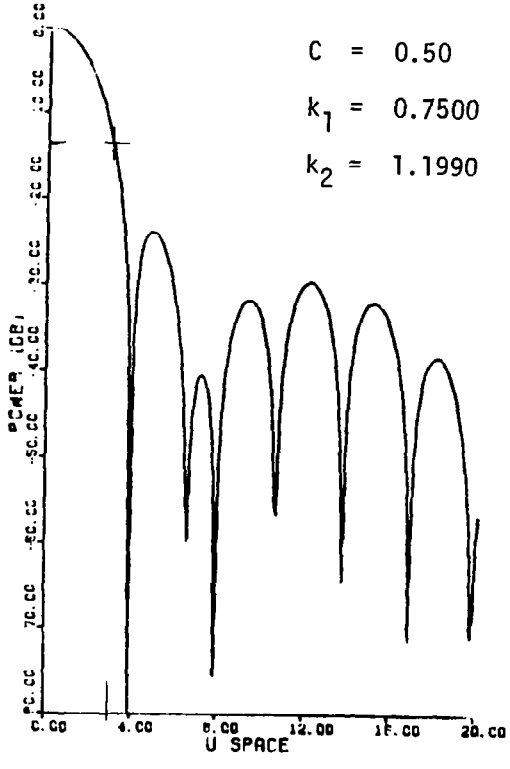

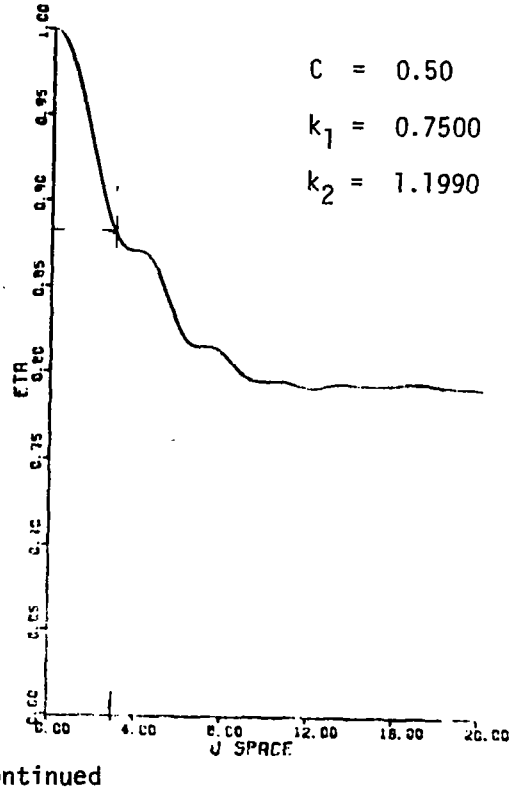

Figure C-5 -- Continued

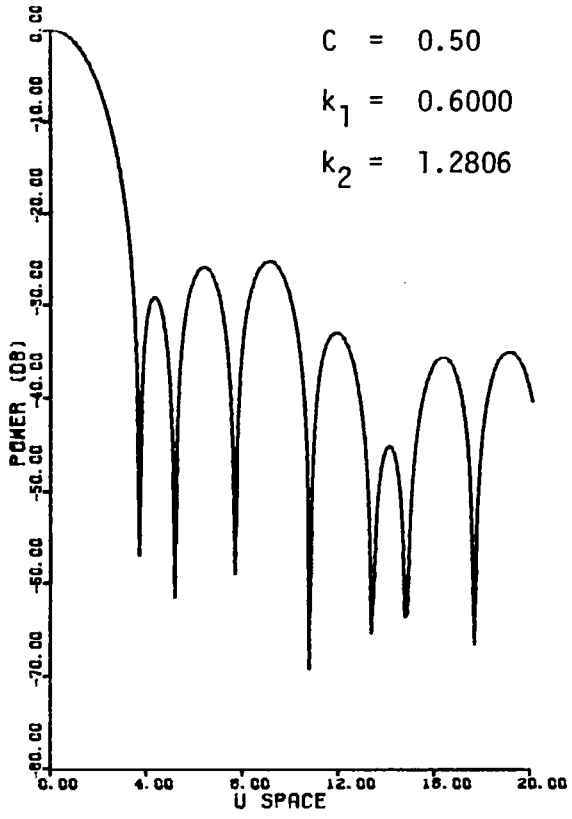

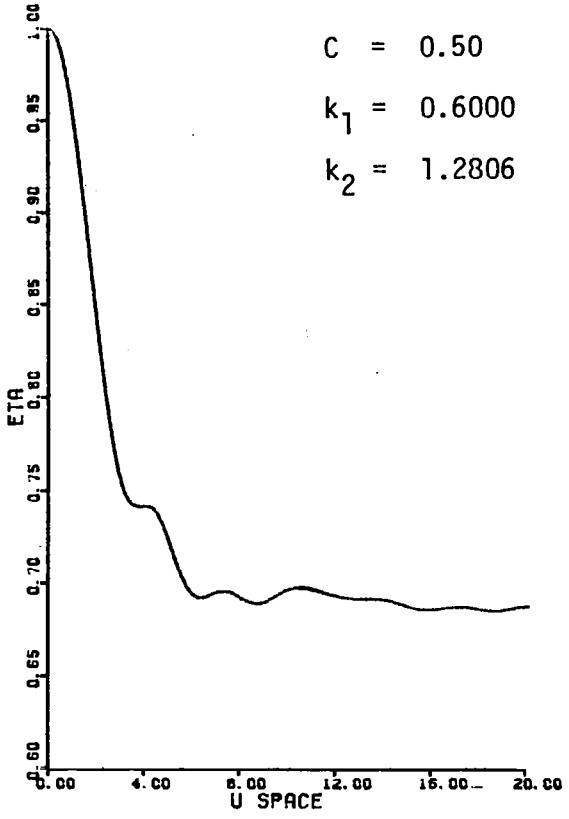

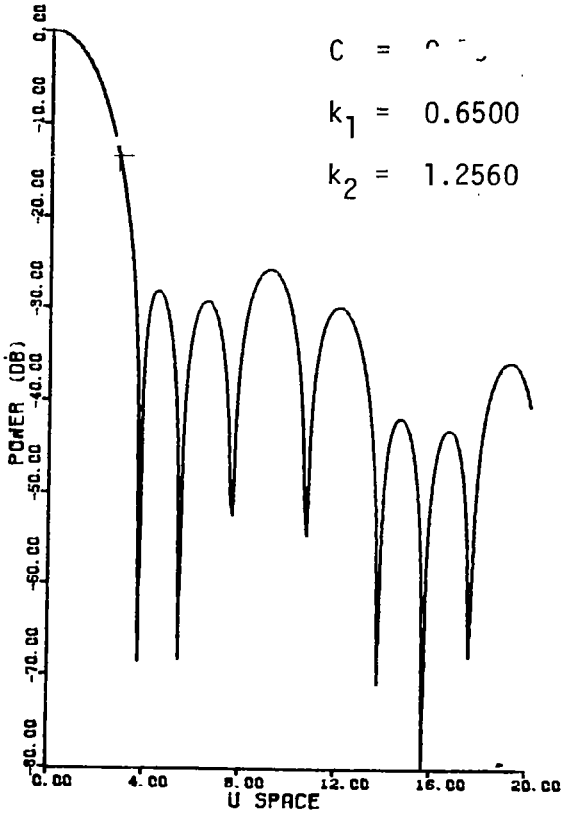

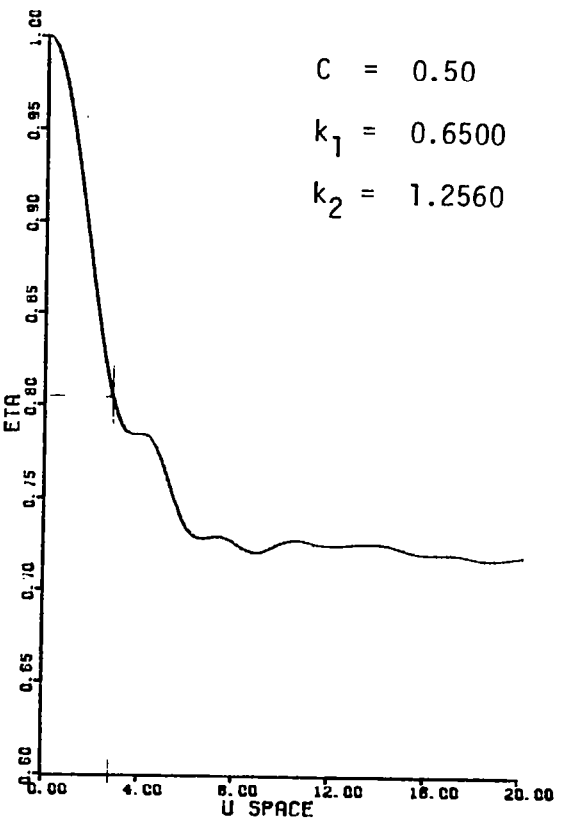

Figure C-5 -- Continued

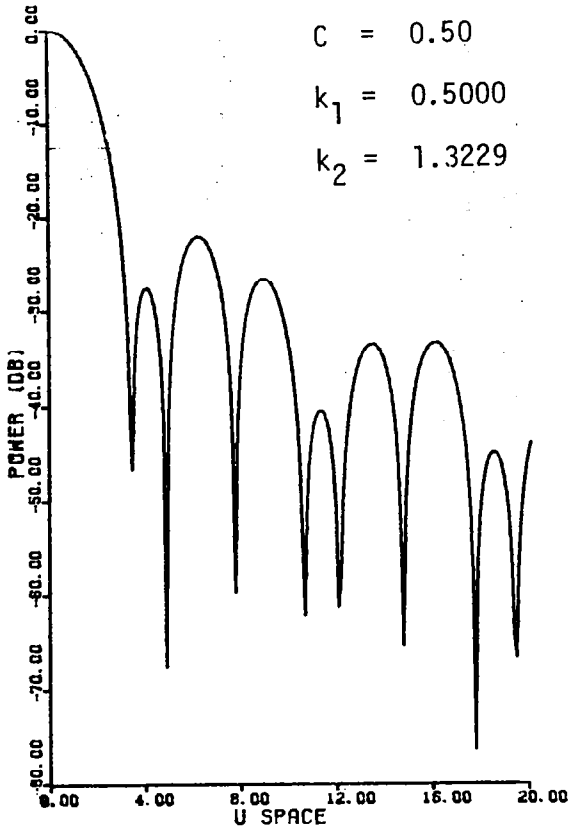

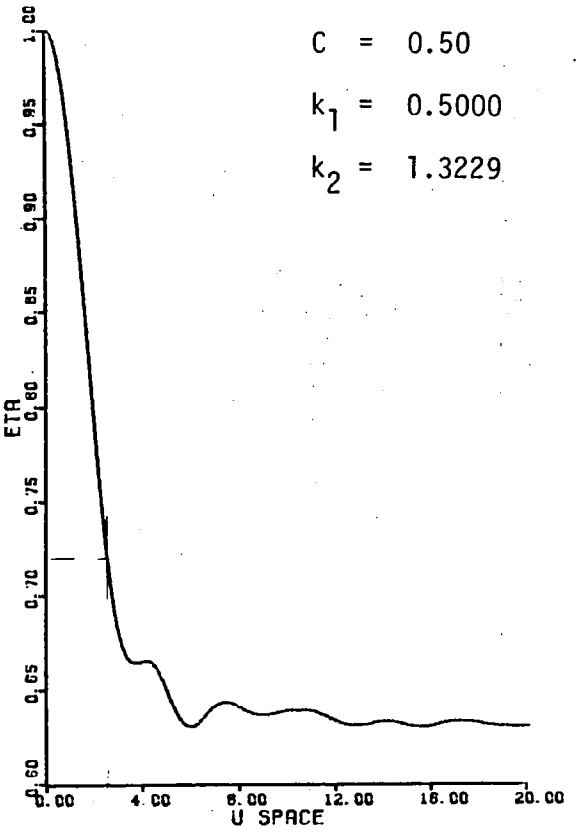

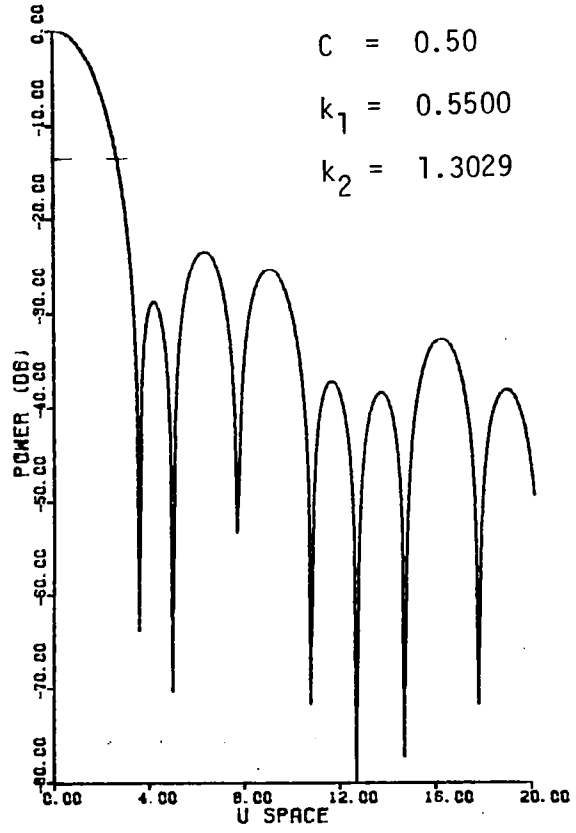

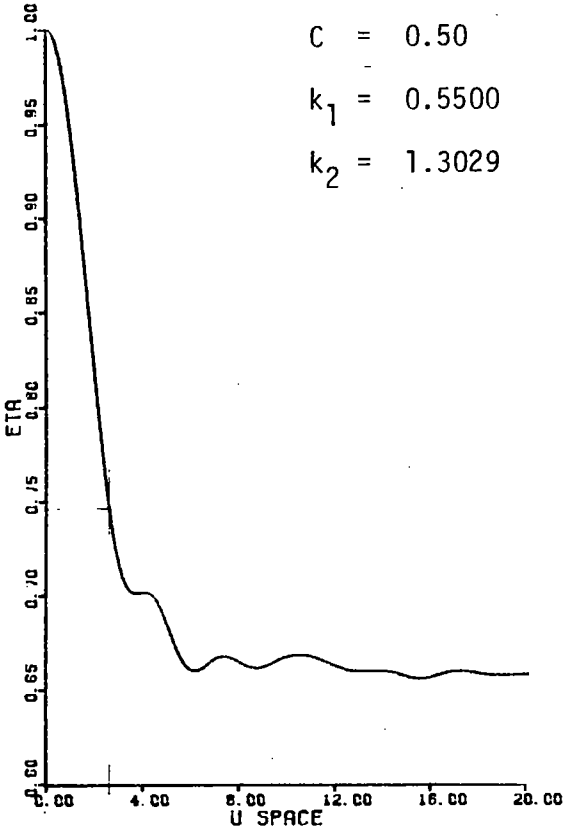

Figure C-5 -- Continued

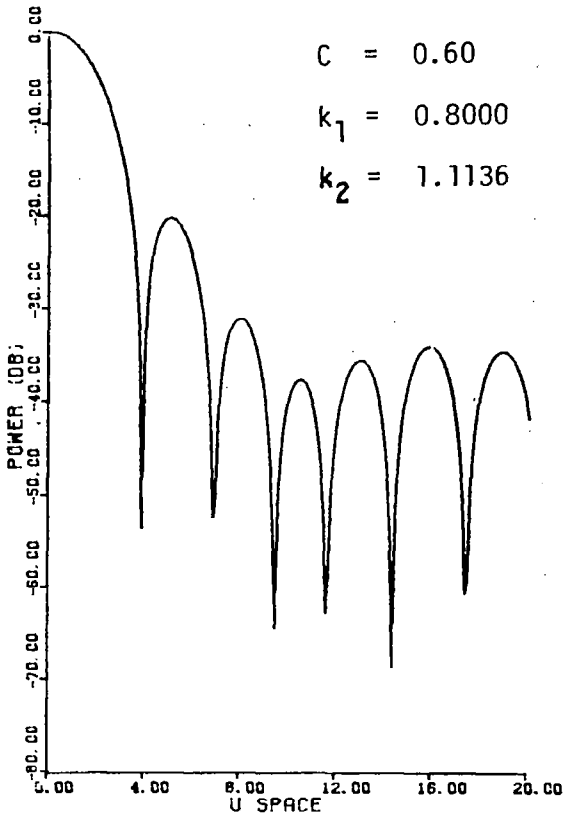

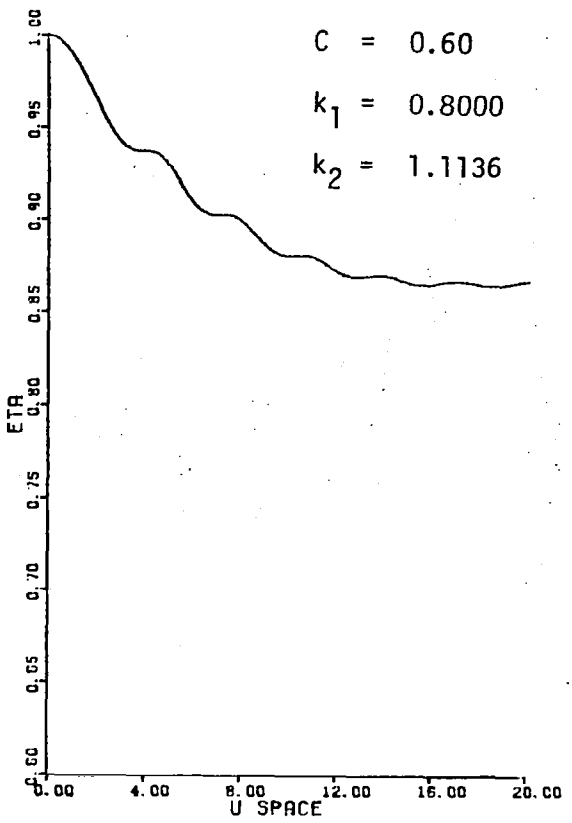

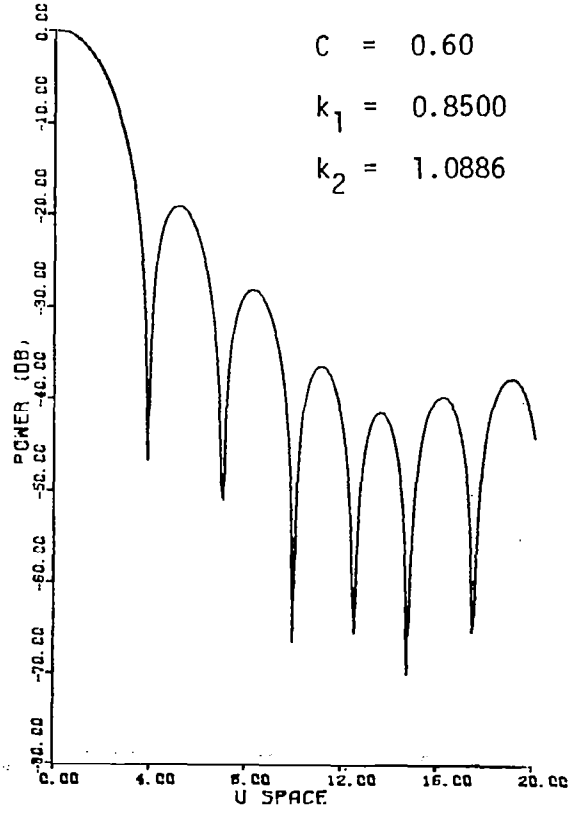

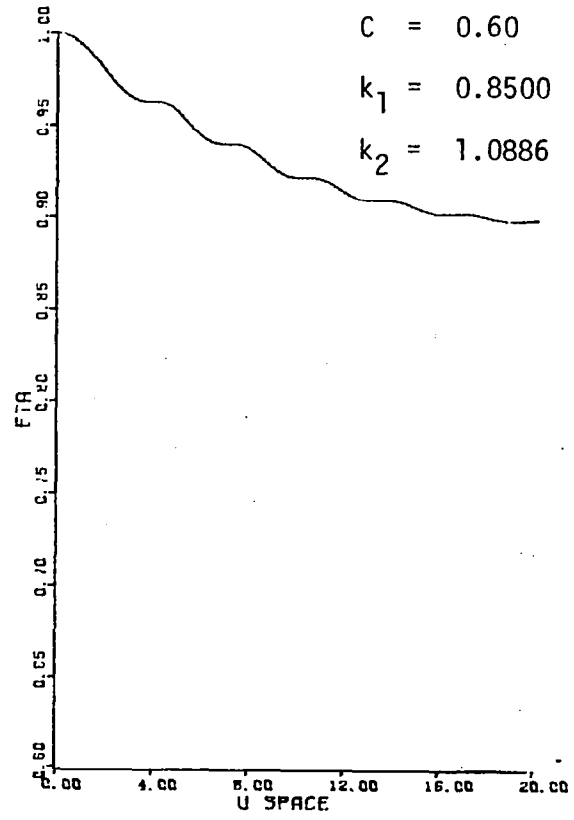

Figure C-5 -- Continued

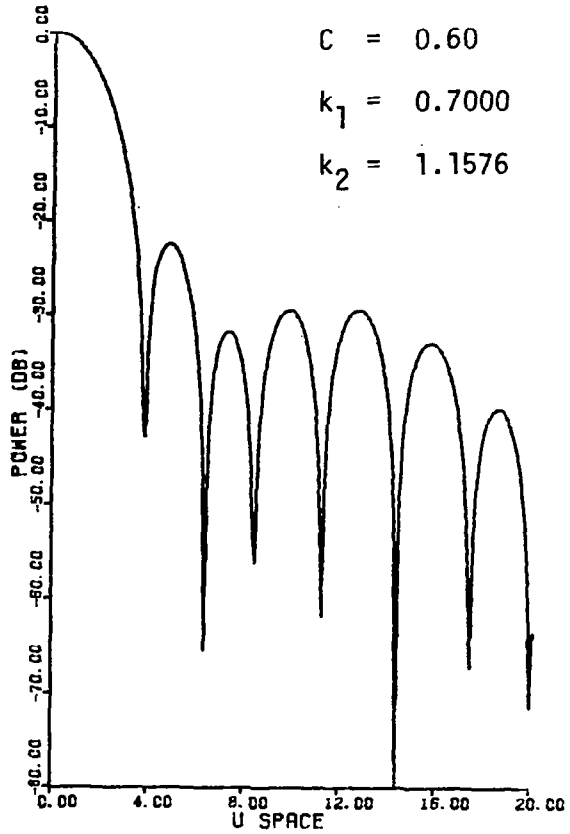

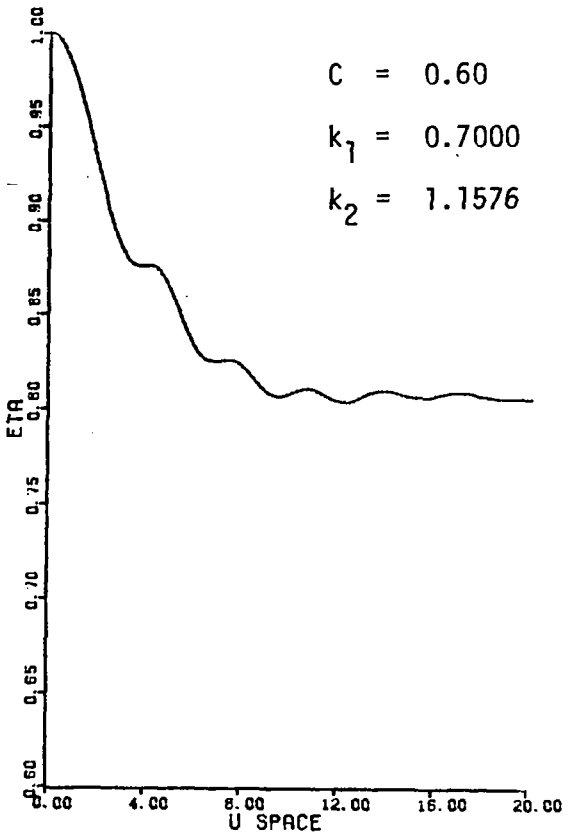

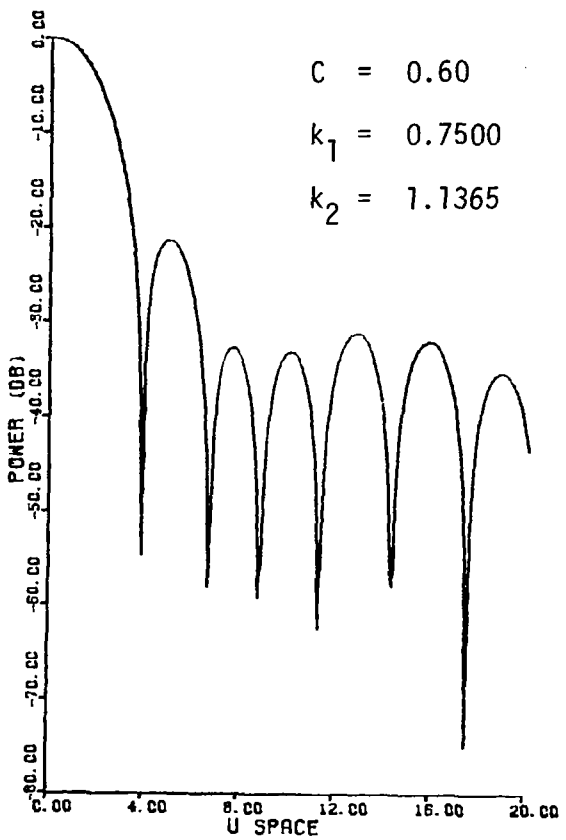

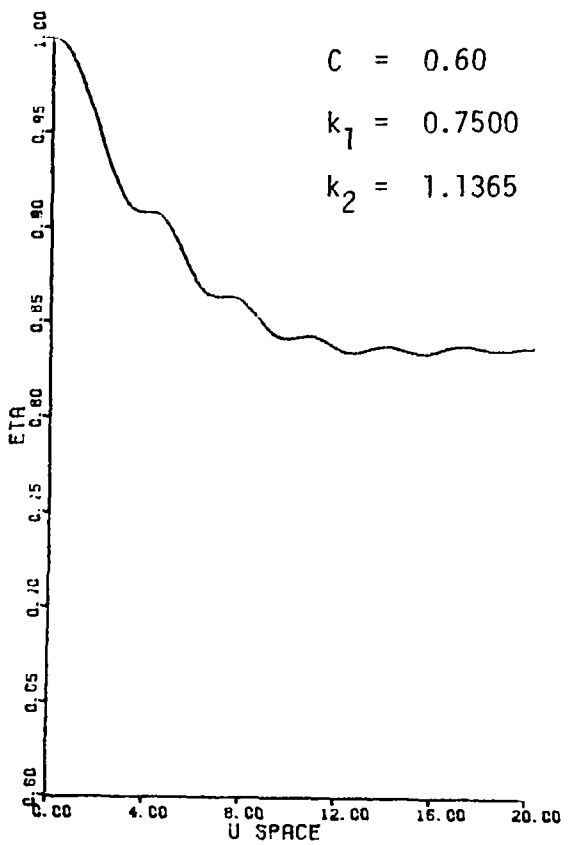

Figure C-5 -- Continued

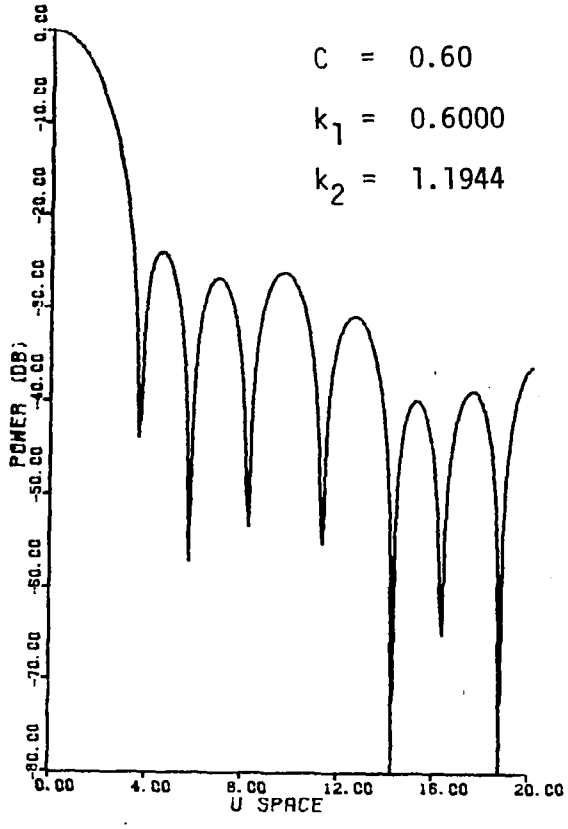

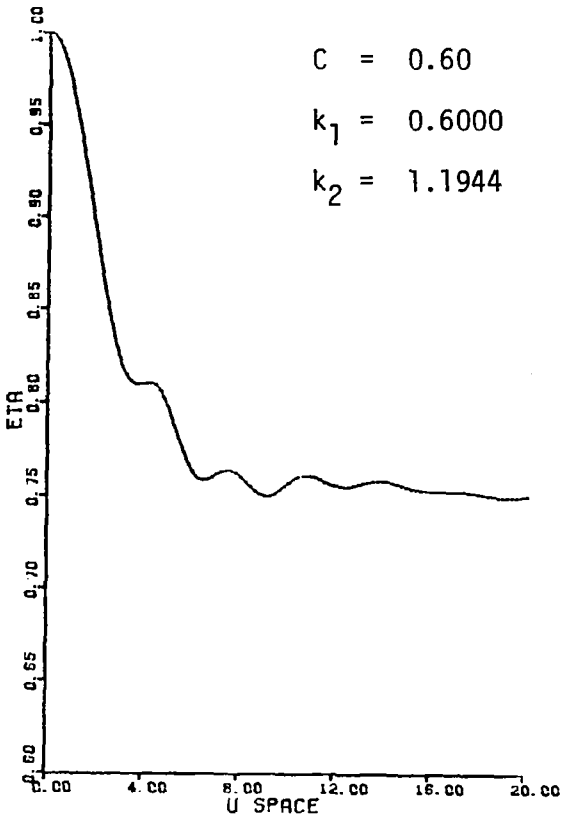

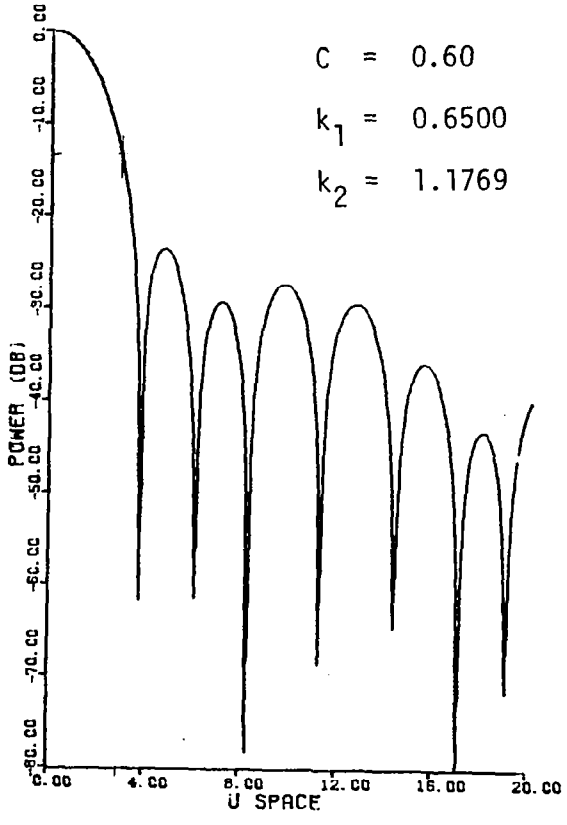

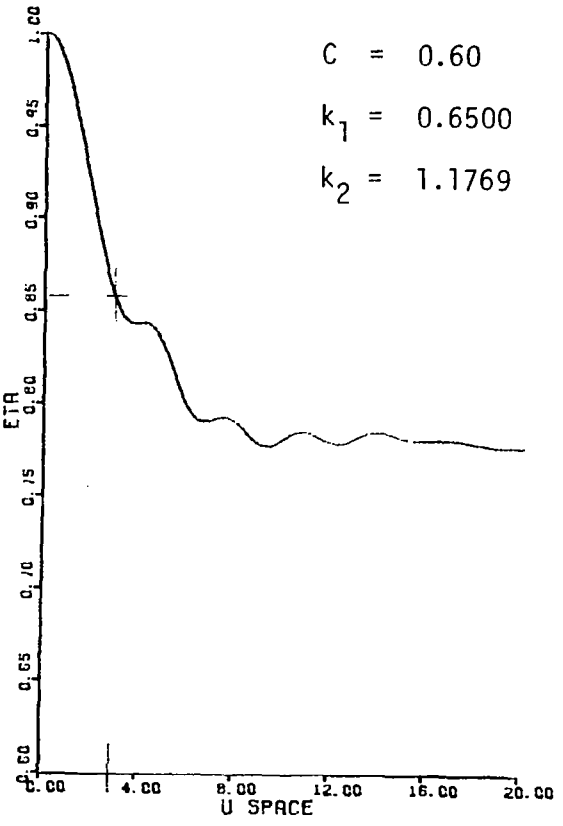

Figure C-5 -- Continued

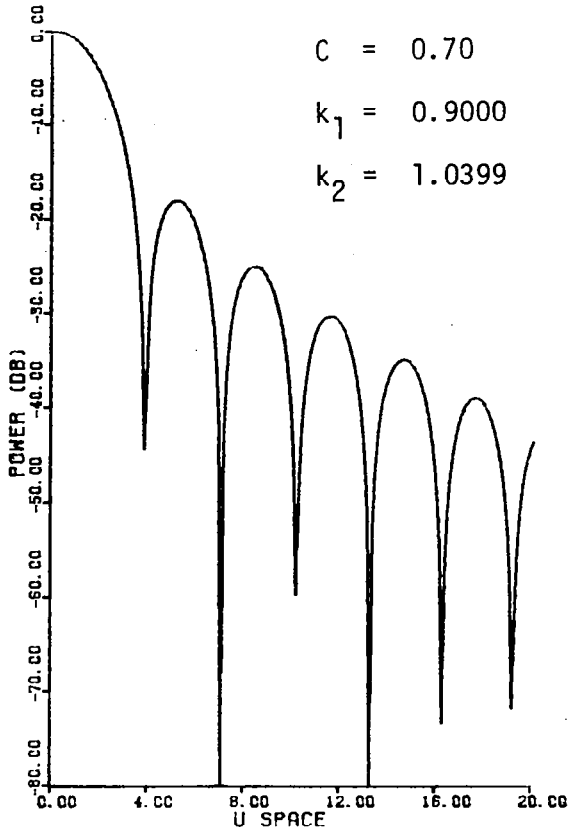

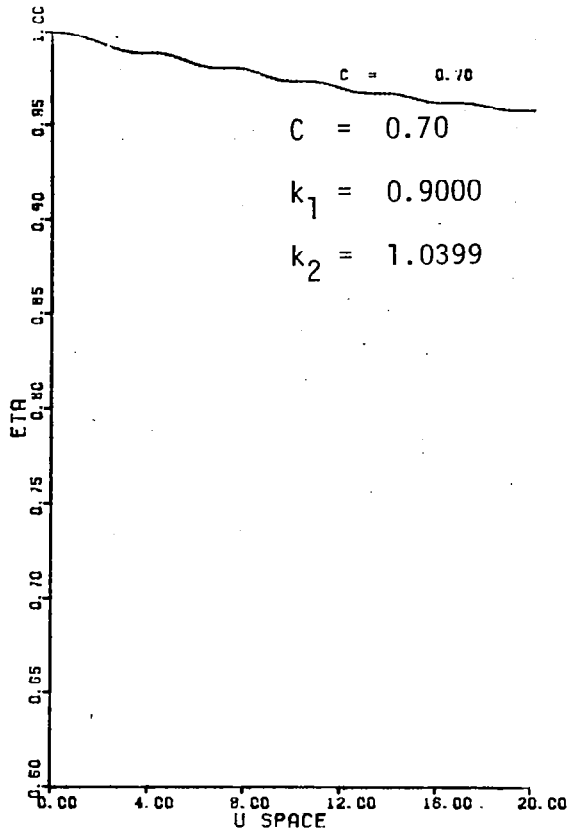

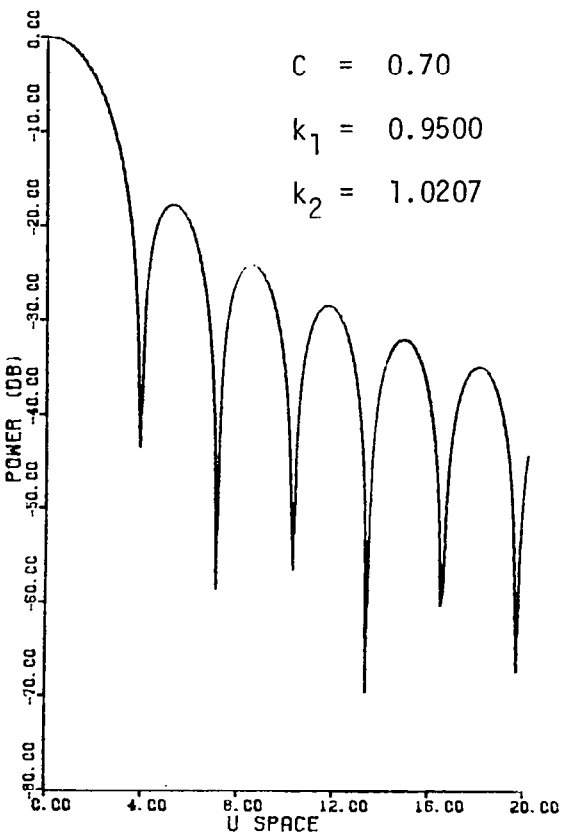

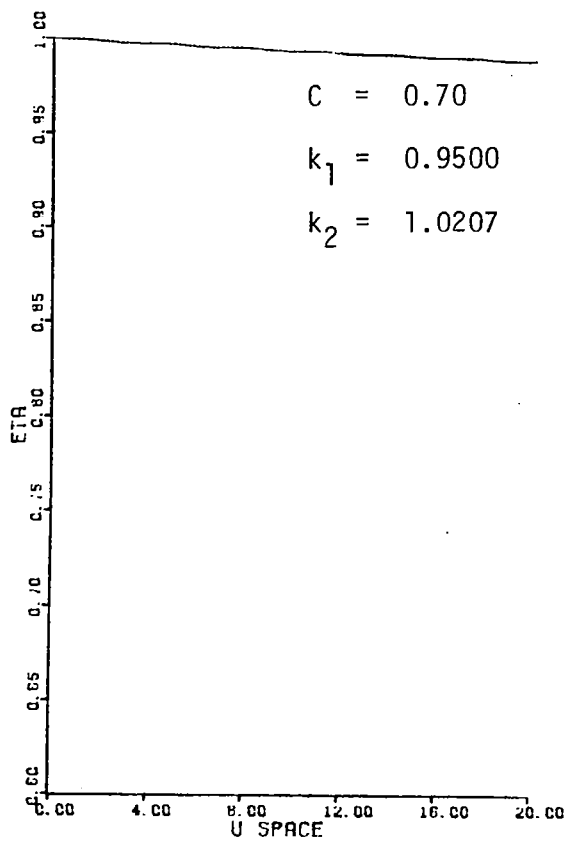

Figure C-5 -- Continued

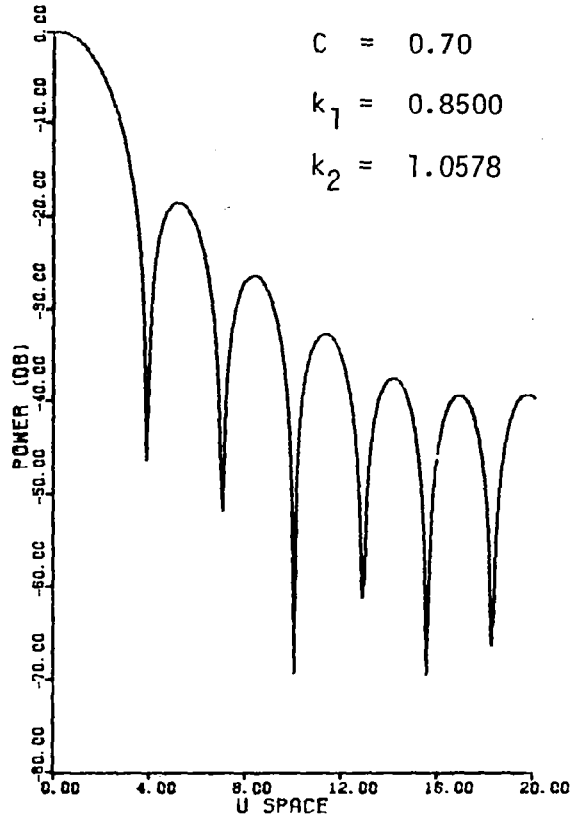

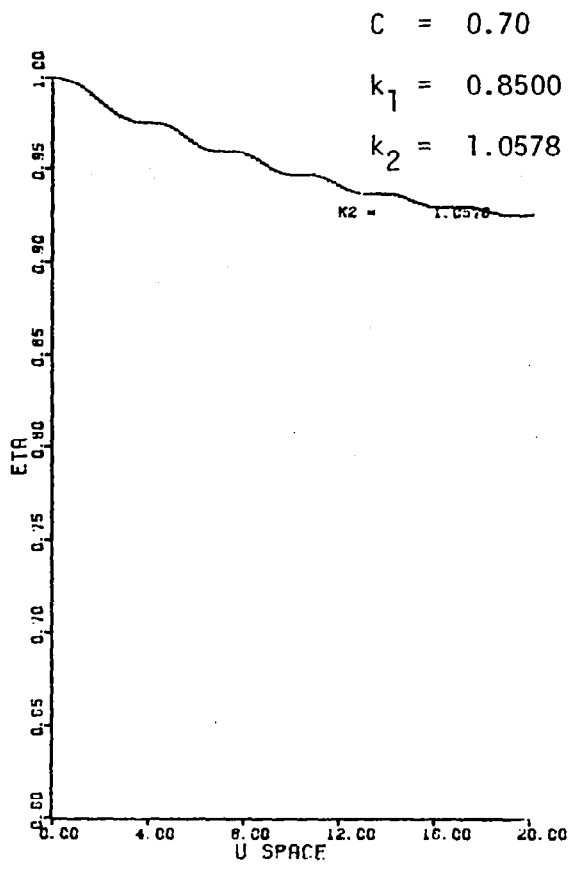

Figure C-5 -- Continued

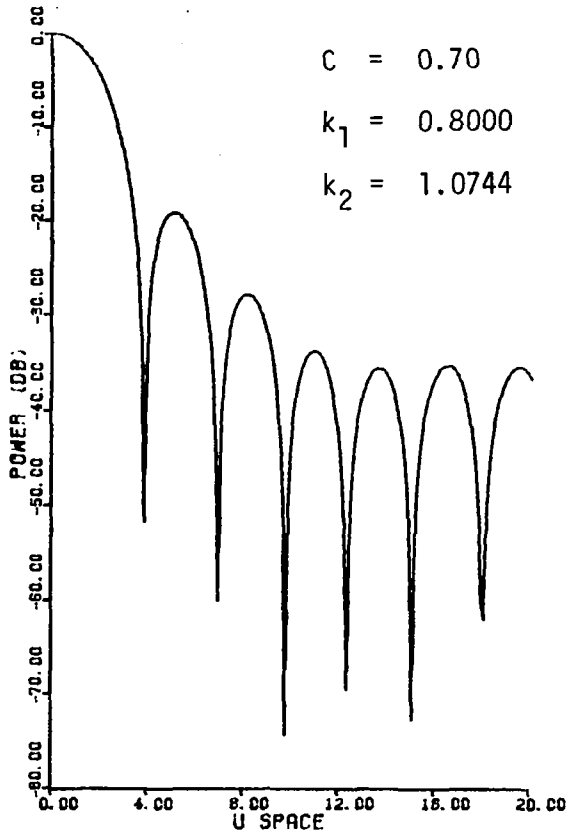

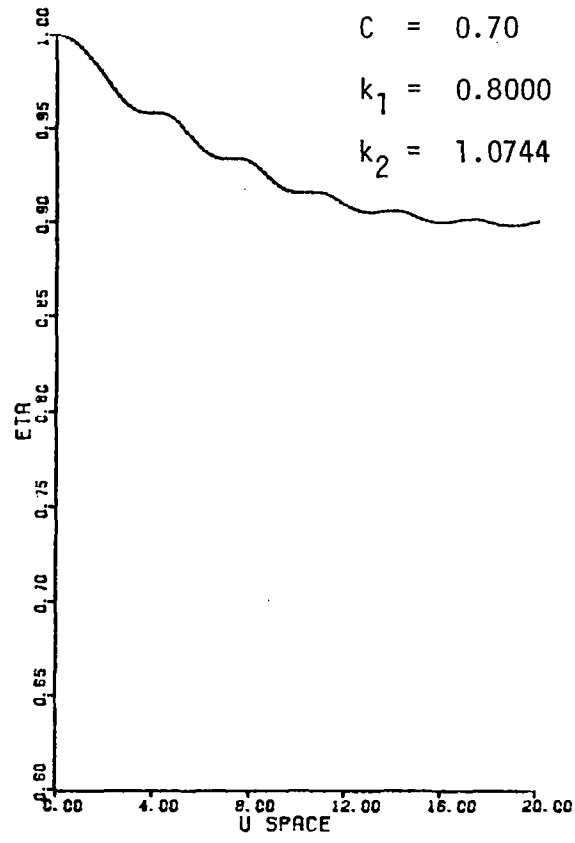

Figure C-5 -- Continued

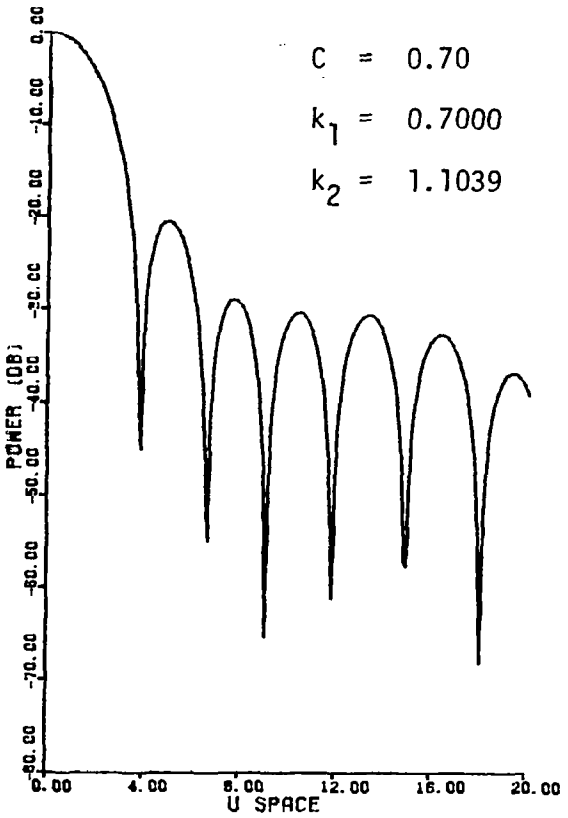

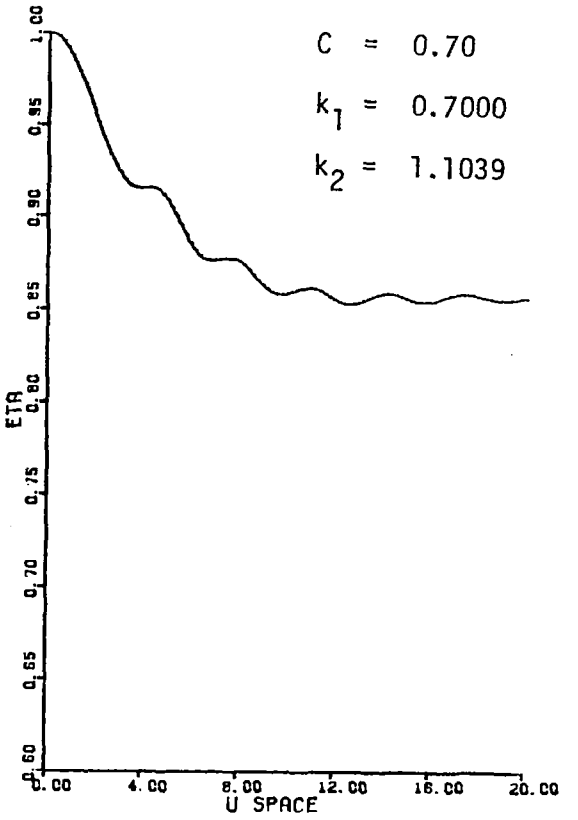

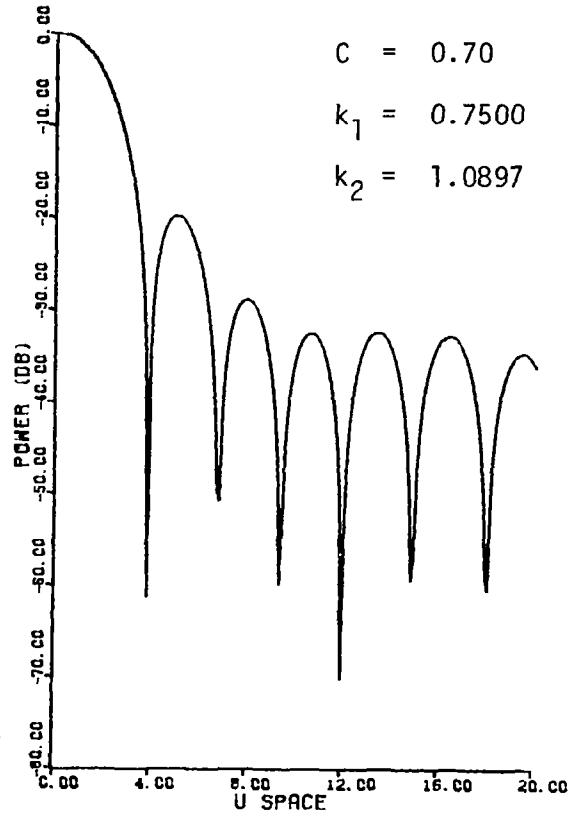

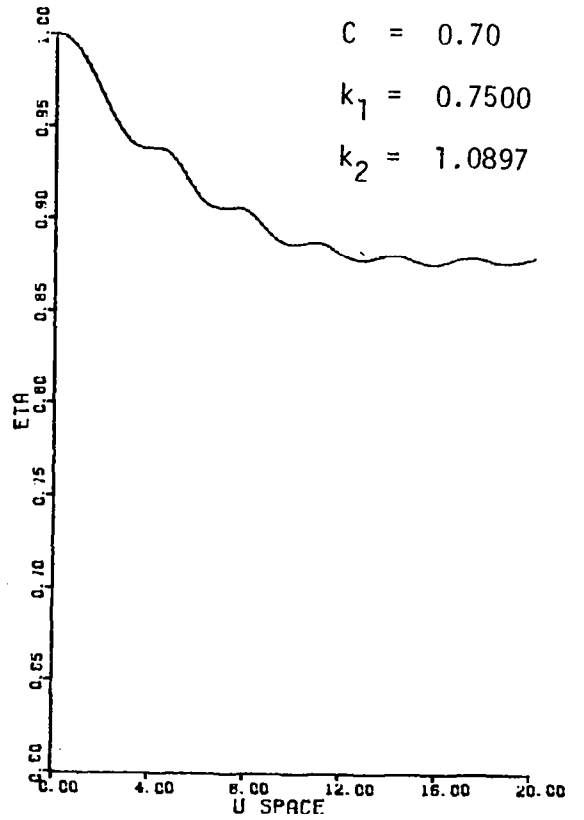

Figure C-5 -- Continued

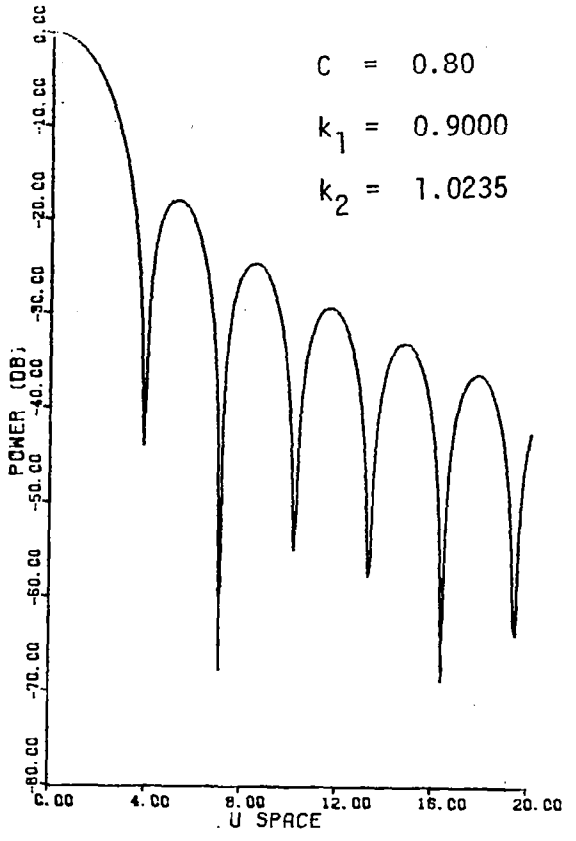

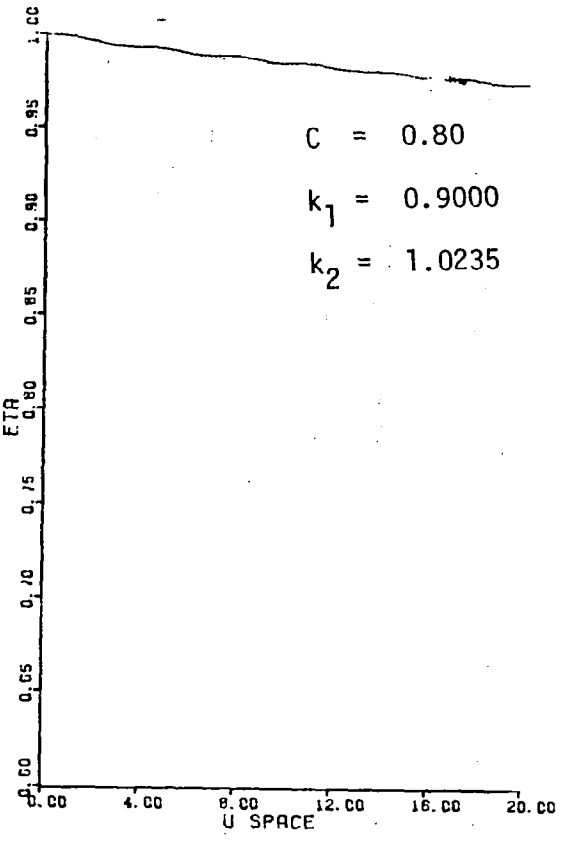

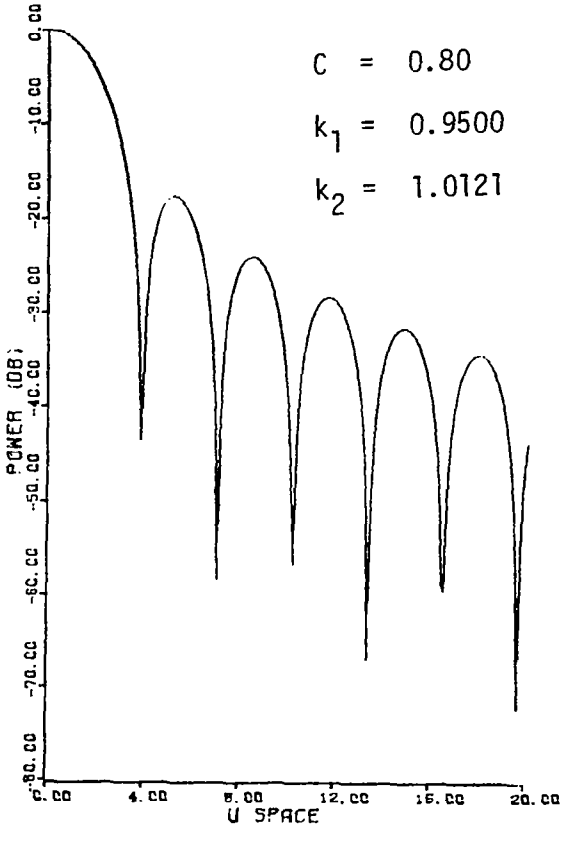

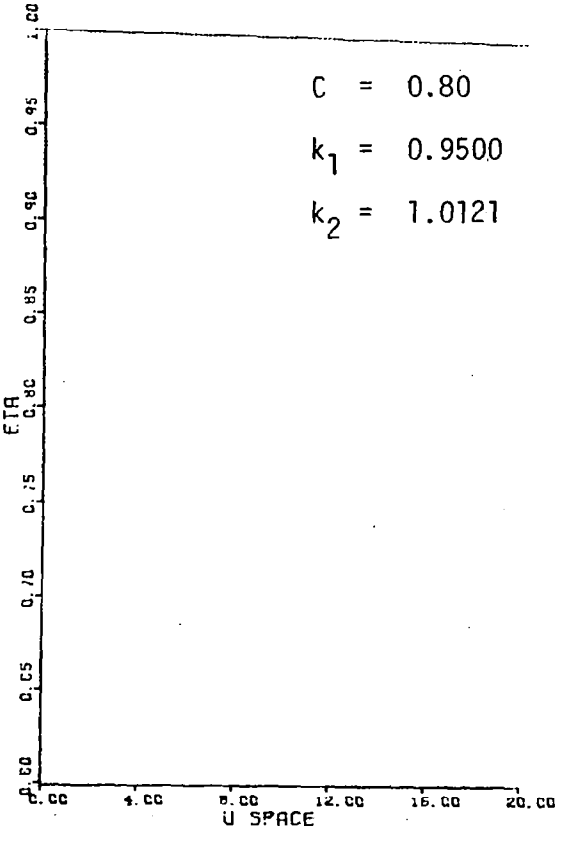

Figure C-5 -- Continued

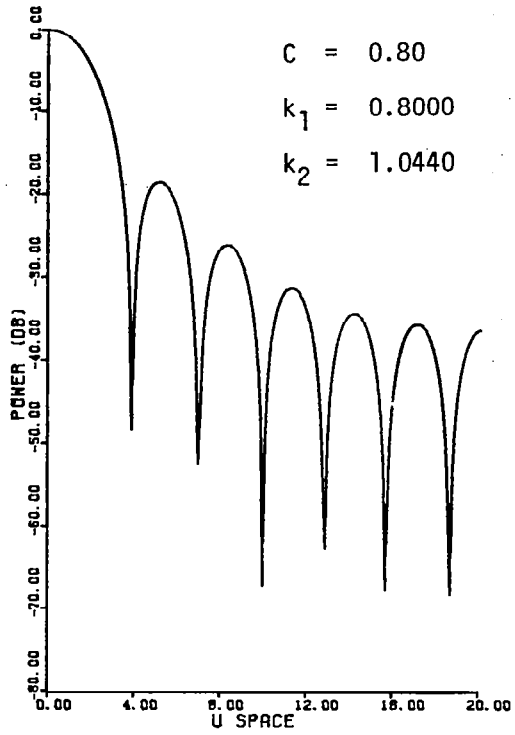

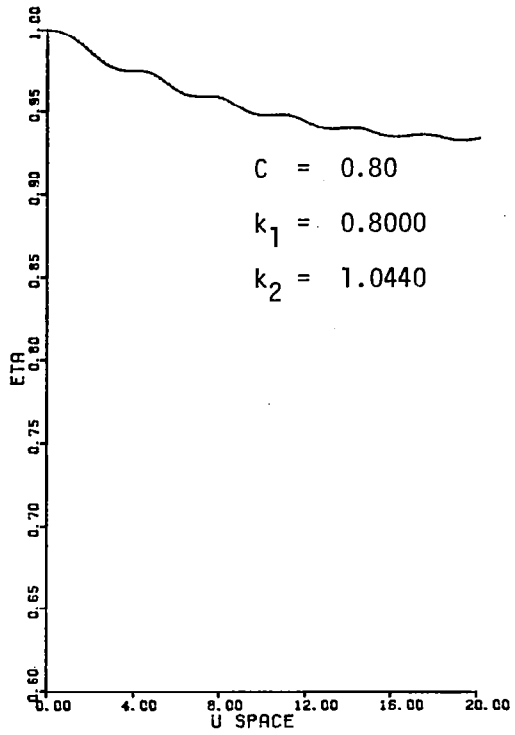

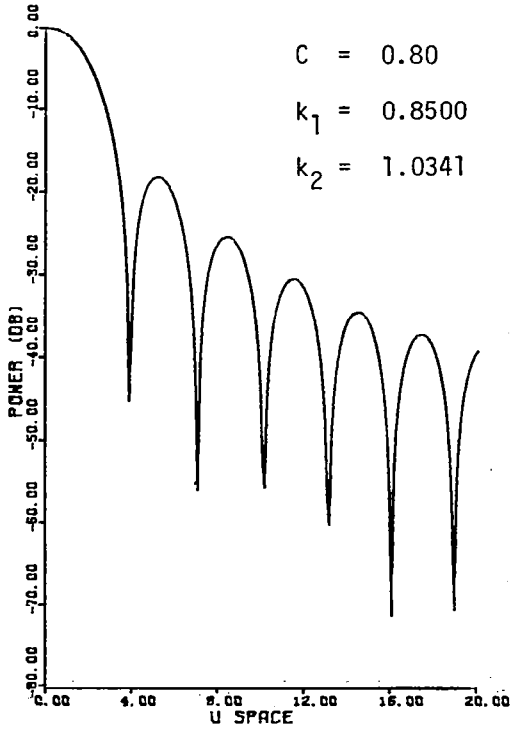

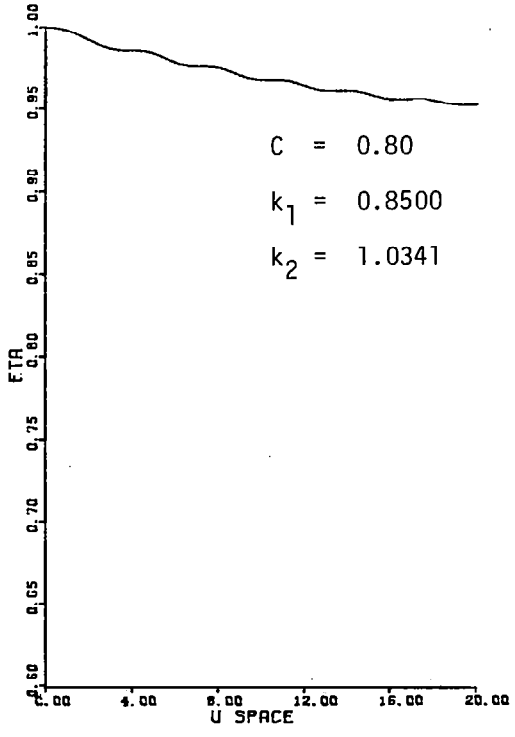

Figure C-5 -- Continued

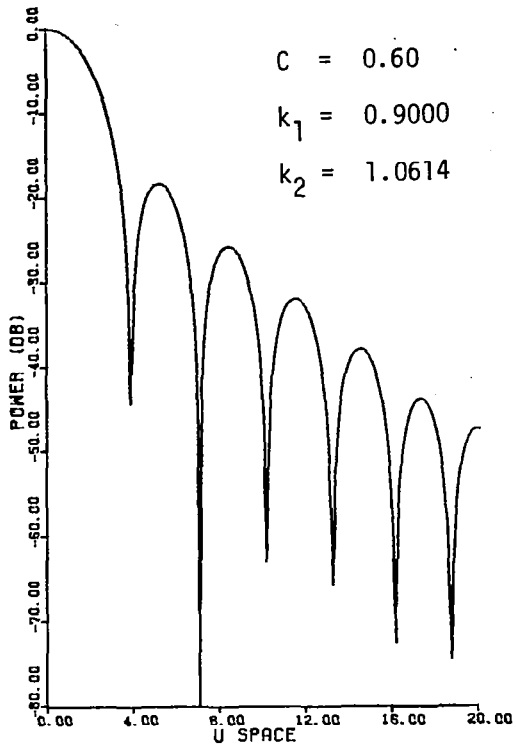

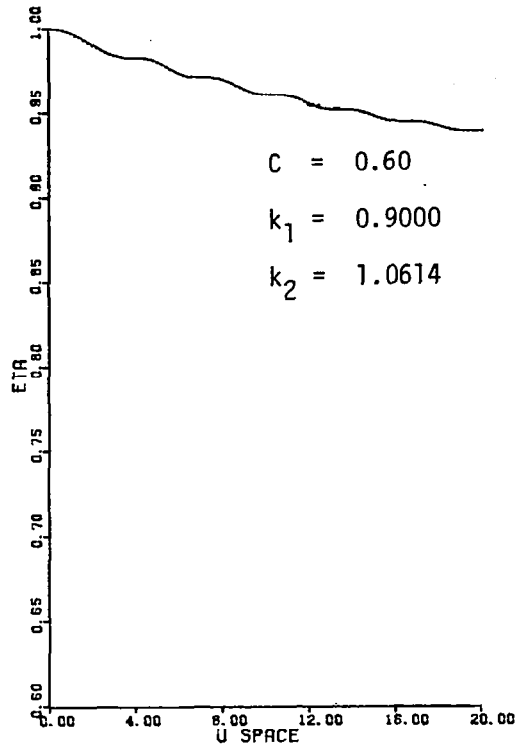

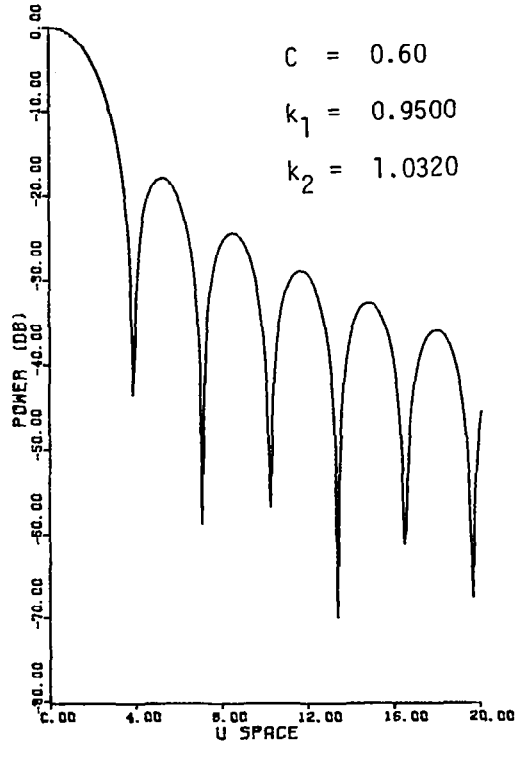

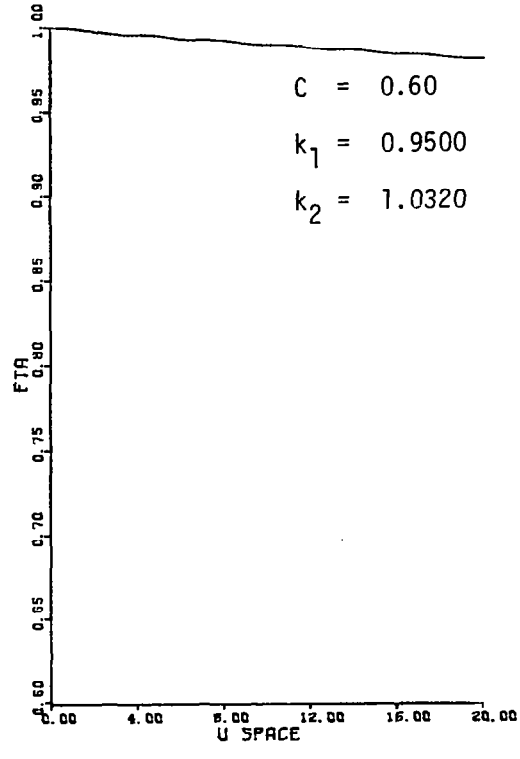

Figure C-5 -- Continued

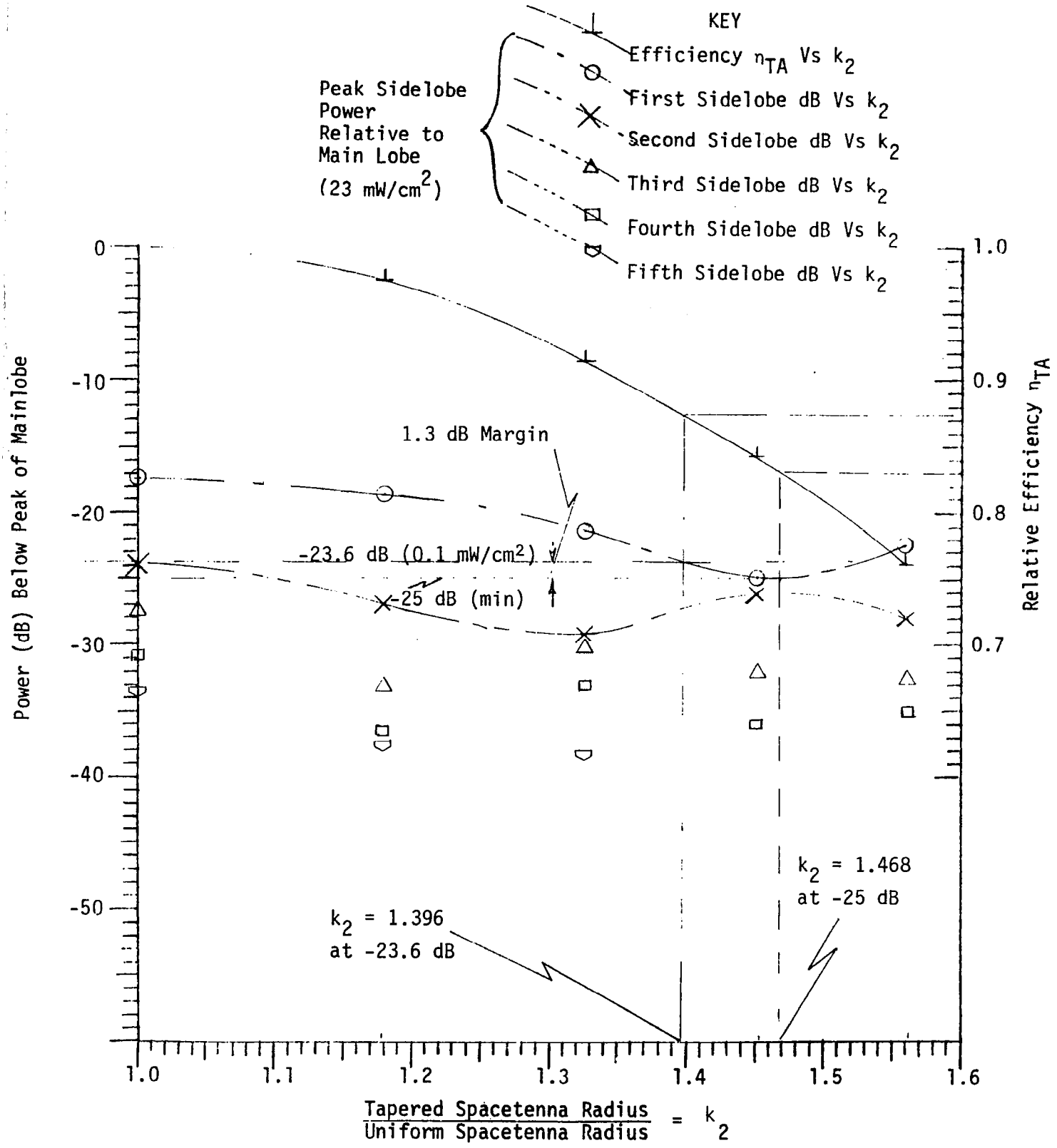

Figure C-6 Sidelobe Envelope and Efficiency For .04 Power Taper

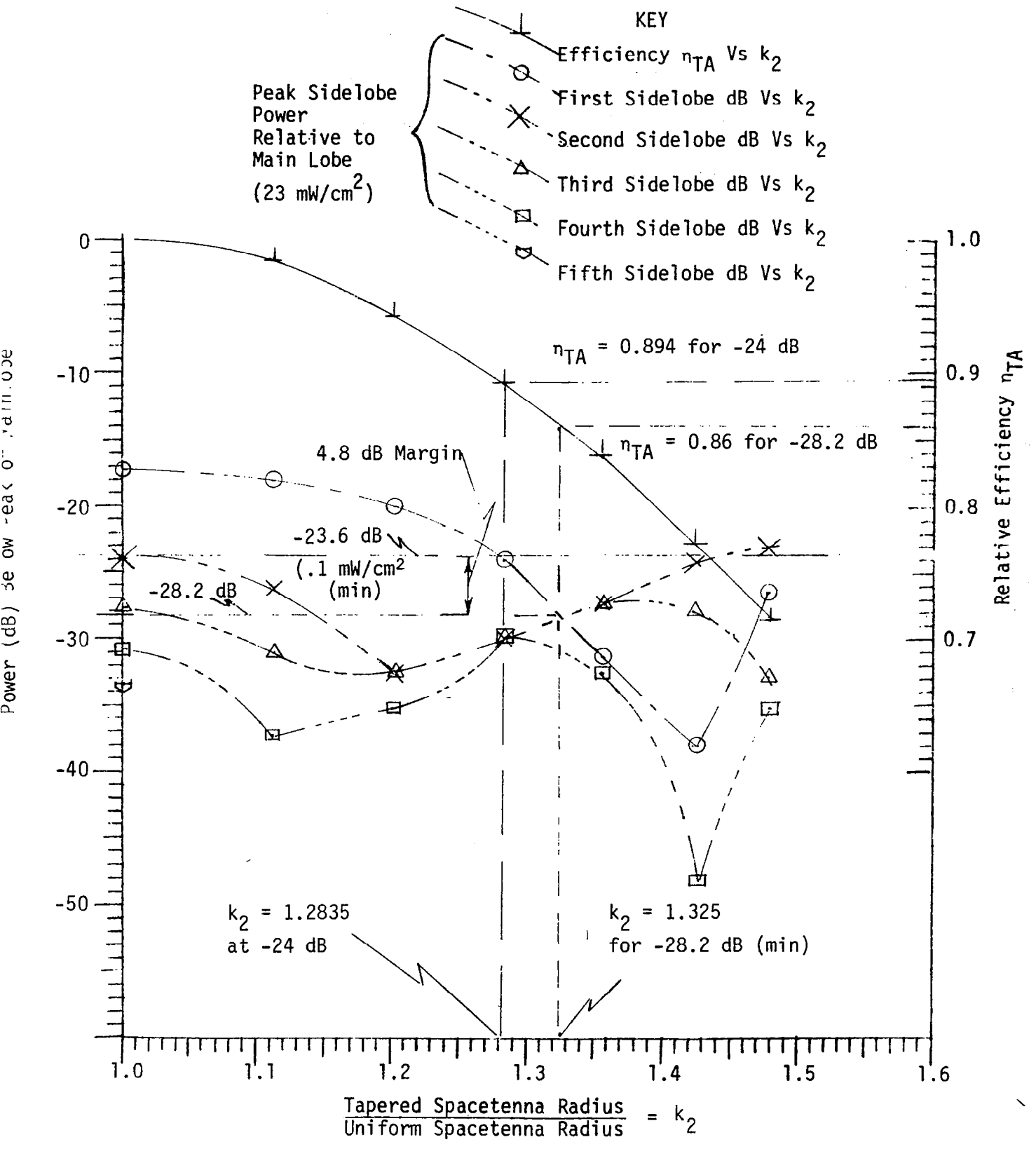

Figure C-7 Sidelobe Envelope and Efficiency For 0.09 Power Taper

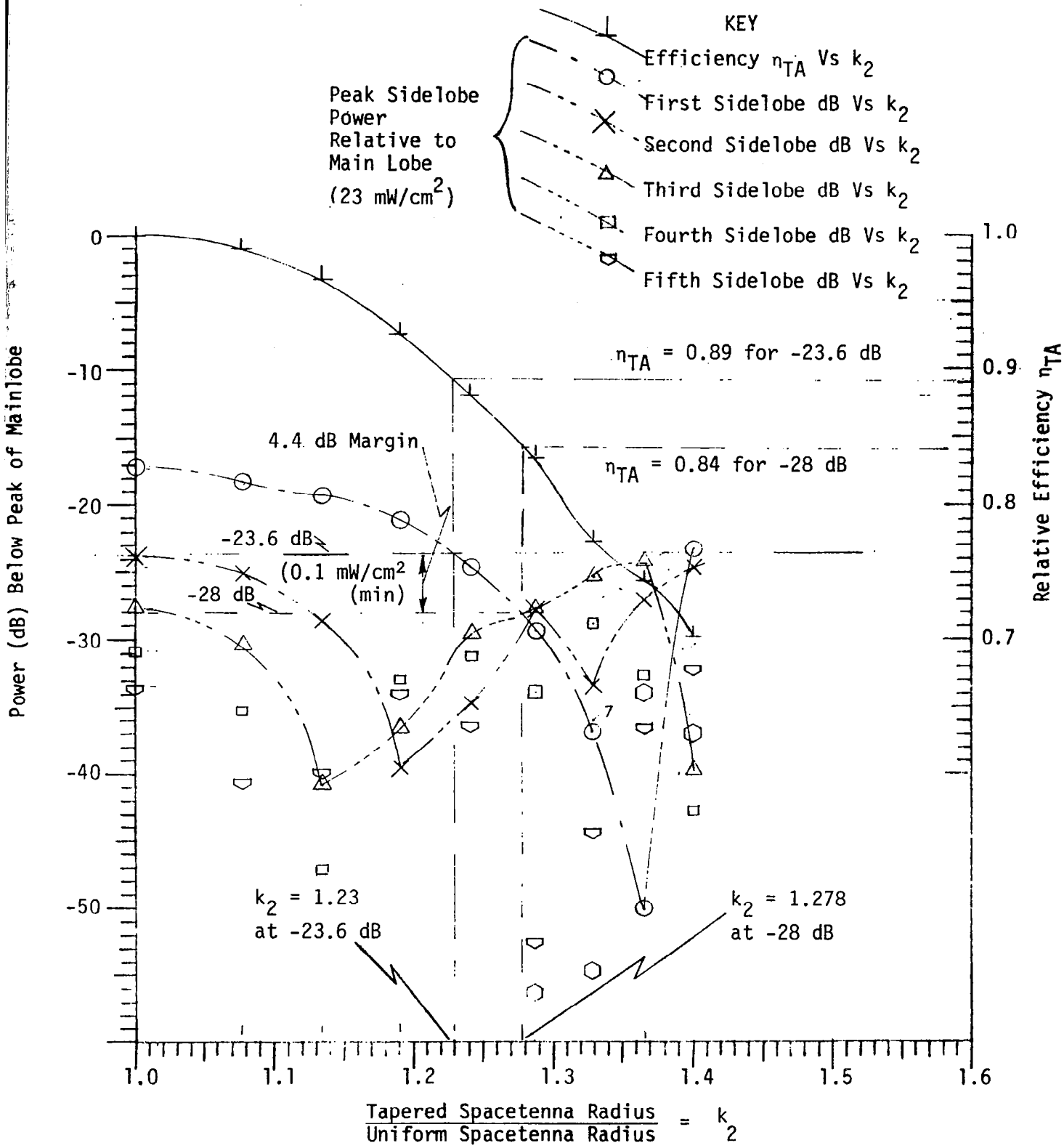

Figure C-8 Sidelobe Envelope and Efficiency For 0.16 Power Taper

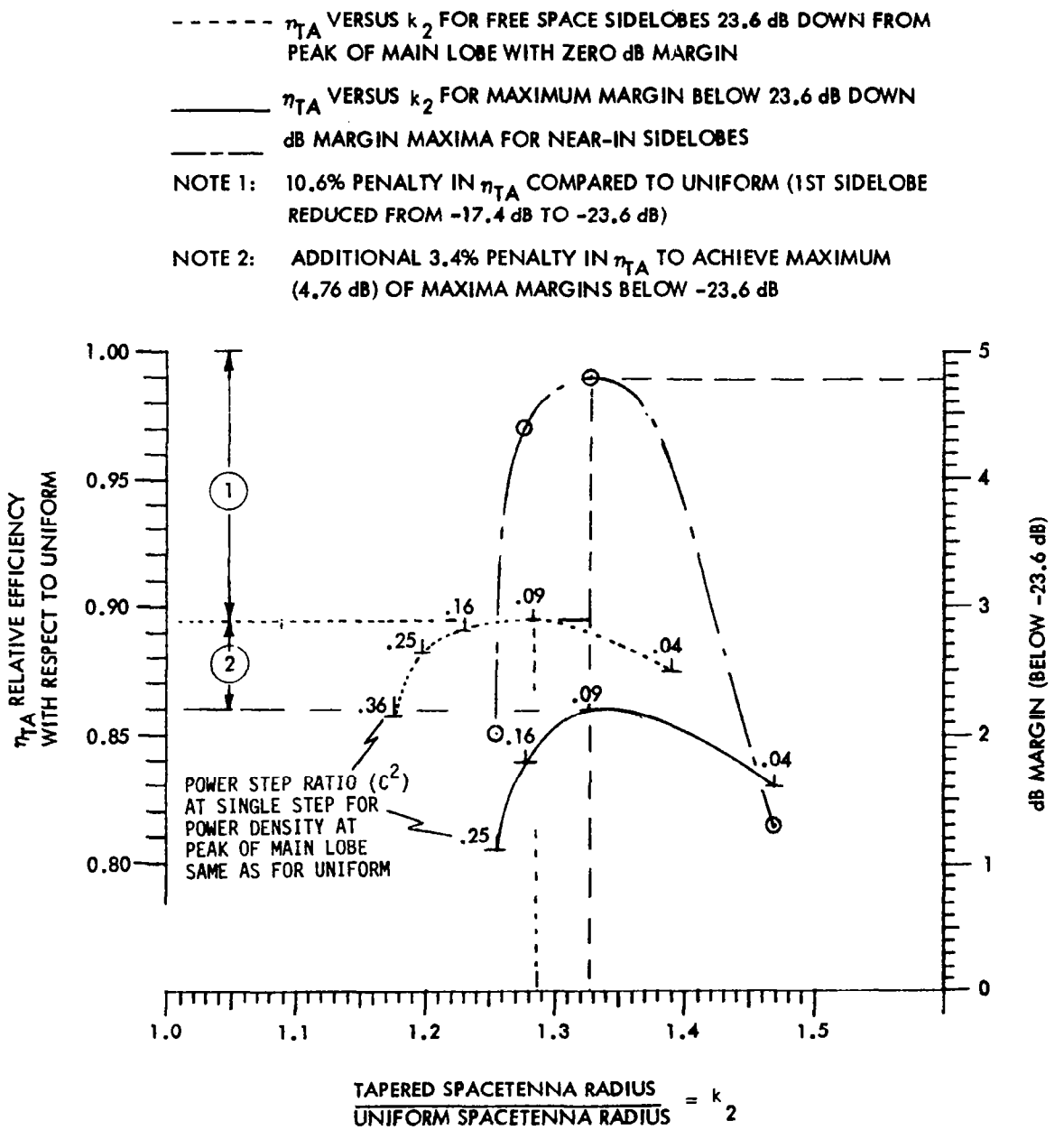

Figure C-9 Single Stepped Taper Aperture Efficiencies and Sidelobe Margins Relative to Uniform

is no dB margin included in the dotted line, while the solid line shows the combinations of C^2 and k_2 to achieve the maximum margin in sidelobes below the -23.6 dB point.

In that the cases for C = 3, 4 and 5 show significant potential for near in sidelobe control, the performance at further out sidelobes was investigated. As shown in Figures C-10 and C-11 the further out sidelobes are well behaved.

A glossary of terms is given in Table C-1.

The power delivered for the step taper (P_{DT}) can be obtained from

$$P_{DT} = \frac{\eta_T \eta_U P_{TT}}{k_1^2(1 - C^2) + C^2 k_2} \tag{C-17}$$

where η_T is the beam efficiency for the tapered case referenced to uniform

$$\eta_T = \frac{P_{D_T}}{P_{D_u}} \tag{C-18}$$

P_{D_u} is the power delivered for uniform illumination which is obtained from η_u the uniform illumination beam efficiency where

$$\eta_u = \frac{P_{D_u}}{P_{T_u}} \tag{C-19}$$

P_{T_u} is the total available power for uniform illumination on the spacetenna. The available power for the step taper is less than this as follows:

$$P_{T_T} = P_{T_u}(k_1^2(1 - C^2) + C^2 k_2^2) \tag{C-20}$$

and

$$P_{D_T} = \eta_T \eta_u P_{T_u} \tag{C-21}$$

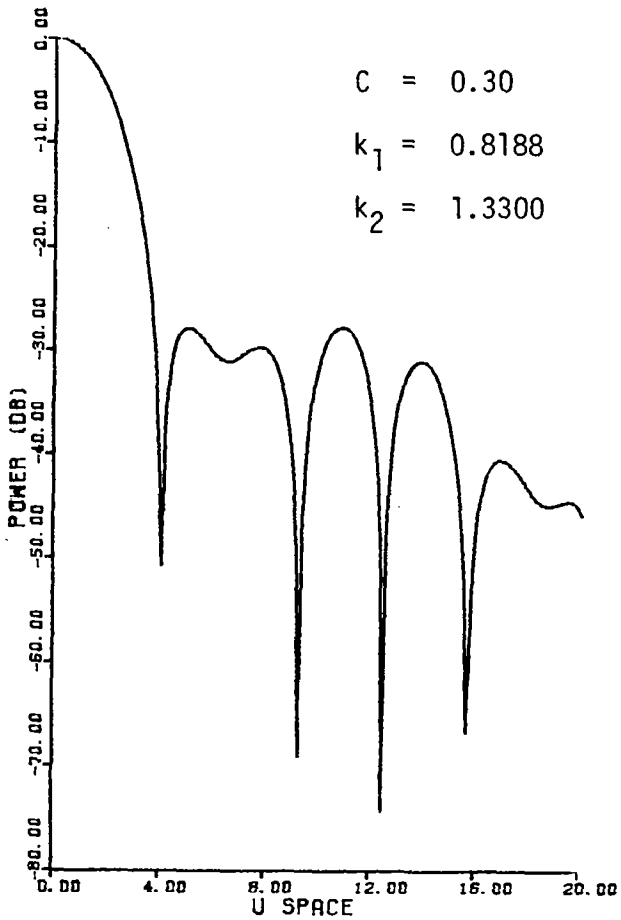

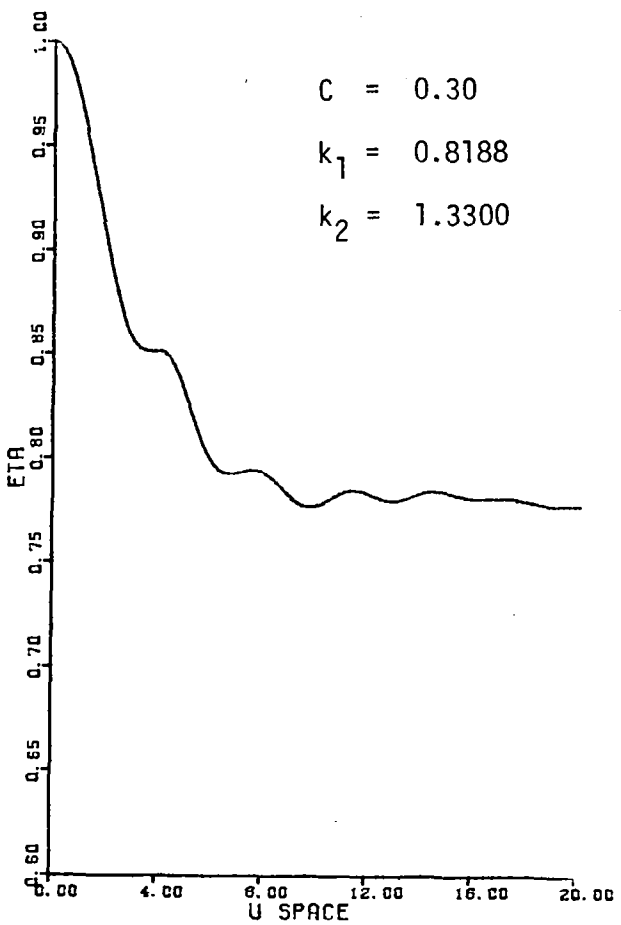

Figure C-10 Typical Near-In Sidelobe and Relative Efficiency Behavior

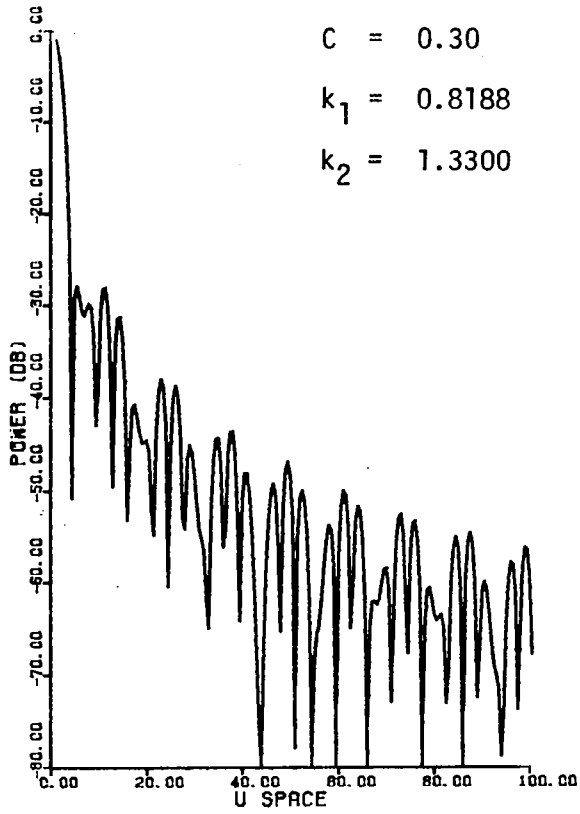

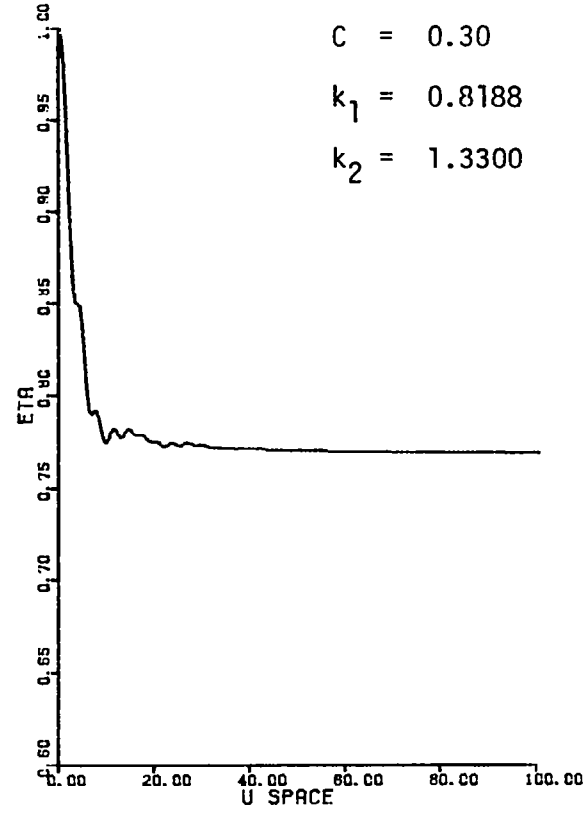

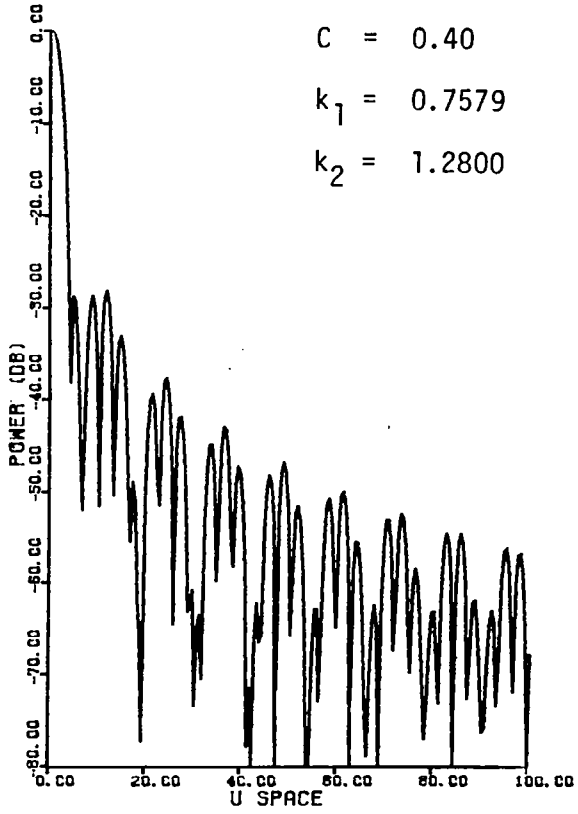

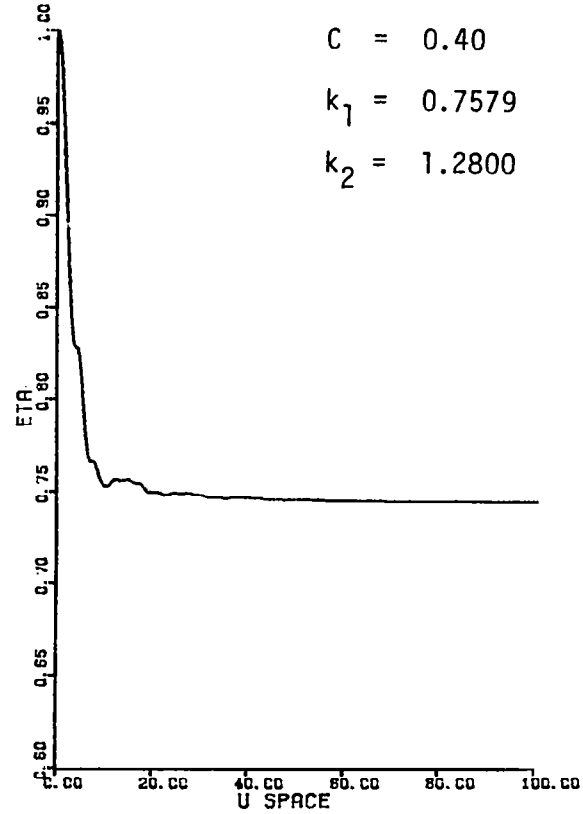

Figure C-11 Typical Far Out Sidelobe and Relative Efficiency Behavior

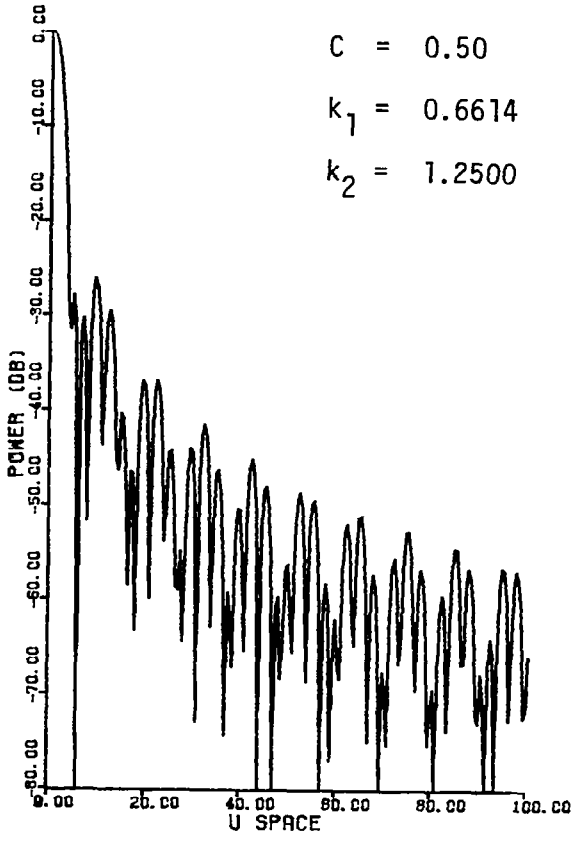

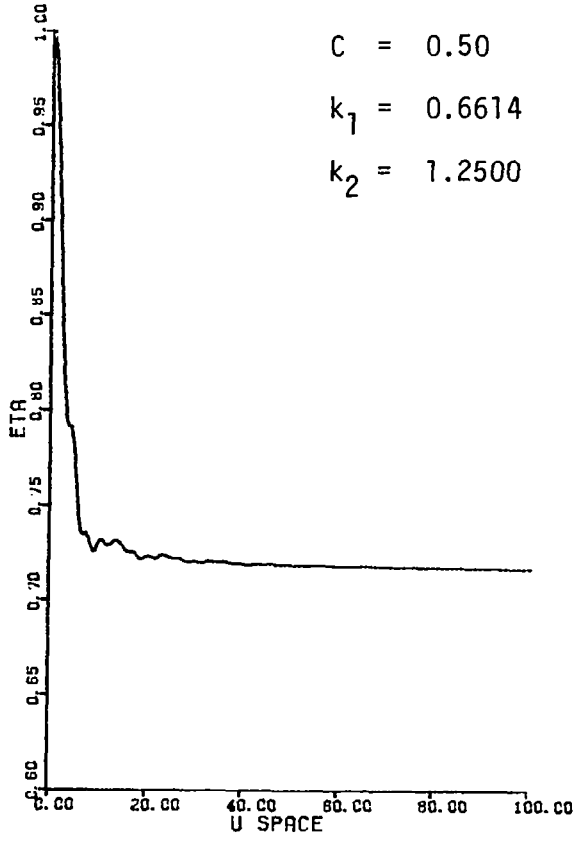

Figure 11 -- Continued

Table C-1 Glossary of Terms

C Step Amplitude

a Spacetenna Radius

k_1 Fractional Radius (Beginning of Step)

k_2 Fractional Radius (End of Step)

(Modified Spacetenna Radius)

U-Space $U = (2\pi a/\lambda) \sin \theta$

λ Operating Wavelength

θ Angle Off Boresight of Spacetenna

Eta (η_r) Ratio of Beam Efficiencies Between Step Taper (η_S) and Uniform (η_u)

$$\eta_r = \eta_S/\eta_u$$

P Ratio of Total Available Power for Step Taper Illumination to Uniform Illumination (Constraint is 23 mW/cm^2 at Beam Peak)

(1) First Sidelobe Peak

(2) Second Sidelobe Peak

(3) Third Sidelobe Peak

(4) Fourth Sidelobe Peak

APPENDIX D

DESIGNS, CONSIDERATIONS AND ISSUES

The Progress Report on Solid State Sandwich Concept presented at Lyndon B. Johnson Space Center in Houston, Texas on 15-18 January 1980 is incorporated in total.

PROGRESS REPORT ON SOLID STATE SANDWICH CONCEPT

- DESIGNS, CONSIDERATIONS AND ISSUES -

Owen E. Maynard
Raytheon Company, Equipment Division

Presented At
Solid State Configurations Session of the SPS Microwave Systems Workshop
15-18 January 1980
Lyndon B. Johnson Space Center, Houston, Texas

ABSTRACT

Progress in analysis and design of solid state approaches to the SPS Microwave Power Transmission System is reviewed with special emphasis on the Sandwich concept and the issues of maintenance of low junction temperatures for amplifiers to assure acceptable lifetime. Ten specific issues or considerations are discussed and their resolution or status is presented.

Introduction and Background

Investigations of Microwave Power Transmission System (MPTS) concepts by Raytheon in the past have not addressed solid state approaches due primarily to the problem of trying to achieve long life (30 years) in an application where high power density and limited waste heat dissipation capabilities are inherent.

Solid state amplifier efficiencies for the current technology are too low (50% to 70% range) requiring 50 to 30% of the DC power to be radiated as waste heat while keeping junction temperatures within acceptable limits. Recent projections of solid state amplifiers have indicated that the efficiency may be as high as 80%, requiring 20% of the DC power to be radiated as waste heat reducing the problem by a factor close to 2.

Solid state amplifiers operate at low voltage, 20 V, compared to 20 kV to 40 kV for tubes and the DC power transmission and conditioning system weights, complexities and cost for known overall system concepts were of major concern for kV power distribution systems and incredible for low voltage systems. The solid state sandwich concept, where the DC power distribution is a simple grid interface with the static microwave portion of the sandwich, is such that investigation of the solid state approach became of considerable interest.

Results have been encouraging and the concept is considered to warrant further and more in-depth investigation. The critical outstanding issues include the need for demonstration of the high efficiency for the amplifiers. When this is accomplished, the issues and considerations discussed herein become important.

Results of Investigation by Raytheon for NASA-MSFC

Raytheon's investigation has included the following tasks:

1. Definition and Math Modeling of Basic Solid State Microwave Devices
2. Initial Conceptual Subsystem and System Design
3. Sidelobe Control and System Selection
4. Assessment of Selected System Concept
5. Parametric Solid State MPTS Data Relevant to SPS Concept

An efficiency goal for the DC to RF amplifiers of 80% has been established. Although this has not been demonstrated it is considered to be a realistic goal and is therefore the basis for the investigation. Parametric data for 75% and 85% are included.

Conceptual subsystem and system design investigations resulted in the following:

(a) 1.95 km diameter transmitting antenna having uniform power density of 500 W/m^2 (RF);

(b) 4.5 km beam diameter or minor axis rectenna having maximum power density of 23 mW/cm^2;

(c) Free space sidelobes < 0.1 mW/cm^2 for 2nd and further out sidelobes;

(d) First sidelobe above 0.1 mW/cm^2 out to the fenced minor axis of 9.2 km;

(e) Subarray size 32 x 32 elements 3.2m x 3.2m;

(f) Microwave subsystem for spacetenna weight of $\sim$3 kg/m^2;

(g) DC to DC efficiency of 0.51;

(h) Total transmitted power of $\frac{\pi \times 1.95^2}{4} \times 500 \times 10^6 = 1.493 \times 10^9$ W RF

(i) DC power into antenna $= \frac{1.493 \times 10^9}{.99 \times .99 \times .8 \times .96 \times .98} = \frac{1.493 \times 10^9}{.738}$

$= 2.02 \times 10^9$ W DC

(j) Power out of rectenna to power grid = $1.49 \times 10^9 \times .98 \times .825 \times .89 \times .97$

$= 1.04 \times 10^9$ W DC

(k) Antenna concept is one amplifier/transmitting antenna element (narrow bandwidth) with element printed on tape 1/4 λ from ground plane. Receiving antenna elements are wide bandwidth and are orthogonal to the transmit elements to minimize adverse coupling.

(l) Waste heat is passively radiated to deep space from pyrographite radiators having $\varepsilon = 0.8$ and $\alpha = 0.05$ thermal control coatings. Waste heat (500 W/m^2) from the photovoltaic array is assumed to add to the heat load on the microwave side.

(m) Single step taper at the transmitting antenna was investigated to determine sensitivity for reduction of 2nd sidelobe. Significant reduction is achievable with single step.

(n) Further parametric investigations indicate that the RF power per element may be increased from 5 W/element to 6, thus permitting a significant reduction in spacetenna diameter for the same power density on the ground.

(o) Further detailed investigation of the concept is warranted.

Issues/Considerations

The issues and considerations along with their resolution and status, shown in the attached table, have evolved during the investigation. Each of them will be discussed in turn in the oral presentation and copies of the visual aids will be made available.

SOLID STATE SANDWICH CONCEPT

DESIGNS AND ISSUES

OWEN MAYNARD
RAYTHEON COMPANY

AT

NASA JSC

15-18 JANUARY 1980

SOLID STATE MPTS SPACETENNA SUBARRAY CIRCUIT DIAGRAM

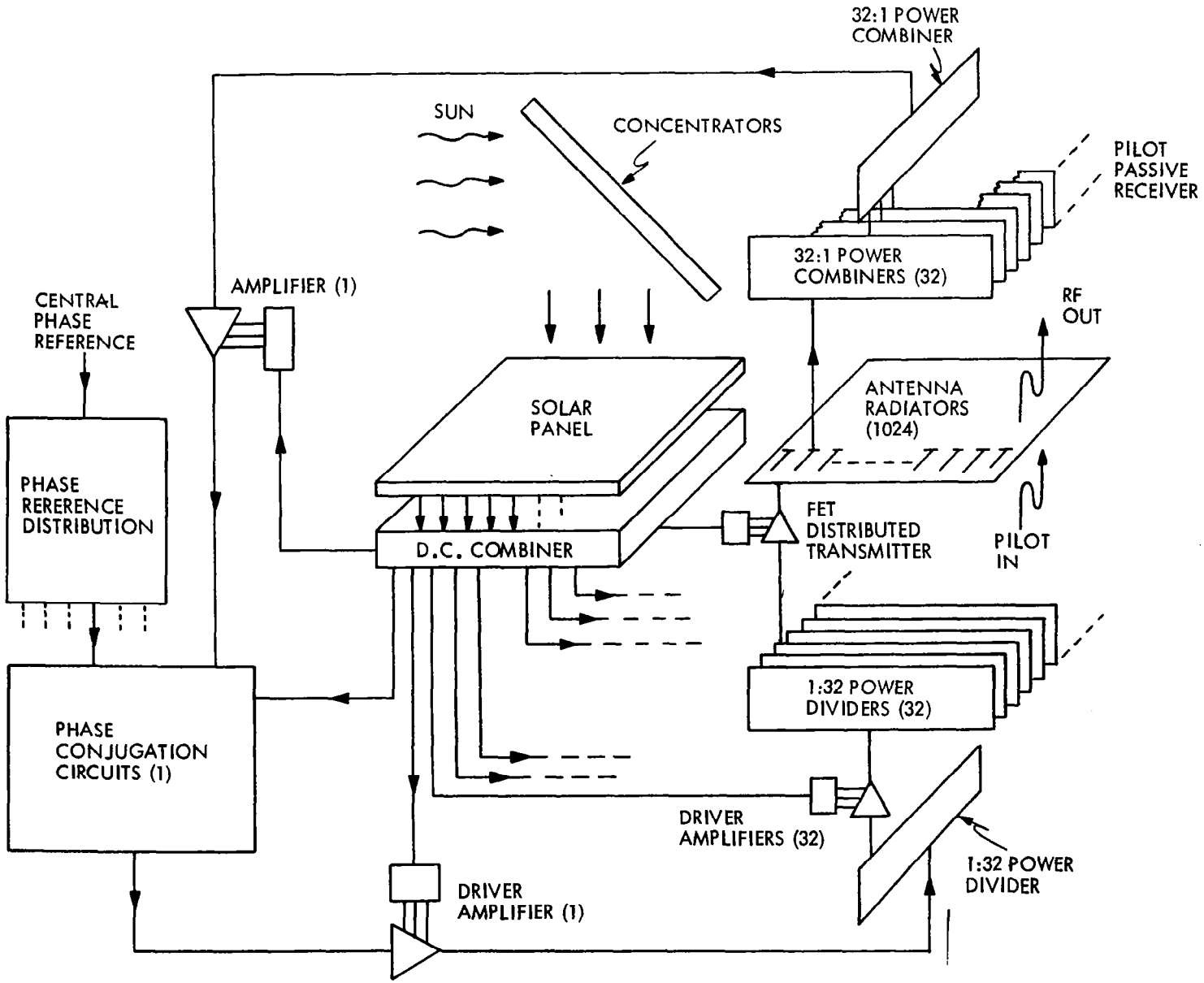

SPACETENNA - DIPOLE CONCEPT

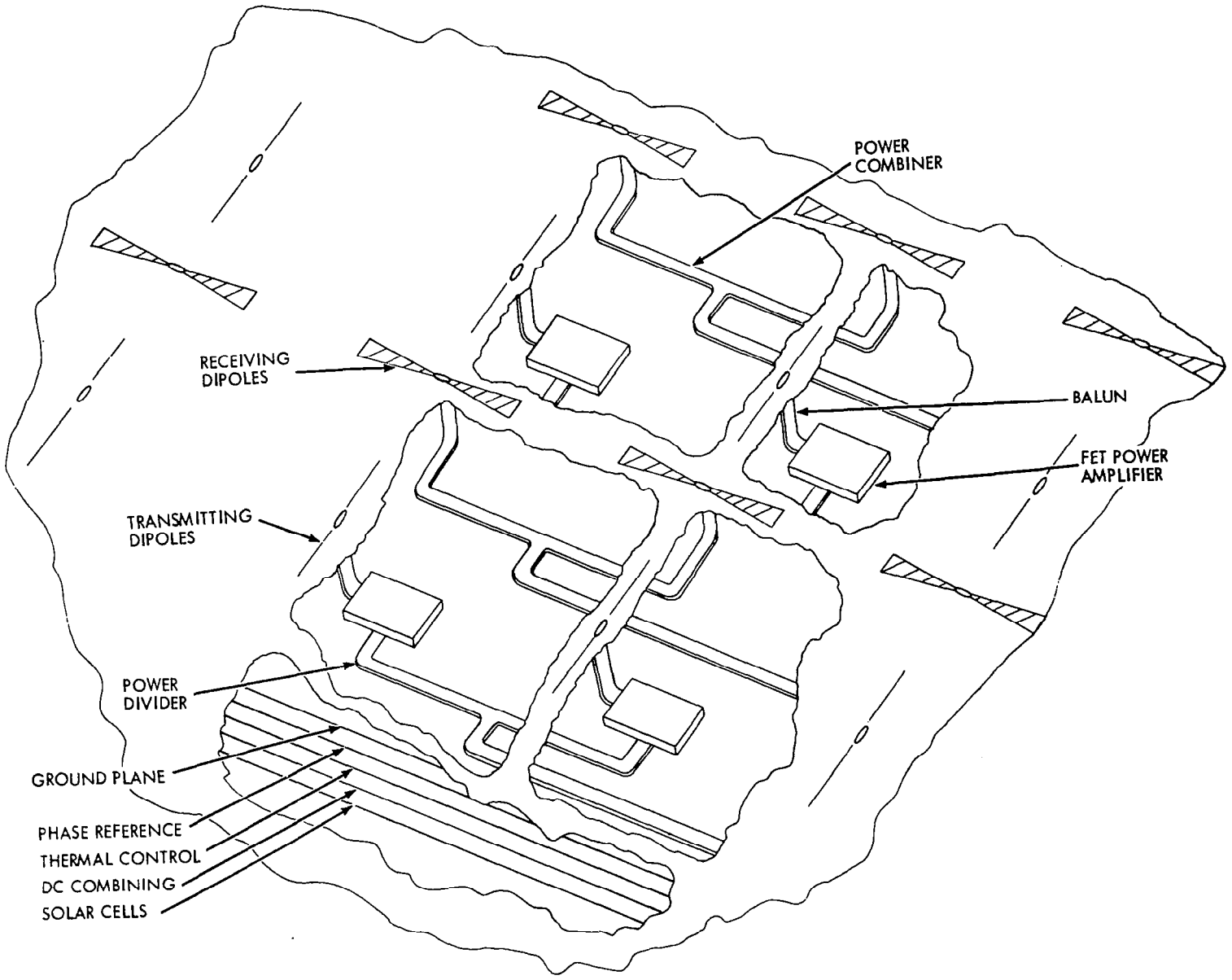

PRELIMINARY ESTIMATES OF POWER TRANSMISSION AND CONVERSION EFFICIENCY CHAIN

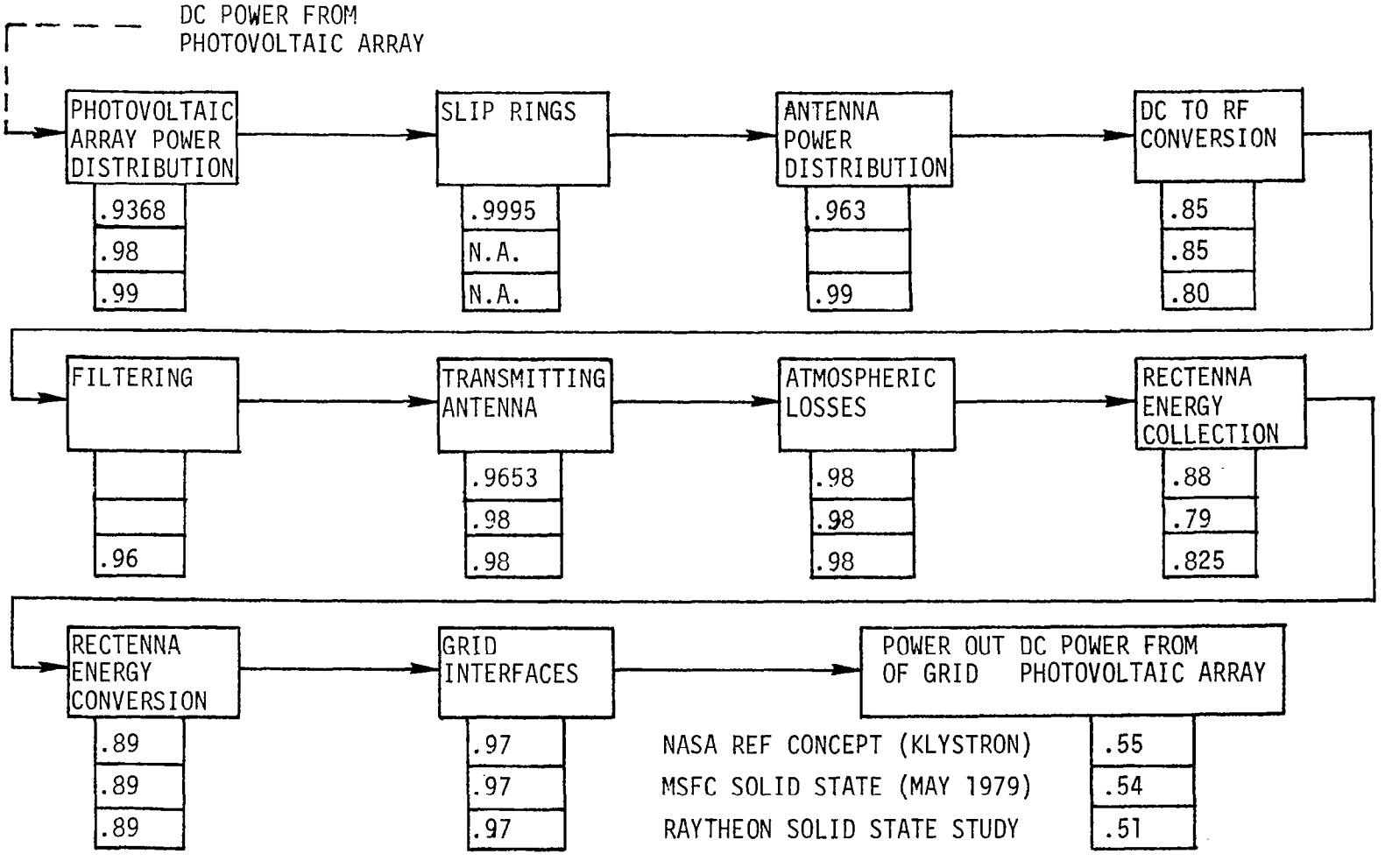

ISSUES/CONSIDERATIONS

- LOW VOLTAGE DISTRIBUTION
- HARMONIC AND NOISE SUPPRESSION
- SUBARRAY SIZE
- MONOLITHIC TECHNOLOGY
- LIFETIME
- MUTUAL COUPLING
- INPUT TO OUTPUT ISOLATION
- CHARGED PARTICLE RADIATION EFFECTS
- TOPOLOGICAL CONSIDERATIONS
- SIDELOBE SUPPRESSION

ISSUES/CONSIDERATIONS	RESOLUTION/STATUS
• LOW VOLTAGE DISTRIBUTION	FURTHER REFINEMENT REQUIRED TO MINIMIZE WEIGHT AND CONTROL THERMAL LEAKAGE

- HARMONIC AND NOISE SUPPRESSION
- SUBARRAY SIZE
- MONOLITHIC TECHNOLOGY
- LIFETIME
- MUTUAL COUPLING
- INPUT TO OUTPUT ISOLATION
- CHARGED PARTICLE RADIATION EFFECTS
- TOPOLOGICAL CONSIDERATIONS
- SIDELOBE SUPPRESSION

DC POWER CHARACTERISTICS OF SANDWICH

- DC POWER FROM PHOTOVOLTAIC BLANKET (PVB) TRANSMITTED TO POWER DISTRIBUTION LAYERS (+ GRID, - GROUND PLANE) (CONDUCTOR LENGTHS <20 CM).
- NEAR-UNIFORM VOLTAGE DIFFERENTIAL IS AVAILABLE CLOSE TO ALL USING EQUIPMENT ACROSS A SUBARRAY (15 V NOMINAL). LOCAL POWER CONDITIONING PROVIDED AT EACH AMPLIFIER MODULE.
- DC CONDUCTOR INCLUDING GROUND PLANE CROSS SECTIONS AND WEIGHT KEPT SMALL TO MINIMIZE "UNCONTROLLABLE" HEAT TRANSFER TO RF DEVICES HAVING LOWER CRITICAL JUNCTION TEMPERATURES THAN THOSE ASSOCIATED WITH PHOTOVOLTAIC PORTION OF SANDWICH.
  - TRANSFER OF POWER BETWEEN SUBARRAYS IS LIMITED BY GENERAL HEAT TRANSFER LIMITS AND BLOCKAGE FROM WASTE HEAT RADIATION POINT OF VIEW.
  - TRANSFER OF POWER FROM POWER GRID AND GROUND PLANE TO USING EQUIPMENT IS BY SHORT (DESIGN CONTROLLED) CONDUCTORS WITH BUILT-IN FUSES TO ISOLATE EQUIPMENT OVER-CURRENT FAILURES FROM THE POWER GRID AND GROUND PLANE.
- SPECIFIC WEIGHT OF GROUND PLANE IS .005 GM/WATT AND OF GRID IS .002 GM/WATT (WATTS ARE DC FROM PVB) FOR A SUBARRAY.

ISSUES/CONSIDERATIONS	RESOLUTION/STATUS
• LOW VOLTAGE DISTRIBUTION	
• HARMONIC AND NOISE SUPPRESSION	FREQUENCY ALLOCATION NEEDS AT HARMONICS SHOULD BE CONSIDERED OR CONSIDER SPREAD SPECTRUM AND ACTIVE SUPPRESSION
• SUBARRAY SIZE	
• MONOLITHIC TECHNOLOGY	
• LIFETIME	
• MUTUAL COUPLING	
• INPUT TO OUTPUT ISOLATION	
• CHARGED PARTICLE RADIATION EFFECTS	
• TOPOLOGICAL CONSIDERATIONS	
• SIDELOBE SUPPRESSION	

HARMONIC NOISE GENERATION, SUPPRESSION AND TRANSMISSION CHARACTERISTICS

- NOISE FILTERS ARE PROVIDED AT THE ELEMENT MODULE LEVEL ON TRANSMIT AND AT THE SUBARRAY CONJUGATING ELECTRONICS LEVEL ON RECEIVE.
- RESIDUAL NOISE IS NON-COHERENT BETWEEN SUBARRAYS.
- RESIDUAL HARMONICS MAY PERIODICALLY BE COHERENT OVER TOTAL TRANSMITTING ARRAY.
- NOISE AT EARTH IS ESTIMATED AS -181 DBW/M^2/4 KHZ.
- HARMONIC POWER DENSITY AT EARTH IS ESTIMATED AS -66 DBW/M^2 AT 3RD HARMONIC AND LESS AT HIGHER HARMONICS. GRATING LOBES FOR LOWER HARMONICS DO NOT INTERSECT THE EARTH.
- FREQUENCY ALLOCATION AT 3RD AND HIGHER HARMONICS SHOULD BE CONSIDERED. SPREAD SPECTRUM AND ACTIVE SUPPRESSION CONCEPTS SHOULD BE INVESTIGATED AS POSSIBLE MITIGATING APPROACHES.

ISSUES/CONSIDERATIONS	RESOLUTION/STATUS
• LOW VOLTAGE DISTRIBUTION	
• HARMONIC AND NOISE SUPPRESSION	
• SUBARRAY SIZE	3M X 3M MAY BE CLOSE TO OPTIMUM, FURTHER STUDY OF IMPLEMENTATION REQUIRED
• MONOLITHIC TECHNOLOGY	
• LIFETIME	
• MUTUAL COUPLING	
• INPUT TO OUTPUT ISOLATION	
• CHARGED PARTICLE RADIATION EFFECTS	
• TOPOLOGICAL CONSIDERATIONS	
• SIDELOBE SUPPRESSION	

SUBARRAY CHARACTERISTICS

THE FOLLOWING HAVE BEEN CONSIDERED IN SIZING OF THE SUBARRAY:

- TOPOLOGICAL CONSIDERATIONS TO MINIMIZE ELEMENT SPACING (MAXIMIZE TRANSMITTED POWER DENSITY), MINIMIZE DIVISIONS OF DRIVE POWER (MAXIMIZE EFFICIENCY) AND PROVIDE FOR OTHER FUNCTIONS WITH MINIMUM LAYERING (MINIMIZE INTER-LAYER CONNECTIONS) RESULTED IN A BASELINE SIZE OF 3.2M X 3.2M.

- SUBARRAY STEERING AND POINTING CONSIDERED SATISFACTORY.

- ARRAY FLATNESS CONSIDERED TO IMPOSE NO OVER-RIDING ISSUES.

- REMAINING COMPLEXITIES ARE PRIMARILY IN PACKAGING, THERMAL AND INTERFACING BETWEEN SUBARRAYS.

- KNOWN SPECIFIC WEIGHT ($\sim$3 KG/M^2) FOR 3.2M X 3.2M SUBARRAY MAY BE REDUCED BY 1% FOR 6.4M x 6.4M SUBARRAY WHILE POSSIBLE COMPLEXITY, HANDLING AND LOSSES NULLIFY THE KNOWN ADVANTAGE.

- LOSSES UNIQUE TO THE SUBARRAY ABOVE THE ELEMENT CELL LEVEL (ELEMENT SPACING 10 CM) HAVE BEEN ESTIMATED TO BE < 0.5%.

- NEAR-IN SIDELOBE INCREASES DUE TO THE SUBARRAY HAVE BEEN ESTIMATED TO BE <0.2 DB.

ISSUES/CONSIDERATIONS	RESOLUTION/STATUS
• LOW VOLTAGE DISTRIBUTION	
• HARMONIC AND NOISE SUPPRESSION	
• SUBARRAY SIZE	
• MONOLITHIC TECHNOLOGY	MONOLITHIC APPROACHES APPLY AND REQUIRE TECHNOLOGY DEVELOPMENT FOR MINIMIZATION OF COST AND WEIGHT
• LIFETIME	
• MUTUAL COUPLING	
• INPUT TO OUTPUT ISOLATION	
• CHARGED PARTICLE RADIATION EFFECTS	
• TOPOLOGICAL CONSIDERATIONS	
• SIDELOBE SUPPRESSION	

MONOLITHIC TECHNOLOGY FOR THE SANDWICH

- THE GENERAL CONCEPT OF MONOLITHIC TECHNOLOGY TO INCORPORATE MULTIPLE FUNCTIONS INTO ONE SERIES OF PROCESS AT BOTH THE AMPLIFIER LEVEL AND AT THE ANTENNA LAYER LEVEL IS THE SELECTED APPROACH FOR HIGH PRODUCTION RATE AND LOW COST PURPOSES.

- TOTAL SANDWICH CONCEPTS INCLUDE INTERCONNECTIONS BETWEEN LAYERS AND BETWEEN SUBARRAYS.

ISSUES/CONSIDERATIONS	RESOLUTION/STATUS
• LOW VOLTAGE DISTRIBUTION	
• HARMONIC AND NOISE SUPPRESSION	
• SUBARRAY SIZE	
• MONOLITHIC TECHNOLOGY	
• LIFETIME	LIFETIME AFFECTED BY JUNCTION TEMPERATURE LIMITS AND CHARGED PARTICLES RADIATION REQUIRING TECHNOLOGY DEVELOPMENT IN BOTH AREAS.
• MUTUAL COUPLING	
• INPUT TO OUTPUT ISOLATION	
• CHARGED PARTICLE RADIATION EFFECTS	
• TOPOLOGICAL CONSIDERATIONS	
• SIDELOBE SUPPRESSION	

LIFETIME CONSIDERATIONS

- LIFETIME GOAL IS 30 YEARS WITH LOW PROBABILITY OF FAILURE.
- PRIMARY FAILURE MECHANISMS RELATE MOST DIRECTLY TO JUNCTION TEMPERATURE.
- RANGE OF INTEREST FOR JUNCTION TEMPERATURE IS $100^{o}C$ TO $150^{o}C$ REQUIRING ADVANCED TECHNOLOGY DEVELOPMENT FOR LONG LIFE.
- HEAT GENERATION AT AMPLIFIER DEVICES IS PRIMARY CONTRIBUTOR TO HIGH JUNCTION TEMPERATURE. ADVANCED TECHNOLOGY DEVELOPMENT REQUIRED FOR HIGH EFFICIENCY.
- HEAT TRANSPORT FROM DEVICE TO WASTE HEAT RADIATOR IS A MAJOR SANDWICH DESIGN CONSIDERATION INVOLVING:
  - HIGH CONDUCTIVITY MATERIALS
  - DEDICATED REGIONS FOR WASTE HEAT RADIATION TO COLD SPACE
  - HIGH EMISSIVITY AND LOW ABSORPTIVITY THERMAL CONTROL SURFACES TO MAXIMIZE WASTE HEAT DISSIPATION WITHOUT EXCEEDING LONG-LIFE JUNCTION TEMPERATURES
- MATERIALS AND COATINGS MUTUAL TECHNOLOGY DEVELOPMENT GOALS HAVE BEEN ESTABLISHED
  - MATERIALS SUCH AS PYROLYTIC GRAPHITE, HAVING HIGH THERMAL CONDUCTIVITY, IN CONJUNCTION WITH HIGH PERFORMANCE THERMAL CONTROL COATINGS NEED TECHNOLOGY DEVELOPMENT TO ASSURE INTEGRITY AND PERFORMANCE OF HIGH EMISSIVITY AND LOW ABSORPTIVITY SURFACES.
  - WHERE WEIGHT IS NOT A SIGNIFICANT FACTOR COPPER MAY BE SATISFACTORY.
- OPTIMIZATION TOOLS HAVE BEEN CONCEIVED TO MAXIMIZE THE ABILITY OF THE TOTAL SANDWICH TO TRANSMIT HIGH POWER DENSITY.

AMPLIFIER JUNCTION TEMPERATURE VS WASTE HEAT

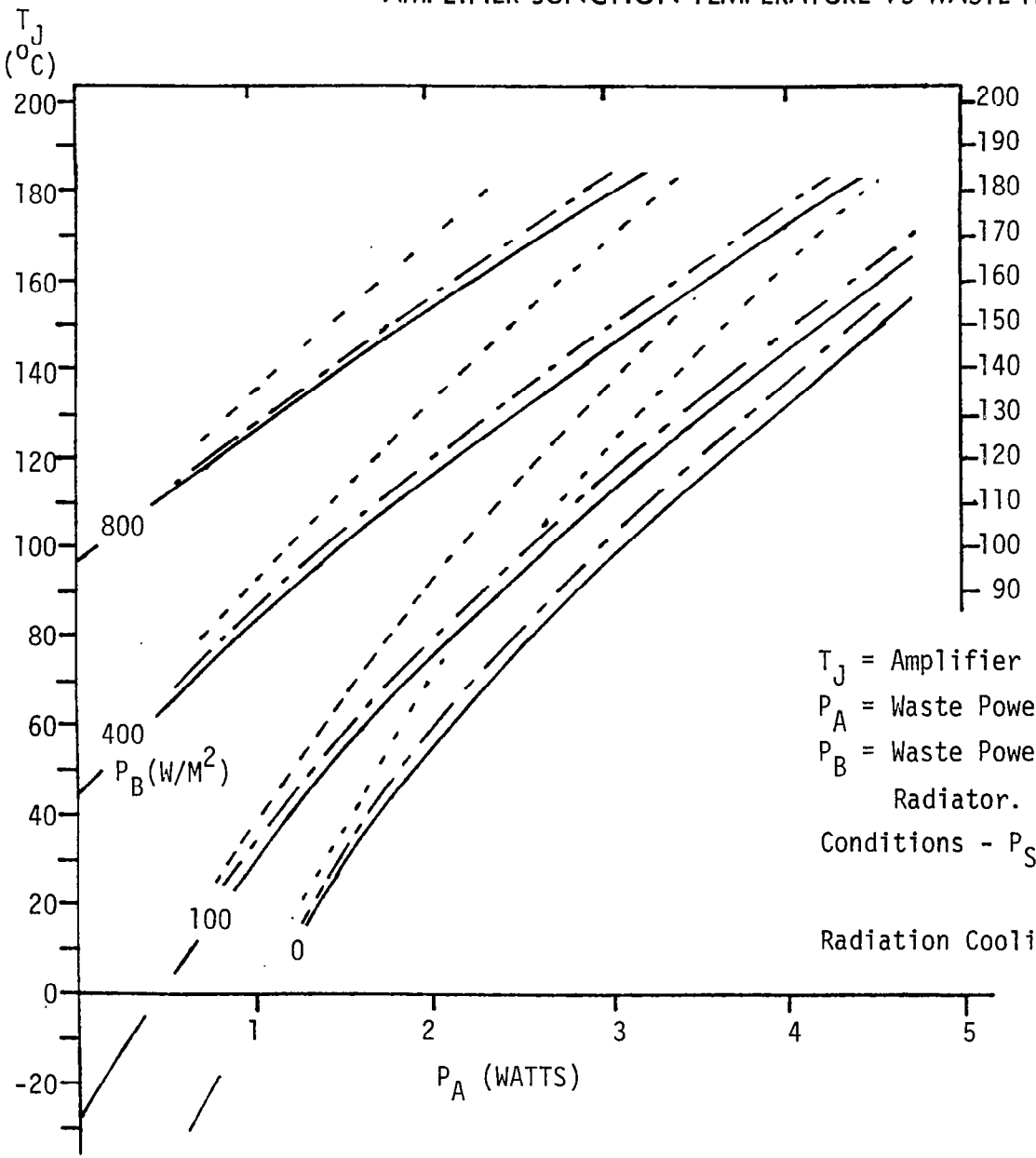

ε = 0.8 Thermal Control
α = 0.05 Coating Wt = 1.59 gm
Dia = 8.66 cm
t_{root} = 1.0 mm
t_{tip} = 0.1 mm

	Thermal Conductor Wt. (gm)
Aluminum _ _ _ _ _ _ _	6.35
Copper ___ _ ___ _ ___	20.94
Pyrographite _____	5.29

T_J = Amplifier Junction Temperature
P_A = Waste Power Generated at Amplifier Junction
P_B = Waste Power w/m^2 - Uniform Over Thermal Radiator.

Conditions - P_S = Incident Solar Power (1300 W/m^2)

Radiation Cooling - To Absolute Zero

SUBARRAY LAYOUT - TYPICAL CORNER AND SECTION

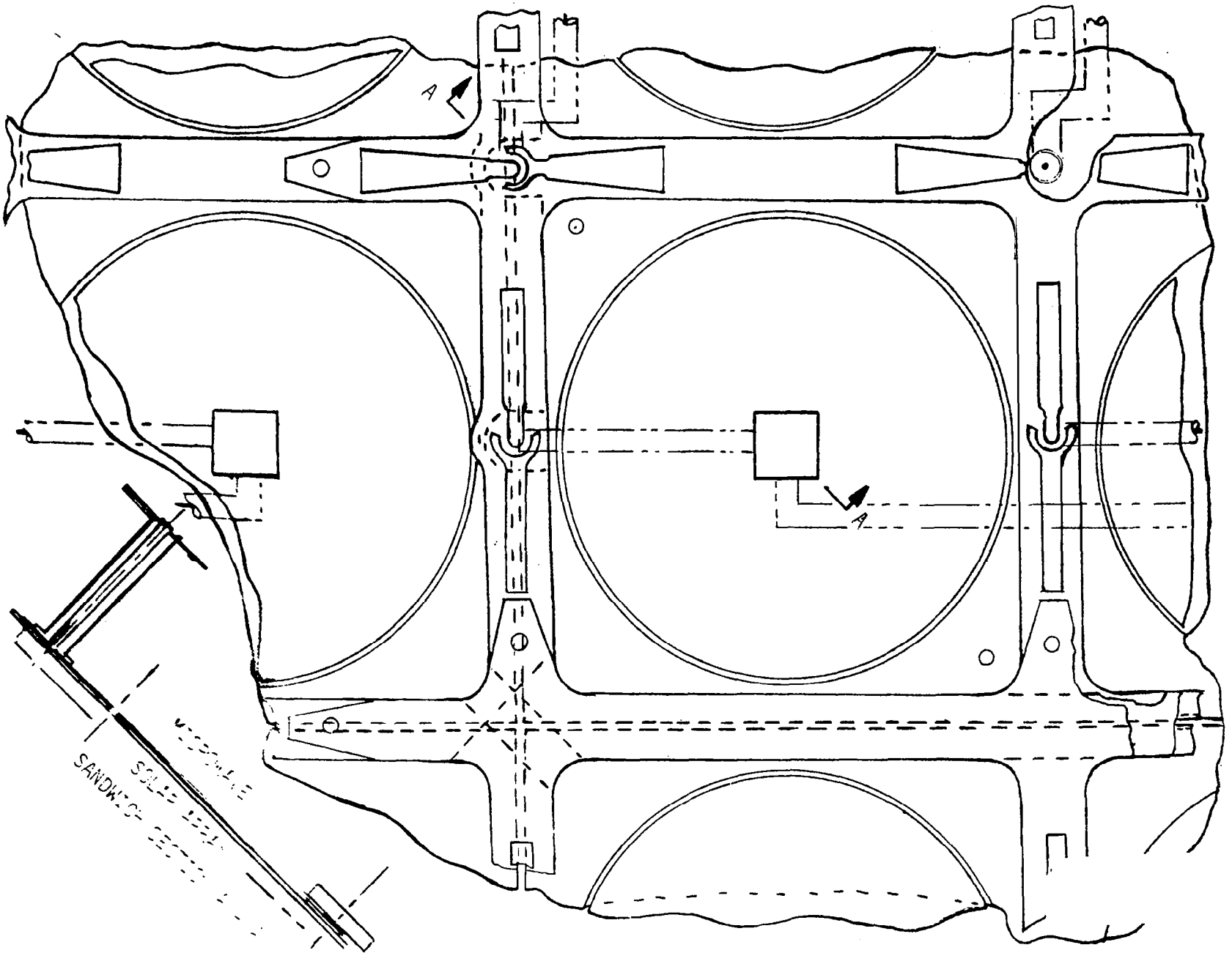

ACCELERATED LIFE DATA AND PROJECTIONS
FOR SOLID STATE SPS MPTS STUDY

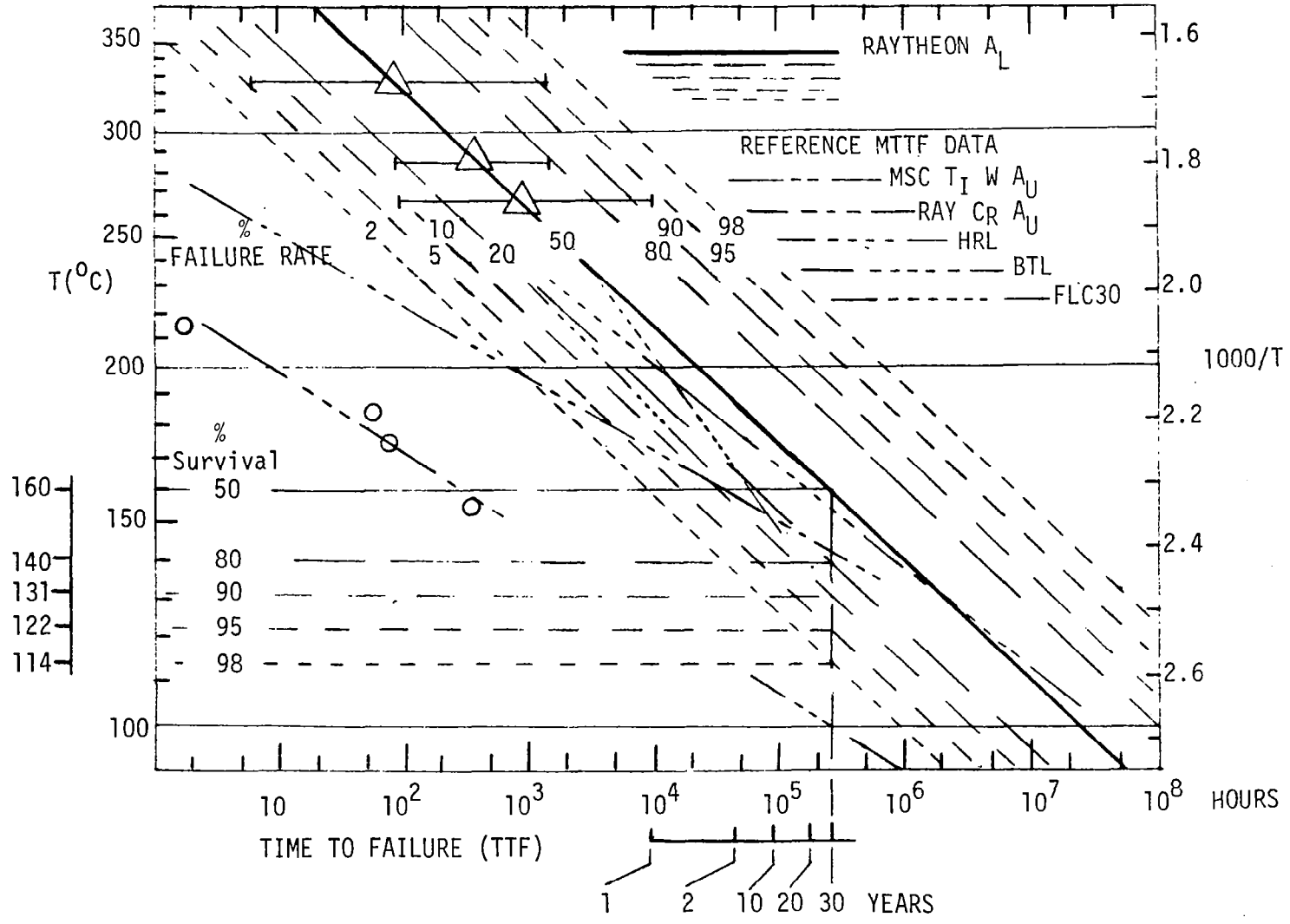

POWER PER ELEMENT CELL (10 CM X 10 CM) RELATIONSHIPS

- o PYROGRAPHITE RADIATORS (8.66 CM DIA)
- o AMPLIFIER EFFICIENCY = 0.8
- o DC TO RF EFFICIENCY = 0.7377

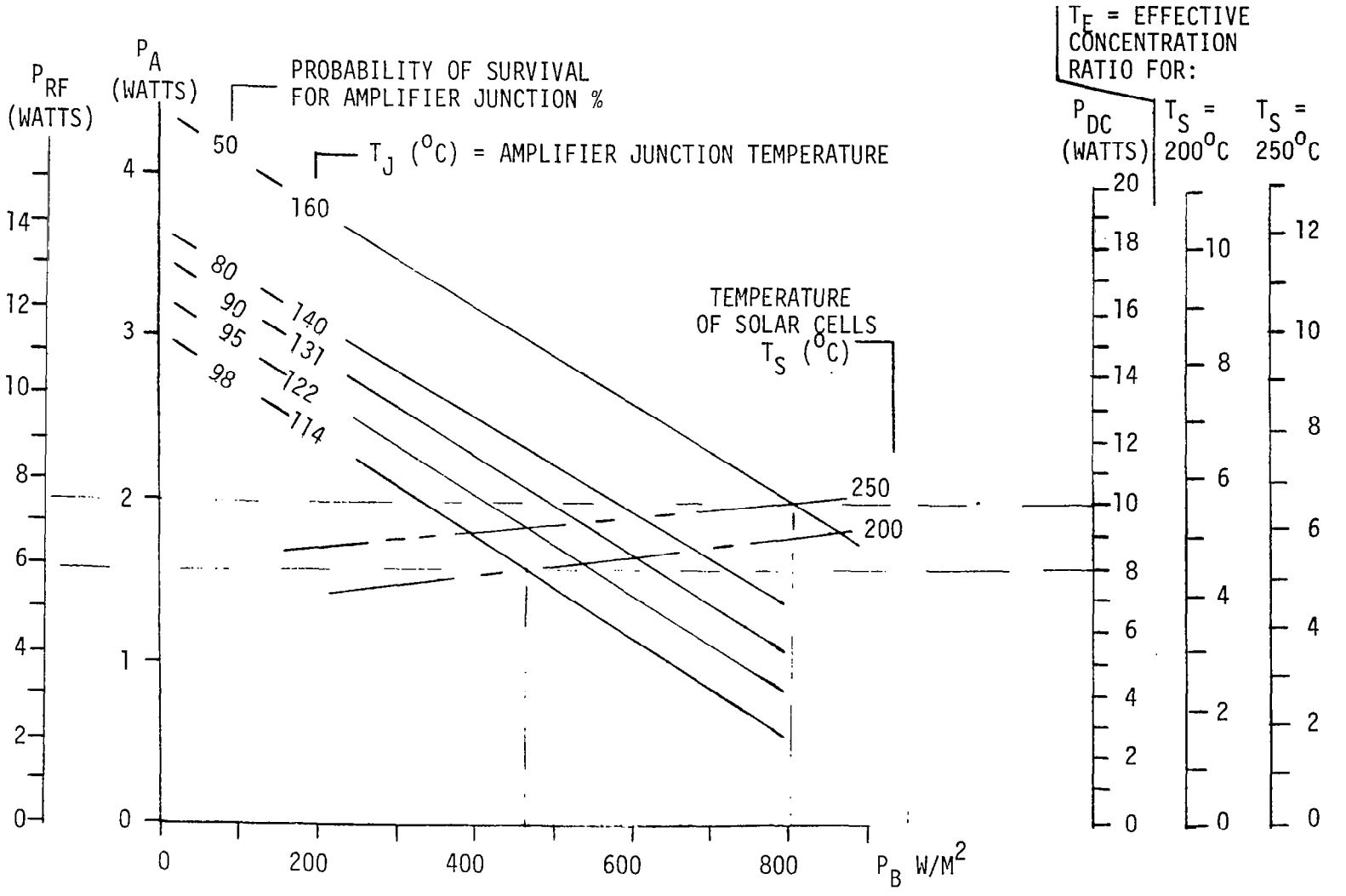

P_B = THERMAL POWER FROM SOLAR CELLS RADIATED FROM MICROWAVE ARRAY

ISSUES/CONSIDERATIONS	RESOLUTION/STATUS
• LOW VOLTAGE DISTRIBUTION	
• HARMONIC AND NOISE SUPPRESSION	
• SUBARRAY SIZE	
• MONOLITHIC TECHNOLOGY	
• LIFETIME	
• MUTUAL COUPLING	IMPLEMENTATION BY PRINTED DIPOLES SPACED FROM GROUND PLANE WITH BALUN IN CIRCUITRY AND CLOSE ELEMENT SPACING TO MINIMIZE DETRIMENTAL MUTUAL COUPLING EFFECTS
• INPUT TO OUTPUT ISOLATION	
• CHARGED PARTICLE RADIATION EFFECTS	
• TOPOLOGICAL CONSIDERATIONS	
• SIDELOBE SUPPRESSION	

MUTUAL COUPLING CONSIDERATIONS

- ELEMENT SPACING (0.8 λ) TO SUPPRESS GRATING LOBES.
- PHYSICAL IMPLEMENTATION OF DIPOLES SUPPORTED ABOVE (0.25 λ) GROUND PLANE TO PREVENT SURFACE WAVE RESONANCES AND PROVIDE BALUN ACTION.
- DIPOLES AND TRANSFORMERS INCORPORATED IN CIRCUITRY USED FOR IMPEDANCE MATCHING IN PRESENCE OF MUTUAL COUPLING AMONG ELEMENTS.

ISSUES/CONSIDERATIONS	RESOLUTION/STATUS
• LOW VOLTAGE DISTRIBUTION	
• HARMONIC AND NOISE SUPPRESSION	
• SUBARRAY SIZE	
• MONOLITHIC TECHNOLOGY	
• LIFETIME	
• MUTUAL COUPLING	
• INPUT TO OUTPUT ISOLATION	ORTHOGONAL DIPOLES, OFFSET FREQUENCIES AND FILTERING PROVIDE SATISFACTORY ISOLATION OF TRANSMIT FROM RECEIVE SIGNALS
• CHARGED PARTICLE RADIATION EFFECTS	
• TOPOLOGICAL CONSIDERATIONS	
• SIDELOBE SUPPRESSION	

INPUT TO OUTPUT ISOLATION

- TRANSMIT AND RECEIVE DIPOLES ARE ORTHOGONAL TO MAXIMIZE INPUT/OUTPUT ISOLATION.
- SEPARATE PILOT FREQUENCIES FROM FUNDAMENTAL (OUTSIDE HIGH NOISE BAND).
- FILTERING PROVIDED ON PILOT RECEIVER WILL BE IMPLEMENTED AT THE PHASE CONJUGATION NETWORK AT THE SUBARRAY LEVEL.

ISSUES/CONSIDERATIONS	RESOLUTION/STATUS
• LOW VOLTAGE DISTRIBUTION	
• HARMONIC AND NOISE SUPPRESSION	
• SUBARRAY SIZE	
• MONOLITHIC TECHNOLOGY	
• LIFETIME	
• MUTUAL COUPLING	
• INPUT TO OUTPUT ISOLATION	
• CHARGED PARTICLE RADIATION EFFECTS	GaAs IS CURRENTLY BEST TECHNOLOGY (REQUIRES MORE ADVANCEMENT IN "MECHANISMS" OF FAILURE)
• TOPOLOGICAL CONSIDERATIONS	
• SIDELOBE SUPPRESSION	

CHARGED PARTICLE RADIATION EFFECTS/CONSIDERATIONS

- VAN ALLEN BELT DISTRIBUTION OF ELECTRONS GEOMAGNETICALLY GO OUT TO 40-50K NAUTICAL MILES. NO SINGLE PEAK BUT VARIES IN TIME.
- 11 YEAR SOLAR SUNSPOT CYCLE RESULTS IN CHARGED ELECTRONS AND PROTONS HAVING POSSIBLY SIGNIFICANT EFFECTS.
- SOLAR WINDS RESULT IN LOW ENERGY ELECTRONS HAVING MUCH SMALLER EFFECTS THAN CHARGED PARTICLES TRAPPED IN VAN ALLEN BELTS.
- GaAs MESFETS TEND TO BE HARDEST OF EXISTING TECHNOLOGIES.
- TEST RESULTS ARE NON-CONCLUSIVE RE FAILURE OR DEGRADATION MECHANISMS AND EFFECTS OF PROTECTIVE SCHEMES.
- SELECTION OF GaAs TECHNOLOGY AND SHIELDING APPEAR TO BE MOST EFFECTIVE APPROACH AT PRESENT.
- ADVANCED TECHNOLOGY DEVELOPMENT REQUIRED TO ADDRESS MATERIALS, FAILURE MECHANISMS AND PROTECTIVE SCHEMES.

ISSUES/CONSIDERATIONS	RESOLUTION/STATUS
• LOW VOLTAGE DISTRIBUTION	
• HARMONIC AND NOISE SUPPRESSION	
• SUBARRAY SIZE	
• MONOLITHIC TECHNOLOGY	
• LIFETIME	
• MUTUAL COUPLING	
• INPUT TO OUTPUT ISOLATION	
• CHARGED PARTICLE RADIATION EFFECTS	
• TOPOLOGICAL CONSIDERATIONS	REQUIRED FUNCTIONS CAN BE IMPLEMENTED IN SANDWICH CONCEPT. FURTHER DETAILS AT SUBARRAY BOUNDARIES REQUIRED.
• SIDELOBE SUPPRESSION	

TOPOLOGICAL CONSIDERATIONS

TOPOLOGICAL CONSIDERATIONS HAVE BEEN GIVEN AT THE TOTAL ARRAY, PHASE DISTRIBUTION SYSTEM, SUBARRAY AND ELEMENT MODULE LEVELS.

- STRUCTURAL SUPPORT FOR THE ARRAY IS CONSIDERED TO BE PROVIDED BY MAJOR STRUCTURAL RING AT PERIPHERY WITH TENSION GRID ASSURING RELATIVE FLATNESS. GRID MEMBERS ARE CONSIDERED TO BE SMALL WITH RESPECT TO SANDWICH THICKNESS AND DO NOT SHIELD RF OR WASTE HEAT RADIATION.

- MECHANICAL SUPPORT AT SUBARRAY BOUNDARIES ARE REQUIRED LARGELY FOR HANDLING, INSTALLATION AND REPLACEMENT PURPOSES. DETAILS OF HOW SUBARRAYS WILL BE MATED TO PRECLUDE ADVERSE DISCONTINUITIES ARE YET TO BE DEVELOPED.

- RF TRANSMIT ELEMENT LATTICE IS MAINTAINED IN REGION OF SUBARRAY EDGES TO MINIMIZE SYSTEMATIC ERROR SIDELOBES.

- FREE RADIATION OF WASTE HEAT FROM RADIATORS NEAR SUBARRAY EDGES IS COMPROMISED REQUIRING CUSTOMIZED EDGE TREATMENT TO MAXIMIZE THE EFFICIENCIES OF THE THERMAL RADIATORS AT THE EXPENSE OF WEIGHT AND COST. FURTHER INVESTIGATION IS REQUIRED.

ISSUES/CONSIDERATIONS	RESOLUTION/STATUS
• LOW VOLTAGE DISTRIBUTION	
• HARMONIC AND NOISE SUPPRESSION	
• SUBARRAY SIZE	
• MONOLITHIC TECHNOLOGY	
• LIFETIME	
• MUTUAL COUPLING	
• INPUT TO OUTPUT ISOLATION	
• CHARGED PARTICLE RADIATION EFFECTS	
• TOPOLOGICAL CONSIDERATIONS	
• SIDELOBE SUPPRESSION	SINGLE STEP EDGE TAPER MAY BE REQUIRED

SIDELOBE SUPPRESSION CONSIDERATIONS

- UNIFORM VERSUS 10 DB GAUSSIAN ILLUMINATION AT SPACETENNA RESULTS IN THE FOLLOWING:

ADVANTAGES FOR UNIFORM

- SMALLEST TRANSMIT ANTENNA
- ALL AMPLIFIER MODULES OPERATE AT SAME POWER LEVEL
- EASY TRANSFER OF DC VOLTAGES FROM SOLAR ARRAY (IF DENSITY TAPERING IS EMPLOYED TO APPROXIMATE GAUSSIAN ILLUMINATION THEN DC DISTRIBUTION AND SOLAR ARRAY ARCHITECTURE BECOMES COMPLEX AND HEAVIER)

DISADVANTAGES FOR UNIFORM

- LOWER POWER BEAM EFFICIENCY
- HIGHER SIDELOBES (-17 DB, -24 DB, -28 DB BELOW 23 MW/CM^2 AND MORE LAND REQUIRED TO FENCE RECTENNA

- SINGLE STEP TAPER VERSUS UNIFORM (CONSTANT POWER DENSITY AT EACH LEVEL)

ADVANTAGES FOR STEP

- LOWER SIDELOBES (-28 DB BELOW 23 MW/CM^2)
- ALL AMPLIFIERS OPERATED AT SAME POWER LEVEL

DISADVANTAGES FOR STEP

- LESS POWER AVAILABLE
- LARGER SPACETENNA

SIDELOBE COMPARISON OF UNIFORM POWER DISTRIBUTION WITH TWO EXAMPLES OF SINGLE STEP EDGE TAPER

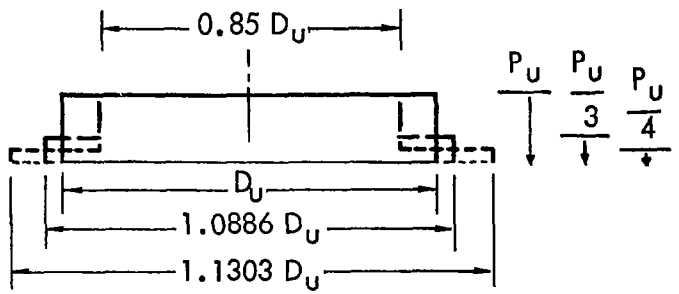

TRANSMITTING ANTENNA

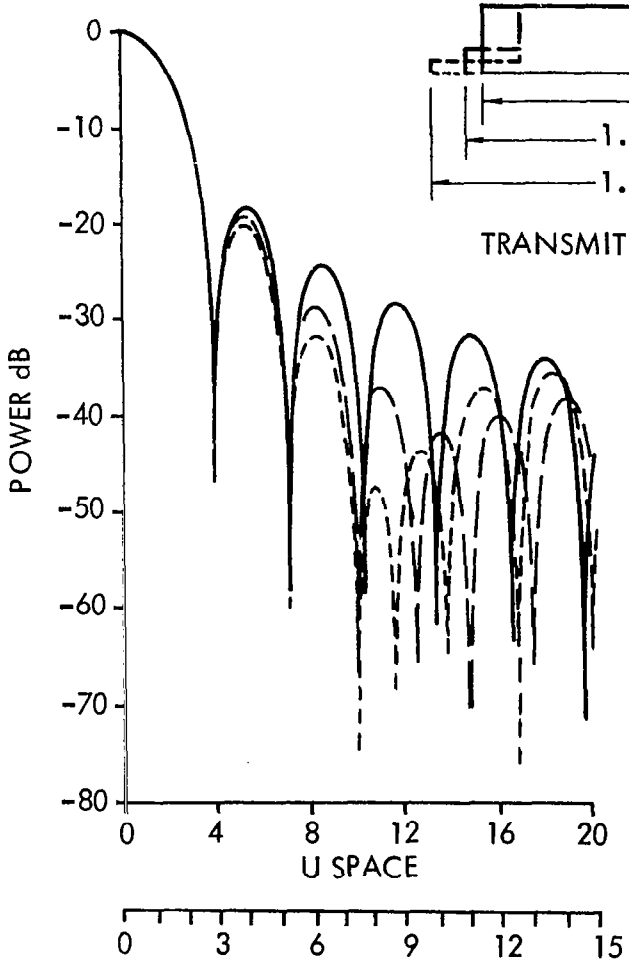

KEY:

——— UNIFORM POWER DISTRIBUTION

— — — 1/3 STEP AT EDGE

------ 1/4 STEP AT EDGE

P_U = POWER DENSITY AT TRANSMITTING ANTENNA

D_U = DIAMETER AT TRANSMITTING ANTENNA FOR UNIFORM POWER DISTRIBUTION

U SPACE

$U = \frac{\pi D_U \sin\theta}{\lambda}$

λ = WAVE LENGTH

θ = BEAM WIDTH (HALF ANGLE)

SUMMARY AND CONCLUSIONS

SOLID STATE SANDWICH CONCEPT ISSUES AND RESOLUTION SUMMARY

ISSUES/CONSIDERATIONS	RESOLUTION/STATUS
LOW VOLTAGE DISTRIBUTION	FURTHER REFINEMENT REQUIRED TO MINIMIZE WEIGHT AND CONTROL THERMAL LEAKAGE
HARMONIC AND NOISE SUPPRESSION	FREQUENCY ALLOCATION NEEDS AT HARMONICS SHOULD BE CONSIDERED OR CONSIDER SPREAD SPECTRUM AND ACTIVE SUPPRESSION
SUBARRAY SIZE	3M X 3M MAY BE CLOSE TO OPTIMUM, FURTHER STUDY OF IMPLEMENTATION REQUIRED
MONOLITHIC TECHNOLOGY	MONOLITHIC APPROACHES APPLY AND REQUIRE TECHNOLOGY DEVELOPMENT FOR MINIMIZATION OF COST AND WEIGHT
LIFETIME	LIFETIME AFFECTED BY JUNCTION TEMPERATURE LIMITS AND CHARGED PARTICLE RADIATION REQUIRING TECHNOLOGY DEVELOPMENT IN BOTH AREAS
MUTUAL COUPLING	IMPLEMENTATION BY PRINTED DIPOLES SPACED FROM GROUND PLANE WITH BALUN IN CIRCUITRY AND CLOSE ELEMENT SPACING TO MINIMIZE DETRIMENTAL MUTUAL COUPLING EFFECTS
INPUT TO OUTPUT ISOLATION	ORTHOGONAL DIPOLES, OFFSET FREQUENCIES AND FILTERING PROVIDE SATISFACTORY ISOLATION OF TRANSMIT FROM RECEIVE SIGNALS
CHARGED PARTICLE RADIATION EFFECTS	GaAs IS CURRENTLY BEST TECHNOLOGY (REQUIRES MORE ADVANCEMENT IN "MECHANISMS" OF FAILURE)
TOPOLOGICAL CONSIDERATIONS	REQUIRED FUNCTIONS CAN BE IMPLEMENTED IN SANDWICH CONCEPT. FURTHER DETAILS AT SUBARRAY BOUNDARIES REQUIRED.
SIDELOBE SUPPRESSION	SINGLE STEP EDGE TAPER MAY BE REQUIRED.

AMPLIFIER THERMAL MODEL

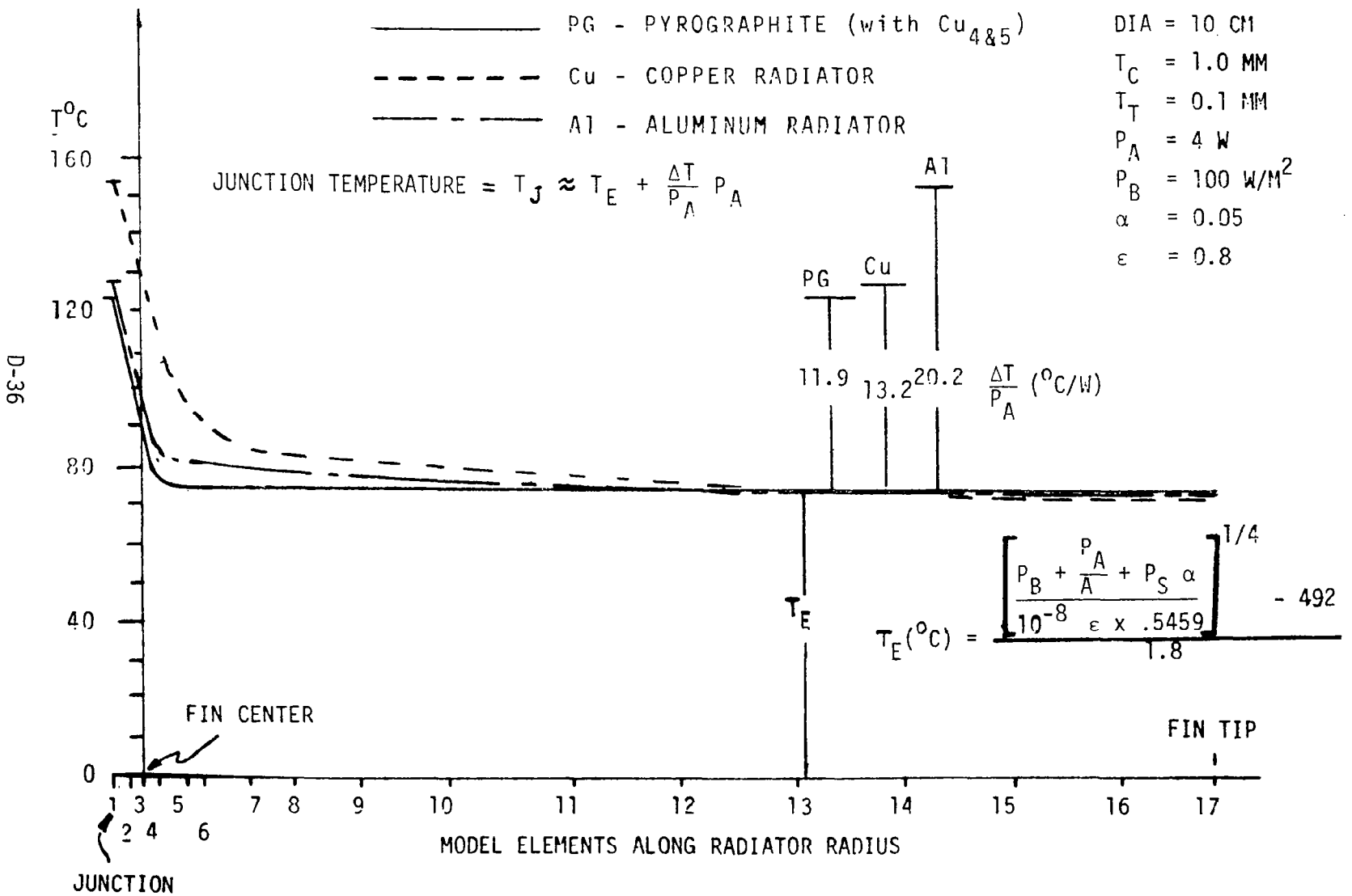

RECTENNA SIZE VS BEAM EFFICIENCY - UNIFORM ILLUMINATION

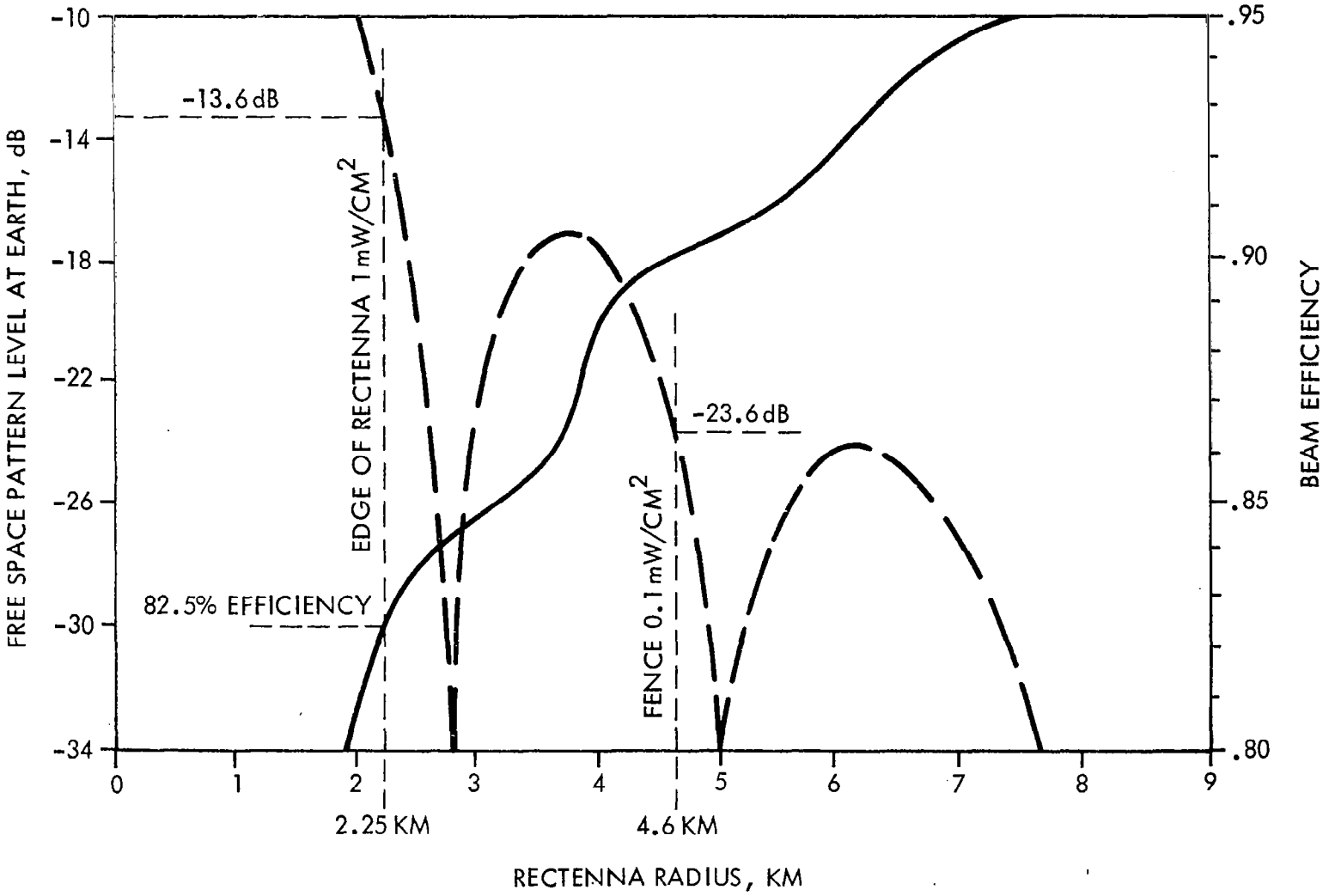

SOLID STATE SANDWICH CONCEPT DESIGNS AND ISSUES

VUGRAPH NUMBERS AND SCREEN LOCATIONS

TIME (MINUTES)	LEFT	CENTER	RIGHT
.01	-	C1	-
1.0	L2	-	-
1.0	-	-	R3
1.0	-	C4	-
0.5	L2	C5	R3
1.0	L6-1	C7	R3
1.0	L6-2	C8	-
0.5	L6-3	C9	R3
0.5	L6-4	C10	R3
2.0	L6-5	C11	-
3.0	L12	C11	R13
1.0	L12	C14	R13
1.0	L12	C14	R15
1.0	L6-5	-	R15
0.5	L6-6	C16	R3
0.5	L6-7	C17	R3
1.0	L6-8	C18	R13
1.0	L6-9	C19	R13
1.0	L6-10	C20	R21
1.0		C22	

1. Report No.	2. Government Accession No.	3. Recipient's Catalog No.
NASA CR-3339		

4. Title and Subtitle	5. Report Date
Solid State SPS Microwave Generation and Transmission Study Volume II - Phase II Final Report Appendices	November 1980 6. Performing Organization Code

7. Author(s)	8. Performing Organization Report No.
Owen E. Maynard	ER80-4074-2

9. Performing Organization Name and Address	10. Work Unit No.
Raytheon Company Equipment Division Advanced Development Laboratory Wayland, MA 01778	M-312 11. Contract or Grant No. NAS8-33157

12. Sponsoring Agency Name and Address	13. Type of Report and Period Covered
National Aeronautics and Space Administration Washington, DC 20546	Contractor Report 14. Sponsoring Agency Code

15. Supplementary Notes

NASA Marshall Technical Monitor: Charles Guttman
Final Report

16. Abstract

The purpose of this investigation was to further define the solid state sandwich concept for SPS. The design effort concentrated on the spacetenna, but did include some system analysis for parametric comparison reasons. The study specifically included definition and math modeling of basic solid state microwave devices, an initial conceptual subsystems and system design, sidelobe control and system selection, an assessment of selected system concept and parametric solid state microwave power transmission system data relevant to the SPS concept. Although device efficiency was not a goal of this study, the sensitivities to design of this efficiency were parametrically treated. Sidelobe control consisted of various single step tapers, multistep tapers and Gaussian tapers. A preliminary assessment of a hybrid concept using tubes and solid state is also included. There is a considerable amount of thermal analysis provided with emphasis on sensitivities to waste heat radiator form factor, emissivity, absorptivity, amplifier efficiency, material and junction temperature.

The document is organized to provide useful design data for future studies, identify issues associated with the solid state sandwich design, and estimate technology requirements.

17. Key Words (Suggested by Author(s))	18. Distribution Statement
SPS Microwave Dipole Subarray Solid State Sandwich Efficiency Power Balance Tapered Illumination Power Density RF Radiating Element Spacetenna Gaussian Pilot Receiver Microwave Power Transmission Sys (MPTS)	Unclassified - Unlimited Subject Category 44

19. Security Classif. (of this report)	20. Security Classif. (of this page)	21. No. of Pages	22. Price
Unclassified	Unclassified	113	A06

For sale by the National Technical Information Service, Springfield, Virginia 22161

NASA-Langley, 1980